Portal fibroblasts with mesenchymal stem cell features form a reservoir of proliferative myofibroblasts in liver fibrosis

Lin Lei, Alix Bruneau, Haquima El Mourabit, Justine Guégan, Trine Folseraas, Sara Lemoinne, Tom Hemming Karlsen, Bénédicte Hoareau, Romain Morichon, Ester Gonzalez-sanchez, et al.

HEPATOLOGY

Portal fibroblasts with mesenchymal stem cell features form a reservoir of proliferative myofibroblasts in liver fibrosis

Journal:	*Hepatology*
Manuscript ID	HEP-21-2383.R1
Wiley - Manuscript type:	Original
Date Submitted by the Author:	n/a
Complete List of Authors:	Lei, Lin; Sorbonne Université, INSERM, Centre de Recherche Saint-Antoine (CRSA) Bruneau, Alix; Charité University Medicine Berlin, Department of Hepatology and Gastroenterology El Mourabit, Haquima; Sorbonne Université, INSERM, Centre de Recherche Saint-Antoine (CRSA) Guégan, Justine; Sorbonne Universite Folseraas, Trine; Norwegian PSC Research Center, Clinic for Specialized Surgery and Medicine, Oslo University Hospital, Rikshospitalet, Research Institute for Internal Medisine Lemoinne, Sara; Saint Antoine Hospital, Hepatology Karlsen, Tom; Oslo Univeristy Hospital Rikshospitalet, Norwegian PSC Reserach Center, Clinic for Specialized Medicine and Surgery Hoareau, Bénédicte; Sorbonne Université, INSERM, UMS Production et Analyse de Données en Sciences de la Vie et en Santé (PASS), Cytométrie Pitié-Salpêtrière (CyPS) Morichon, Romain; Sorbonne Université, INSERM, Centre de Recherche Saint-Antoine (CRSA) Gonzalez-Sanchez, Ester; Sorbonne Université, INSERM, Centre de Recherche Saint-Antoine (CRSA); Instituto de Salud Carlos III, National Biomedical Research Institute on Liver and Gastrointestinal Diseases; Bellvitge Institute for Biomedical Research, Oncobell Program Goumard, Claire; Hopital Universitaire Pitie Salpetriere, Department of Hepato-Biliary and Pancreatic Surgery and Liver Transplantation, AP-HP Pitié-Salpêtrière Hospital; Sorbonne Universite, Sorbonne Université, Paris, France; Saint Antoine Research Centre, Centre de Recherche de Saint-Antoine (CRSA), INSERM, UMRS-938, Paris, France Ratziu, Vlad; Hôpital Pitié Salpêtrière and Université Pierre et Marie Curie Charbord, Pierre; Sorbonne Universite Gautheron, Jérémie Tacke, Frank; Charité Universitätsmedizin Berlin, Hepatology & Gastroenterology; Jaffredo, Thierry; Sorbonne Universite Cadoret, Axelle; Sorbonne Université, INSERM, Centre de Recherche Saint-Antoine (CRSA) Housset, Chantal; Sorbonne Université, INSERM, Centre de Recherche Saint-Antoine (CRSA); Assistance Publique-Hôpitaux de Paris (AP-HP), Department of Hepatology
Keywords:	Cirrhosis, Hepatic stellate cells, Perivascular, Single-cell RNA-sequencing, SLIT2

Note: The following files were submitted by the author for peer review, but cannot be converted to PDF. You must view these files (e.g. movies) online.
PMSC video.mp4 HSC video.mp4

Portal fibroblasts with mesenchymal stem cell features form a reservoir of proliferative myofibroblasts in liver fibrosis

Lin Lei,[1] Alix Bruneau,[2] Haquima El Mourabit,[1] Justine Guégan,[3] Trine Folseraas,[4] Sara Lemoinne,[1,5] Tom Hemming Karlsen,[4] Bénédicte Hoareau,[6] Romain Morichon,[1] Ester Gonzalez-Sanchez,[1] Claire Goumard,[1,7] Vlad Ratziu,[7] Pierre Charbord,[8] Jérémie Gautheron,[1] Frank Tacke,[2] Thierry Jaffredo,[8] Axelle Cadoret,[1]* Chantal Housset[1,5]*

[1]Sorbonne Université, INSERM, Centre de Recherche Saint-Antoine (CRSA), Institute of Cardiometabolism and Nutrition (ICAN), Paris, France;
[2]Charité University Medicine Berlin, Department of Hepatology and Gastroenterology, Berlin, Germany;
[3]Sorbonne Université, INSERM, Institut du Cerveau (ICM), Bioinformatics/Biostatistics iCONICS Facility, Paris, France;
[4]Oslo University Hospital Rikshospitalet, Norwegian PSC Research Center, Research Institute of Internal Medicine, Division of Surgery, Inflammatory Medicine and Transplantation, Oslo, Norway;
[5]Assistance Publique-Hôpitaux de Paris (AP-HP), Department of Hepatology, Reference Center for Inflammatory Biliary Diseases and Autoimmune Hepatitis (CRMR MIVB-H, ERN RARE-LIVER), Saint-Antoine Hospital, Paris, France;
[6]Sorbonne Université, INSERM, UMS Production et Analyse de Données en Sciences de la Vie et en Santé (PASS), Cytométrie Pitié-Salpêtrière (CyPS), Paris, France ;
[7]AP-HP, Sorbonne Université, ICAN, Departments of Hepatology, Hepatobiliary surgery and liver transplantation, Pitié-Salpêtrière Hospital, Paris, France ;
[8]Sorbonne Université, CNRS, INSERM, Institut de Biologie Paris Seine (IBPS), Laboratoire de Biologie du Développement, Paris, France.

*These authors share senior authorship

Keywords: Angiogenesis; Cirrhosis; Hepatic stellate cell; Single-cell RNA-sequencing; SLIT2.

Corresponding authors:

Chantal Housset, M.D., Ph.D.

Sorbonne Université, Faculté de Médecine, Site Saint-Antoine, 27 rue Chaligny, 75571 Paris cedex 12, France.

E-mail: chantal.housset@inserm.fr; Phone: (33) 1-40-01-13-59

Axelle Cadoret, Ph.D.

Sorbonne Université, Faculté de Médecine, Site Saint-Antoine, 27 rue Chaligny, 75571 Paris cedex 12, France.

E-mail: axelle.cadoret@inserm.fr; Phone: (33) 1-40-01-13-53

Abbreviations: ABCB4, ATP-binding cassette B4; α-SMA, alpha-smooth muscle actin; CK19, cytokeratin 19; CCl4, carbon tetrachloride; CDAA, choline-deficient, L-amino acid-defined; CFU-F, colony forming unit-fibroblast; CSAA, choline-sufficient, L-amino acid-defined; DDC, 3,5-diethoxycarbonyl-1,4-dihydrocollidine; DEG, differentially expressed gene; EC, endothelial cell; ECM, extracellular matrix; FISH, fluorescent *in situ* hybridization; GO, gene ontology; HSC, hepatic stellate cell; HUVEC, human umbilical vein endothelial cell; LSEC, liver sinusoidal endothelial cell; MSC, mesenchymal stem cell; NAFLD, non-alcoholic fatty liver disease; NASH, non-alcoholic steatohepatitis; NCD, normal chow diet; PCA, principal component analysis; PMSC, portal fibroblast with mesenchymal stem cell features; PSC, primary sclerosing cholangitis; ROBO, Roundabout; RT-qPCR, Reverse transcription-quantitative PCR; scRNAseq, single-cell RNA-sequencing; *t*-SNE, *t*-distributed stochastic neighbor embedding; VSMC, vascular smooth muscle cell.

Electronic word count: / 6037 words; 5 Figures

Conflict of interest: The authors have no conflict of interest to declare.

Financial support: This work was supported by funding from ANRS (ECTZ35217), FRM (EQU202003010517) and the Microbiome Foundation. Lin Lei received a fellowship from the China Scholarship Council (CSC).

Authors contributions: L.L., T.J., A.C., C.H. designed the study; L.L., A.B., H.E.M., J.Gu., T.F., T.H.K., B.H., R.M., E.G-S., C.G., V.R., J.Ga., T.J. acquired experimental and clinical data; L.L., A.B., H.E.M., J.Gu., S.L., P.C., F.T., T.J., C.H., A.C. analyzed and interpreted the data; L.L., S.L., A.C., C.H. drafted the manuscript, with critical revision from all authors.

Abstract

Background & Aims: In liver fibrosis, myofibroblasts derive from hepatic stellate cells (HSCs) and as yet undefined mesenchymal cells. We aimed to identify portal mesenchymal progenitors of myofibroblasts. **Approach & Results:** Portal mesenchymal cells were isolated from mouse bilio-vascular tree and analyzed by scRNAseq. Thereby, we uncovered the landscape of portal mesenchymal cells in homeostatic mouse liver. Trajectory analysis enabled inferring a small cell population further defined by surface markers used to isolate it. This population consisted of portal fibroblasts with mesenchymal stem cell features (PMSCs), *i.e.*, high clonogenicity and tri-lineage differentiation potential, that generated proliferative myofibroblasts, contrasting with non-proliferative HSC-derived myofibroblasts (-MFs). Using bulk RNAseq, we built oligogene signatures of the two cell populations, that remained discriminant across myofibroblastic differentiation. *SLIT2*, a prototypical gene of PMSC/PMSC-MF signature, mediated pro-fibrotic and angiogenic effects of these cells, whose conditioned medium promoted HSC survival and endothelial cell tubulogenesis. Using PMSC/PMSC-MF 7-gene signature and *SLIT2* FISH, we showed that PMSCs display a perivascular portal distribution in homeostatic liver and largely expand with fibrosis progression, contributing to the myofibroblast populations that form fibrotic septa, preferentially along neo-vessels, in murine and human liver disorders, irrespective of aetiology. We also unraveled a 6-gene expression signature of HSCs/HSC-MFs that did not vary in these disorders, consistent with their low proliferation rate. **Conclusions:** PMSCs form a small reservoir of expansive myofibroblasts, which in interaction with neo-vessels and HSC-MFs that mainly arise *via* differentiation from a preexisting pool, underlie the formation of fibrotic septa in all types of liver diseases.

Mesenchymal cells are key players in tissue homeostasis and wound healing. In the liver, mesenchymal cells comprise hepatic stellate cells (HSCs), that reside in sinusoids, and perivascular cells including vascular smooth muscle cells (VSMCs) and fibroblasts, that reside in the portal tracts and around central veins. Genetic-based lineage-tracing analyses have demonstrated that HSCs and perivascular mesenchymal cells as well as mesothelial cells all derive from the septum transversum during liver development (1). Over the past 30 years, HSCs have been extensively investigated for their capacity to undergo myofibroblastic differentiation, and have been identified as a major source of myofibroblasts in liver fibrosis (2). However, the other liver mesenchymal cells, particularly portal mesenchymal cells have gained increasing interest as evidence has accumulated that indicates they could also generate myofibroblasts (3-6). The portal tracts contain three main structures referred to as the portal triad, *i.e.*, the portal vein, hepatic artery and bile duct, surrounded by a mesenchyme, which has remained poorly defined so far. Little is known regarding the identity, spatial distribution or functions of portal mesenchymal cells and how they contribute to fibrosis. A major limitation has been the lack of markers, especially surface markers that would allow to isolate portal mesenchymal cells or track them *in vivo*. Using a model of outgrowth from fragments of the bilio-vascular tree isolated from rat liver, we previously showed that portal cells distinct from HSCs could generate myofibroblasts, that we referred to as portal myofibroblasts, characterized by COL15A1 expression, a high proliferation rate and pro-angiogenic properties (4, 7, 8). However, the precursors of portal myofibroblasts have not been truly identified in these studies. In the present study, we isolated portal mesenchymal cells from mouse liver as a single-cell preparation and analyzed their diversity using single-cell RNA-

sequencing (scRNAseq). A minimal set of surface markers enabled us to isolate a subset of portal fibroblasts with mesenchymal stem cell features (PMSCs) and the ability to generate myofibroblasts. Markers of PMSCs were discovered and used to examine the expansion potential of these cells in murine and human liver fibrosis.

Experimental procedures

Details are provided in Supplementary material.

Animals. Male mice of C57BL/6J or FVB.129 genetic background, were used at the age of 8-12 weeks for cell isolation and liver fibrosis models, in compliance with ARRIVE guidelines.

Cell isolation and culture. The bilio-vascular tree was isolated from mouse liver, by adapting a procedure we previously described in rat (7), and further processed using cell sorting and flow cytometry analysis to collect and analyze mesenchymal cells. Ultrapure HSCs and other liver cell types were isolated using established methods. Cell clonogenicity, trilineage and myofibroblastic differentiation were examined in cell culture.

RNAseq. ScRNAseq of the bilio-vascular tree Lin-negative cells (gated as $Epcam^-$ $CD31^-CD45^-CD11b^-$ cells), was performed using the 10X Genomics 3' v3 kit (10× Genomics). NextSeq500 (Illumina) device was used for single-cell and bulk RNAseq. ScRNAseq analyses were performed using CellRanger, Seurat and Monocle, and bulk RNAseq analyses, using STAR, RSEM and edgeR R package.

Human liver samples. Fresh and frozen samples of normal and pathological liver tissue were collected with the approval of ethical committees, from patients who gave written informed consent.

Reverse transcription-quantitative PCR (RT-qPCR), Immunofluorescence and fluorescent *in situ* hybridization (FISH). Primers, antibodies and probes are listed in Table S1-3.

Microarray analyses. Pangenomic analysis of frozen liver tissue samples, was performed using the Affymetrix human gene 1.0 st microarray.

SLIT2-mediated functions analyses. The conditioned medium of PMSC-derived myofibroblasts (PMSC-MFs) was tested for potential effects on the viability of the LX-2 HSC cells, and the tubulogenesis of human umbilical vein endothelial cells (HUVECs). In these experiments, SLIT2 signaling was blocked using siRNA, CRISPR/Cas9, anti-ROBO1 antibody or a recombinant ROBO1/Fc chimera.

Statistical analyses. Unless otherwise stated, statistical analyses were performed using Graphpad Prism v6.0 and R. Unpaired two-sided Wilcoxon test and ANOVA with a Scheffe post-hoc test were used to compare differences between two groups, and more than two groups, respectively. A significant difference was defined as $p<0.05$.

Results

Landscape of the portal mesenchyme revealed by scRNAseq

Portal mesenchymal cells represent a small cell population. They are tightly bound to the portal triad, relying on basement membranes. This makes them more difficult to isolate than hepatocytes or sinusoidal cells, which reside in a loose, basement membrane-free, extracellular matrix (ECM). In the present study, we set up a specific procedure to isolate portal mesenchymal cells, for scRNAseq analysis. We adapted a method we previously established for the culture of rat portal myofibroblasts (7), to isolate fragments of the bilio-vascular tree from mouse liver. The bilio-vascular tree fragments were submitted to enzymatic digestion, resulting in a single-cell suspension,

which was depleted in cells expressing the lineage (Lin) markers of cholangiocytes (EpCAM), endothelial cells (CD31), and hematopoietic cells (CD45 and CD11b) using cell sorting. Lin-negative single-cell suspension was then processed to generate a scRNAseq cDNA library (Fig. 1A). We captured 4,976 sequenced cells that met quality control metrics (Fig. S1A) from healthy mouse liver. Unsupervised clustering identified 16 distinct clusters that were assigned to fibroblast (5 clusters), VSMC (5 clusters), endothelial (4 clusters), HSC (1 cluster) and mesothelial (1 cluster) identities (Fig. 1B). The hierarchical clustering of gene expression profiles supported this classification except for the very small cluster of VSMC-5 (Fig. 1C). The most selective expressed genes that allowed to segregate cell clusters are shown in Fig. 1D, Fig. S2 and Table S4. In all clusters, the expression of cell cycle-related genes, *e.g.*, *Mki67*, was at the limit of detection, as expected from resting cells in homeostatic liver (Fig. S3).

The non-mesenchymal components: mesothelial and endothelial cells

Mesothelial cells display an intermediate phenotype between epithelial and mesenchymal cells and form a single layer that covers the liver surface (9). The liver capsule also covers the intrahepatic parenchyma surrounding the Glissonean pedicles including bile ducts (10), which can explain the presence of mesothelial cells in our cell suspension. Genes expressed in these cells included previously reported mesothelial markers, among which the most specific were *Msln* and *Upk1b* as well as epithelial markers, such as *Krt8* and *Krt19*, and mesenchymal markers, such as *Vim* but almost no *Pdgfrb.* Additional putative markers restricted to this cluster included *Fxyd3, Myl7* and *Slpi* (Fig. S4A).

We identified four clusters of endothelial cells (ECs), enriched in markers such as *Pecam1*, *Cdh5*, *Kdr* and *Egfl7* (Fig. S4B). The PECAM1 protein (alias CD31) has been

shown to be intracellular in liver sinusoidal endothelial cells (LSECs) (11), which explains, at least partly, why ECs escaped our negative selection according to the membrane antigen CD31. Moreover, even though cells from the bilio-vascular tree were preferentially retrieved by our method, basement membrane-free LSECs adhere to other cell types and are prone to be collected during isolation procedures, as previously reported (12). As shown in Fig. S5, we found markers of EC zonation in the liver, *i.e.*, of peri-central LSECs in EC-1, of peri-portal LSECs and/or portal vascular ECs in EC-2, of lymphatic ECs in EC-3, and of hepatic arterial ECs in EC-4 (12, 13).

The mesenchymal components: fibroblasts, HSCs and VSMCs

Our single-cell analysis revealed five clusters of fibroblasts (Fig. 1B-D), which predominantly expressed genes involved in vascular ECM such as *Mmp19*, *Col6a5*, *Col6a6* or *Col15a1*, and also expressed genes of interstitial collagens such as *Col1a1*, *Col1a2*, *Col3a1* at higher levels than other clusters. Both fibroblasts and HSCs expressed *Pdgfra*, whereas *Eln* previously reported as a marker of portal fibroblasts (5), was expressed in many other clusters (Fig. S4C). Fib-3 highly expressed *Ptn* (Fig. 1D), a pericyte-derived trophic factor for ECs (14), suggesting a particular interaction of this cluster with portal vessels, whereas Fib-5 was enriched in HSC markers, such as *Lrat* (2) and *Reln* (5) (Fig. S4D), which was not driven by doublets (Fig. S1B), and may thus represent an intermediate population between fibroblasts and HSCs. All five fibroblast clusters were enriched in the gene ontology (GO) terms “ECM organization” and “Wound healing” (Fig. S6, Table S5). Individual clusters were also enriched in terms related to cell (including leucocyte) chemotaxis (Fib-1), epithelial cell proliferation and migration (Fib-2), tissue development or morphogenesis (Fib-3, Fib-4, Fib-5).

Cells of cluster 8 were recognized as HSCs. They were enriched in GO terms related to immunity and cell differentiation (Fig. S6). Among classical markers of HSCs, *Lrat* and *Reln* (2, 5) appeared to be not fully specific, being expressed notably in Fib-2 and Fib-5 (Fig. S4D). Like others (2, 15), we found virtually no expression of *Gfap*, whereas *Des* and *Cygb* (2, 3), were expressed at variable levels in virtually all clusters. Among HSC markers newly identified by scRNAseq (15-18) or bulk RNAseq (19), our analysis confirmed that some of them were restricted to HSCs, such as *Tmem56*, *Colec10, Mapt* or *Bco1*. Others such as *Fcna* or *Angptl6*, although not fully specific, were largely overexpressed in HSCs, whereas yet others such as *Rgs5*, *Pcdh7*, *Adamtsl2*, *Gucy1a1/b1* or *Colec11* were expressed at relatively high levels in several other mesenchymal cells, in addition to HSCs. Both *Ngfr* and *Il34* on one hand, *Vipr1* and *Pth1r* on the other one, previously reported to preferentially mark peri-portal and peri-central HSCs, respectively (15), were expressed in the HSC cluster, indicating that this cluster was representative of all HSCs (Fig. S4D).

We identified 5 clusters of VSMCs that expressed at highest levels markers such as *Myh11, Cnn1, Acta2* or *Tagln* (13, 15) (Fig. S4E). VSMC clusters were enriched in GO terms related to muscle functions but also to “Inflammatory response” (Fig. S6).

Identification of PMSCs

As a first approach to assess differentiation potency of the different clusters, we computed single-cell entropy, an approximation of single-cell differentiation potency based on predicted signalling promiscuity (20). Of all clusters, Fib-3 displayed the highest differentiation potency as suggested by the highest entropy value (Fig. 2A). We also examined the differentiation dynamics among mesenchymal cells, and analyzed all cells except mesothelial and endothelial cells, using Monocle 2 (21). This

analysis showed a common trajectory of mesenchymal cells with one bifurcation and three branches defining states (Fig. 2B). On the basis of entropy analysis, the branch containing Fib-3 was defined as the root state. As shown in Fig. 2B, the root state was mainly populated by Fib-3 and Fib-4 cells, which were consequently assumed to be progenitor cells, contrasting with the two other states populated by VSMCs, notably VSMC-1, and HSCs, both well-differentiated cell types with high pseudotime values. Consistent with this assumption, GO terms related to development were concentrated in Fib-3 and Fib-4, suggesting multilineage potential of these two clusters (Fig. 2C). Genes previously reported to demarcate universal fibroblasts in mouse tissues, *i.e. Pi16* and *Col15a1* (22), or portal fibroblasts/myofibroblasts, *i.e.*, *Col15a1* (4), *Cd34* (6, 15), *Thy1* alias CD90 (6, 23, 24), *Gli1* (19, 25), *Clec3b* (15), *Fbln2* (26) and *Entpd2* (27), were mainly expressed in these two clusters (Fig. 2D). *Pi16*$^{+}$ cells, were recently shown to serve as resource fibroblasts that would pass through *Col15a1*$^{+}$ fibroblasts able to secrete basement membrane proteins, before developing into specialized fibroblasts, in all steady-state mouse tissues (22). In addition, CD34, Thy1 and Gli1 are all considered as stem cell markers. To further analyze Fib-3 and Fib-4 clusters, we defined a minimal set of surface markers enabling to isolate them together. As shown in Fig. 2E, a high expression of *Pdgfra*, *Cd34* and *Cd9* combined with a low expression of *Cd200* appeared to discriminate Fib-3 and Fib-4 from other Lin-negative cells. We FACS-sorted Lin (Epcam/CD31/CD45/CD11b)-negative, PDGFRα/CD34/CD9-positive, and CD200-low cells (Gate 4 in Fig. 2F) and examined this population for stem cell features. The percentage of cells recovered was approximately 0.03 % of total liver cells. The cells of this population were highly clonogenic (80 colony forming unit-fibroblast (CFU-F) per 2,000 cells) (Fig. 2G) irrespective of whether they were Thy1-positive or negative (Fig. S7). They also

displayed the expression of classical mesenchymal stem cell (MSC) markers*, i.e.*, CD105, Sca-1, CD29 (Fig. 2H), and the ability to undergo trilineage (adipogenic, osteogenic and chondrogenic) differentiation, in culture (Fig. 2I). Taken together, the cells isolated by our gating strategy displayed MSC attributes and were designated PMSCs. When cultured on a stiff substratum (Fig. 2J, bottom panels), PMSCs proliferated and gave rise to cells phenotypically similar to portal myofibroblasts expressing COL15A1 (4), here referred to as PMSC-MFs. This phenotypic change was accompanied by the expected up-regulation of *Acta2*, the gene encoding alpha-smooth muscle actin (α-SMA), no change in *Col1a1* expression, and a down-regulation of *Col15a1* (Fig. 2K). Despite such down-regulation, *Col15a1* demarcates both PMSCs and portal myofibroblasts (4). It was possible to maintain PMSCs in a resting state by cultivating them in spheroids, on ultra-low attachment plates, in which case the expression of α-SMA was not induced and that of Col15a1, less reduced (Fig. 2J-K). Overall, these data indicate that our screening strategy and isolation procedure enabled identifying portal fibroblasts with MSC properties and high collagen expression as precursors of portal myofibroblasts.

Specific phenotypes and molecular profiles of PMSCs, HSCs and derived myofibroblasts

The isolation of PMSCs provided a unique opportunity to compare them with HSCs, and uncover specific markers of the two cell populations and of their myofibroblastic progenies. We performed transcriptomic analyses using bulk RNAseq, to compare PMSCs with ultrapure HSCs (28), as ascertained by vitamin A fluorescence (Fig. S8A). We identified 3,273 genes expressed at higher levels in PMSCs, and 3,122, in HSCs (Fig. 3A, upper panel). Projections onto *t*-SNE plot (Fig. 3A, lower panel), showed that

the top 10 differentially expressed genes in PMSCs included common markers of portal fibroblasts, as expected from a comparison with HSCs, but were expressed at highest levels in Fib-3/Fib-4, indicating that PMSCs comprised mainly if not exclusively Fib-3/Fib-4 fibroblasts. The top 10 differentially expressed genes of HSCs included common markers with ECs, but none with the other mesenchymal cells. Consistent with the GO analyses of scRNAseq (Fig. S6, Table S5), bulk RNAseq analysis showed enrichment in pathways related to “Extracellular matrix organization” in PMSCs and “Immunity” in HSCs, and further highlighted pathways related to “Angiogenesis” in PMSCs and to “Metabolism of fat-soluble vitamins” in HSCs (Fig. 3B).

Both PMSCs (Fig. 2J-K), and HSCs (3, 4), undergo phenotypic changes into myofibroblasts in primary culture. Phenotypically, the major difference we observed between the two cell populations, was an intense proliferation in PMSCs as they became myofibroblastic, whereas HSCs differentiated into myofibroblasts without dividing (Fig. S8A, D-E including videomicroscopy). We extended bulk RNAseq analyses to the myofibroblasts derived from both cell populations in culture, including an early and late stage of differentiation for PMSC-MFs (Table S6). Principal component analysis (PCA) showed a clear discrimination of PMSCs and HSCs from their myofibroblastic progenies according to PC1, while PMSC-MFs were discriminated from HSC-derived myofibroblasts (HSC-MFs) according to PC2 (Fig. 3C). The molecular profiles of PMSCs and HSCs became more similar as they differentiated into myofibroblasts. Yet, they retained specificities at the stage of myofibroblasts as confirmed by GO analysis (Fig. 3D). When fully differentiated into myofibroblasts, *i.e.*, after 7 days of culture, both cell populations were enriched in themes related to muscle differentiation, whereas additionally, PMSC-MFs were enriched in themes related to axonogenesis and ECM organization. To a large extent,

PMSCs/PMSC-MFs overexpressed genes encoding fibrillar collagens (*Col1a1*, *Col1a2*, *Col3a1*), *Timp1* and *Acta2*, the hallmarks of liver fibrosis, whereas *Col4a1*, a major component of sinusoidal ECM was overexpressed in HSC-MFs (Fig. S9). At an early stage of myofibroblastic differentiation, *i.e.*, after 3 days of culture, PMSC transcriptome was highly enriched in pathways related to cell proliferation (Fig. 3D). At a later stage of myofibroblastic differentiation, *i.e.*, after 7 days of culture, PMSC-MFs compared to HSC-MFs still markedly overexpressed genes involved in cell proliferation, consistent with videomicroscopy and CFU-F assays, showing that only PMSCs as opposed to HSCs were clonogenic and divided in culture (Fig. S8B-E).

Next, we looked for gene expressions that would demarcate the two cell populations both in their resting and myofibroblastic states, and that could thus be used in fibrotic liver tissue analyses to assess if PMSCs/PMSC-MFs were more expansive than HSCs/HSC-MFs, also *in vivo*. Altogether, comparative analyses of gene expressions indicated that 100 genes in PMSCs (or Fib-3/Fib-4) and 112 genes in HSCs, i) were overexpressed according to both scRNAseq and bulk RNAseq analyses, and ii) remained differentially expressed in these cells throughout myofibroblastic differentiation (Fig. 3E). Among such genes, we selected those that combined the highest differential expression (>3.5-fold), a relatively high expression (CPM>40) in the demarcated cell population, limited variation with myofibroblastic differentiation, and no or little expression in the other liver cell types, to build an oligogene expression signature of PMSCs/PMSC-MFs (7 genes) and HSCs/HSC-MFs (6 genes) (Fig. 3F-G). Projection of the two signatures onto current (Fig. 1B) and previous scRNAseq datasets (15, 18) showed that the PMSC/PMSC-MF signature demarcated liver fibroblasts, with highest intensity in Fib-3/Fib-4 (Fig. S10A) and in liver fibroblasts accumulating in liver fibrosis induced either by carbon tetrachloride (CCl4) or bile duct

ligation (BDL) (Fig. S10B-C), with little or no signal in other liver cell types. The HSC/HSC-MF signature demarcated the HSC cluster (Fig. S10A), as well as the vast majority of HSCs in mouse liver, including in CCl4- and BDL-induced liver fibrosis, and virtually no other liver cell populations except a small portion of ECs (Fig. S10B-C).

Implication of PMSCs and PMSC-MFs in liver fibrosis

Our transcriptome analyses highlighted *Slit2* as a prototypical gene of PMSC/PMSC-MF signature. Its expression was particularly stable in PMSCs throughout their myofibroblastic differentiation and virtually absent from all other liver cell types including HSCs/HSC-MFs (Fig. 4A, left panel). Using FISH, we confirmed that PMSC-MFs in culture were distinguishable from HSC-MFs by *Slit2* expression (Fig. 4A, right panel). SLIT2 is an axon guidance molecule, which was previously shown to trigger HSC activation and fibrosis (29-31) as well as angiogenesis, in the liver (32). However, so far, the endogenous source of SLIT2 in the liver, had not been accurately identified. Our scRNAseq data showed that *Slit2* expression was concentrated in Fib-3/Fib-4, whereas its roundabout (ROBO) receptors were mainly expressed in the HSC and EC clusters, and to a lesser extent in the fibroblast clusters (Fig. 4B). Therefore, previous and current findings suggested that PMSCs had the potential to signal towards HSCs and ECs via *Slit2*, to promote their pro-fibrotic and pro-angiogenic activity, respectively. Supporting such mechanisms, PMSC-MF conditioned medium prevented the decrease in cell viability induced by an oxidative stress in the LX-2 HSC cell line and this effect was abolished by silencing *Slit2 via* SiRNA in PMSC-MFs (Fig. 4C). PMSC-MF conditioned medium also increased tubulogenesis in HUVECs and this effect was largely SLIT2-dependent. It was prevented in the presence of anti-ROBO1 antibody or recombinant ROBO1/Fc chimera that entraps soluble SLIT2 and it was reduced by

Slit2 depletion *via* CRISPR/Cas9 in PMSC-MFs (Fig. 4D). We used *SLIT2* FISH to demarcate PMSCs/PMSC-MFs and address their connections with other cell types in normal and cirrhotic human liver. In normal liver, *SLIT2*$^{+}$ cells were scarce, although more abundant in large portal tracts than in the small ones. They were virtually restricted to portal tracts and displayed a perivascular distribution (Fig. 4E, left panel, Fig. S11, upper panel). In cirrhotic liver, irrespective of aetiology (*i.e.*, alcoholic liver disease, non-alcoholic steatohepatitis (NASH) or chronic hepatitis C), *SLIT2*$^{+}$ cells were much more abundant than in normal liver (Fig. 4E, middle and right panels). They were mainly located in the fibrotic septa, displayed α-SMA expression and were thus identified as PMSC-MFs. Within fibrotic septa, SLIT2^{+}/α-SMA^{+} PMSC-MFs were intermingled with, and outnumbered by SLIT2^{-}/α-SMA^{+} myofibroblasts, and were frequently located in the surrounding of vascular lumens (Fig. 4E, middle panel). Consistent with PMSC/PMSC-MF interacting with HSCs/HSC-MFs and ECs, we found that in cirrhosis, SLIT2^{+} PMSC-MFs often lined up along CD31^{+} neo-vessels, and thus appeared as a scaffold for the accumulation of abundant SLIT2^{-}/α-SMA^{+} myofibroblasts, most likely largely derived from HSCs (Fig. 4F). Both in normal and cirrhotic human livers, *SLIT2*$^{+}$ cells were clearly distinct from cytokeratin 19 (CK19)-labeled cholangiocytes (Fig. S11).

To further ascertain that PMSCs/PMSC-MFs accumulated in liver fibrosis, we measured SLIT2 mRNA levels in mouse and human injured livers. We found that the hepatic expression of *Slit2* increased in mouse models of either cholestatic diseases, *i.e.*, 3,5-diethoxycarbonyl-1,4-dihydrocollidine (DDC), *Abcb4*$^{-/-}$, or NASH, *i.e.*, choline-deficient, L-amino acid-defined (CDAA) and cytotoxic injury, *i.e.*, CCl4 (Fig. S12), along with those of fibrosis markers (*Acta2*, *Col1a1*) in all models, and of an angiogenesis marker (*vWF*) in the cholestatic models (Fig. 5A and S13). The complete

PMSC/PMSC-MF 7-gene signature was increased in the DDC, *Abcb4*$^{-/-}$ and CDAA models, whereas the HSC/HSC-MF 6-gene signature that was tested in the DDC and CDAA models, was not (Fig. 5A and S13). The analysis of a cohort of patients with non-alcoholic fatty liver disease (NAFLD) showed that the expression of *SLIT2* was increased in the group with advanced fibrosis, *i.e.* F3-F4 according to the SAF score (33) (Fig. 5B). We also examined the microarray data of liver tissue samples from patients with NASH, primary sclerosing cholangitis (PSC) and other chronic liver diseases (alcoholic liver disease, haemochromatosis, primary biliary cholangitis, autoimmune hepatitis), for *SLIT2* expression and the oligogene expression signatures of PMSCs/PMSC-MFs and of HSCs/HSC-MFs. This analysis showed that *SLIT2* expression and the 7-gene expression signature of PMSCs/PMSC-MFs were both significantly increased in the liver of patients with all types of chronic liver diseases, as compared to normal liver (Fig. 5C-D, left panels and S14A). *SLIT2* expression and the 7-gene expression signature were both similarly correlated with *ACTA2*, *COL1A1* and *vWF* expression in these samples (Fig. 5C-D). The analysis of the microarray data also indicated that in contrast to the PMSC/PMSC-MF 7-gene signature, the 6-gene expression signature of HSCs/HSC-MFs was not significantly different between any group of diseased livers and normal livers (Fig. 5E and S14B). This finding is consistent with a low proliferation rate of HSCs and further supports the assumption that HSC-MFs would primarily derive from myofibroblastic differentiation of the HSC preexisting pool. We concluded from these results that PMSCs give rise to a highly expansive population of myofibroblasts in liver fibrosis irrespective of the cause.

Discussion

In the present study, we provide a detailed atlas of portal mesenchymal cells, that were obtained *via* dissociation of the bilio-vascular tree. While being consistent with previous scRNAseq studies of the liver, notably from a *Pdgfrb*-GFP reporter mouse (15), our analysis revealed the existence of several clusters of fibroblasts. Among them, the Fib-3 and Fib-4 clusters, displayed relatively low levels of *Pdgfrb* expression compared to the other clusters of liver mesenchymal cells (Fig. S4A), and thus may have been underestimated in the study of PDGFRβ^{+} cells (15). Fib-3 and Fib-4 were highlighted as potential progenitor cells on the basis of entropy, GO and trajectory analyses as well as the expression of stem cell markers. Thus, Fib-3 and Fib-4 appeared as the most primitive of liver mesenchymal cells, which form a continuum of cells with overlapping markers, along a gradient of differentiation that bifurcates towards mature VSMCs on one hand and HSCs on the other one. In this context, PMSCs were isolated as a cell population, that primarily comprised Fib-3 and Fib-4. MSCs were first identified in the bone marrow as clonogenic, multipotent cells, able to differentiate into lineages of mesenchymal tissues including osteoblasts, chondrocytes and adipocytes in culture (34). Subsequently, cells with similar properties were identified in multiple organs and also referred to as MSCs (35), although a controversy over the MSC terminology has been fueled by studies showing that MSCs from different tissues exhibited different differentiation capacities (36). Yet, MSCs from different tissues share common features including a small cell population, clonogenicity, the ability to differentiate into the afore-mentioned mesenchymal cell lineages *in vitro* and a frequent perivascular distribution (35, 36). PMSCs displayed all these characteristics. Thy1 and Gli1, two stem cell markers predominantly expressed in Fib-3, as well as fibulin-2 and ENTPD2, predominantly expressed in Fib-4, were previously immunolocalized in the portal tracts of homeostatic liver, with a perivascular or periductal distribution (19, 23-

25, 27, 37-39). We found that the sub-populations of Thy1^{+} and Thy1^{-} PMSCs were equally clonogenic (Fig. S7), implying that both Fib-3 and Fib-4 are resource fibroblasts in the liver. COL15A1 (4) and SLIT2, that we identified as PMSC markers, are expressed in both clusters, and also display a perivascular or periductal distribution in the homeostatic liver. As formerly proposed for other MSCs, *e.g.,* in the skeletal muscle (36), we suggest that Fib3 and Fib4 represent subsets of the same original population, recruited to the surface of nascent portal blood vessels or later, of developing bile ducts.

The lack of markers that would enable to differentiate HSC-derived from non-HSC-derived myofibroblasts has been a major hurdle so far, to gain insight into the specificities of the different types of liver myofibroblasts and their contributions to liver fibrosis. The isolation of PMSCs allowed us to gain such insight and seek invaluable markers of the two populations. The comparison of transcriptional profiles indicated that in their resting state, PMSCs primarily ensure ECM organization and vasculature integrity whereas HSCs are mainly involved in immunity and the metabolism of vitamin A. A striking difference between the two cell populations as they transform into myofibroblasts *in vitro*, is that PMSCs intensely proliferate whereas HSCs do not divide. In addition, whereas the expression of α-SMA is induced in both cell types, that of ECM genes such as *Col1a1*, is up-regulated in HSCs but not in PMSCs, so that they both converge towards more similar phenotypes. As a result, most of gene expressions that could demarcate the two cell populations in their resting state are lost or no longer discriminant between their myofibroblastic progenies. Thus, among markers of PMSCs, the expression of *Gli1* or *Entpd2* is totally suppressed in PMSC-MFs, whereas that of *Fbln2* expression is induced in HSC-MFs (Fig. S15). Our strategy was to build

oligogene expression signatures, which included only markers of the two cell populations that maintained high differential expression, with limited variation (average fold-change of approximately one), throughout their myofibroblastic differentiation. Specificity of the cell signatures for liver fibroblasts and HSCs *in vivo*, was attested by their projection onto previous scRNAseq datasets of mouse liver fibrosis (15, 18). PMSC gene signature was predominantly expressed in Fib-3/Fib-4, but also to a lesser extent in other fibroblast clusters (Fig. S10A), which therefore could also proliferate in liver injury.

Slit2, known as a profibrotic and proangiogenic factor in the liver (29-32), is a prototypical gene of PMSC/PMSC-MF signature. From the present data, we may postulate that following liver injury, SLIT2, produced by proliferating PMSCs/PMSC-MFs, promotes the formation of new vessels and the survival of HSC-MFs. Supporting this view, FISH analyses showed that *SLIT2*$^{+}$ PMSCs/PMSC-MFs accumulated along neo-vessels in the fibrotic septa of cirrhotic livers, surrounded by *SLIT2*$^{-}$ myofibroblasts, likely mostly HSC-derived. As we previously showed for *COL15A1* (4), the hepatic expression of *SLIT2* increased in injured liver in correlation with that of *COL1A1* and *vWF*, in all types of liver fibrosis. Akin to *SLIT2*, the complete PMSC/PMSC-MF 7-gene signature increased, indicating that this cell population expanded in mouse and human liver fibrosis of multiple causes. As they expand, PMSCs/PMSC-MFs may promote liver fibrosis *via* several mechanisms including the SLIT2/ROBO axis, but also the production of COL15A1, a multiplexin that anchors interstitial collagen to basement membranes forming a scaffold for fibrosis progression (4, 40), the overproduction of COL1A1 and COL1A2, that form the major interstitial collagen in liver fibrosis, and of LOXL1, which promotes elastin cross-linking, among

others. ScRNAseq analysis of human liver mesenchymal cells in cirrhosis (13), previously identified a cluster distinguished by PDGFRA expression that expanded in cirrhotic livers and was annotated scar-associated mesenchymal cells. We found that the expression of all PMSC/PMSC-MF signature genes is largely predominant in this population (Fig. S16), supporting the clinical relevance of our findings and our conclusion regarding the expansion of PMSC-MFs in liver fibrosis. In a previous study, a 122-gene HSC signature was shown to be increased in experimental and human liver fibrosis (41). However, this latter signature was designed in comparison with other liver cell types that did not include other liver mesenchymal cells, and highlighted genes such as *Pcdh7* that were herein found to be expressed not only in HSCs/HSC-MFs but also in PMSCs/PMSC-MFs (Fig. S4D and S15). Our HSC/HSC-MF 6-gene expression signature did not increase in human fibrosis, which is consistent with a low proliferation rate of HSCs/HSC-MFs *in vitro*, as shown here and *in vivo*, in recent scRNAseq analysis of HSCs/HSC-MFs in mouse models of liver fibrosis (17, 18). Despite little or no proliferation, HSC-MFs that derive from the large preexisting pool of HSCs, likely form the major part of liver myofibroblasts. However, as they proliferate and expand within the lobule, PMSC-MFs may develop interactions with ECs and HSCs anticipated to play crucial roles in fibrosis progression.

Acknowledgements: The authors acknowledge Tatiana Ledent (CRSA Animal Facility), Yannick Marie and Delphine Bouteiller (ICM Sequencing Facility), Pierre-Antoine Soret (CRSA), Filomena Conti, Lynda Aoudjehane (Human HepCell) and Pierre-Emmanuel Rautou (CRI, Université de Paris) for their contributions.

Data availability: All sequencing data are deposited in the Gene Expression Omnibus (GEO) with the accession numbers GSE163777 (scRNAseq), GSE164037 (bulk RNAseq) and GSE159676 (microarrays).

References

1. Asahina K, Zhou B, Pu WT, Tsukamoto H. Septum transversum-derived mesothelium gives rise to hepatic stellate cells and perivascular mesenchymal cells in developing mouse liver. Hepatology 2011;53:983-995.

2. Mederacke I, Hsu CC, Troeger JS, Huebener P, Mu X, Dapito DH, Pradere JP, et al. Fate tracing reveals hepatic stellate cells as dominant contributors to liver fibrosis independent of its aetiology. Nat Commun 2013;4:2823.

3. Bosselut N, Housset C, Marcelo P, Rey C, Burmester T, Vinh J, Vaubourdolle M, et al. Distinct proteomic features of two fibrogenic liver cell populations: hepatic stellate cells and portal myofibroblasts. Proteomics 2010;10:1017-1028.

4. Lemoinne S, Cadoret A, Rautou PE, El Mourabit H, Ratziu V, Corpechot C, Rey C, et al. Portal myofibroblasts promote vascular remodeling underlying cirrhosis formation through the release of microparticles. Hepatology 2015;61:1041-1055.

5. Lua I, Li Y, Zagory JA, Wang KS, French SW, Sevigny J, Asahina K. Characterization of hepatic stellate cells, portal fibroblasts, and mesothelial cells in normal and fibrotic livers. J Hepatol 2016;64:1137-1146.

6. Nishio T, Hu R, Koyama Y, Liang S, Rosenthal SB, Yamamoto G, Karin D, et al. Activated hepatic stellate cells and portal fibroblasts contribute to cholestatic liver fibrosis in MDR2 knockout mice. J Hepatol 2019;71:573-585.

7. El Mourabit H, Loeuillard E, Lemoinne S, Cadoret A, Housset C. Culture Model of Rat Portal Myofibroblasts. Front Physiol 2016;7:120.

8. Loeuillard E, El Mourabit H, Lei L, Lemoinne S, Housset C, Cadoret A. Endoplasmic reticulum stress induces inverse regulations of major functions in portal myofibroblasts during liver fibrosis progression. Biochim Biophys Acta Mol Basis Dis 2018;1864:3688-3696.

9. Lua I, Asahina K. The Role of Mesothelial Cells in Liver Development, Injury, and Regeneration. Gut Liver 2016;10:166-176.

10. Sugioka A, Kato Y, Tanahashi Y. Systematic extrahepatic Glissonean pedicle isolation for anatomical liver resection based on Laennec's capsule: proposal of a novel comprehensive surgical anatomy of the liver. J Hepatobiliary Pancreat Sci 2017;24:17-23.

11. **Poisson J**, **Lemoinne S**, Boulanger C, Durand F, Moreau R, Valla D, Rautou PE. Liver sinusoidal endothelial cells: Physiology and role in liver diseases. J Hepatol 2017;66:212-227.

12. **Halpern KB**, **Shenhav R**, Massalha H, Toth B, Egozi A, Massasa EE, Medgalia C, et al. Paired-cell sequencing enables spatial gene expression mapping of liver endothelial cells. Nat Biotechnol 2018;36:962-970.

13. Ramachandran P, Dobie R, Wilson-Kanamori JR, Dora EF, Henderson BEP, Luu NT, Portman JR, et al. Resolving the fibrotic niche of human liver cirrhosis at single-cell level. Nature 2019;575:512-518.

14. Copes F, Ramella M, Fusaro L, Mantovani D, Cannas M, Boccafoschi F. Pleiotrophin: Analysis of the endothelialisation potential. Adv Med Sci 2019;64:144-151.

15. Dobie R, Wilson-Kanamori JR, Henderson BEP, Smith JR, Matchett KP, Portman JR, Wallenborg K, et al. Single-Cell Transcriptomics Uncovers Zonation of Function in the Mesenchyme during Liver Fibrosis. Cell Rep 2019;29:1832-1847 e1838.

16. Krenkel O, Hundertmark J, Ritz TP, Weiskirchen R, Tacke F. Single Cell RNA Sequencing Identifies Subsets of Hepatic Stellate Cells and Myofibroblasts in Liver Fibrosis. Cells 2019;8:503.

17. Rosenthal SB, Liu X, Ganguly S, Dhar D, Pasillas MP, Ricciardelli E, Li RZ, et al. Heterogeneity of HSCs in a Mouse Model of NASH. Hepatology 2021;74:667-685.

18. **Yang W**, **He H**, Wang T, Su N, Zhang F, Jiang K, Zhu J, et al. Single-Cell Transcriptomic Analysis Reveals a Hepatic Stellate Cell-Activation Roadmap and Myofibroblast Origin During Liver Fibrosis in Mice. Hepatology 2021;74:2774-2790.

19. Gupta V, Gupta I, Park J, Bram Y, Schwartz RE. Hedgehog Signaling Demarcates a Niche of Fibrogenic Peribiliary Mesenchymal Cells. Gastroenterology 2020;159:624-638 e629.

20. Chen W, Teschendorff AE. Estimating Differentiation Potency of Single Cells Using Single-Cell Entropy (SCENT). Methods Mol Biol 2019;1935:125-139.

21. Trapnell C, Cacchiarelli D, Grimsby J, Pokharel P, Li S, Morse M, Lennon NJ, et al. The dynamics and regulators of cell fate decisions are revealed by pseudotemporal ordering of single cells. Nat Biotechnol 2014;32:381-386.

22. **Buechler MB**, **Pradhan RN**, Krishnamurty AT, Cox C, Calviello AK, Wang AW, Yang YA, et al. Cross-tissue organization of the fibroblast lineage. Nature 2021;593:575-579.

23. Dudas J, Mansuroglu T, Batusic D, Ramadori G. Thy-1 is expressed in myofibroblasts but not found in hepatic stellate cells following liver injury. Histochemistry and cell biology 2009;131:115-127.

24. Katsumata LW, Miyajima A, Itoh T. Portal fibroblasts marked by the surface antigen Thy1 contribute to fibrosis in mouse models of cholestatic liver injury. Hepatol Commun 2017;1:198-214.

25. Kramann R, Schneider RK, DiRocco DP, Machado F, Fleig S, Bondzie PA, Henderson JM, et al. Perivascular Gli1+ progenitors are key contributors to injury-induced organ fibrosis. Cell Stem Cell 2015;16:51-66.

26. Knittel T, Kobold D, Saile B, Grundmann A, Neubauer K, Piscaglia F, Ramadori G. Rat liver myofibroblasts and hepatic stellate cells: different cell populations of the fibroblast lineage with fibrogenic potential. Gastroenterology 1999;117:1205-1221.

27. Dranoff JA, Kruglov EA, Robson SC, Braun N, Zimmermann H, Sevigny J. The ecto-nucleoside triphosphate diphosphohydrolase NTPDase2/CD39L1 is expressed in a novel functional compartment within the liver. Hepatology 2002;36:1135-1144.

28. **Mederacke I**, **Dapito DH**, Affo S, Uchinami H, Schwabe RF. High-yield and high-purity isolation of hepatic stellate cells from normal and fibrotic mouse livers. Nat Protoc 2015;10:305-315.

29. **Chang J**, **Lan T**, Li C, Ji X, Zheng L, Gou H, Ou Y, et al. Activation of Slit2-Robo1 signaling promotes liver fibrosis. J Hepatol 2015;63:1413-1420.

30. Zeng Z, Wu Y, Cao Y, Yuan Z, Zhang Y, Zhang DY, Hasegawa D, et al. Slit2-Robo2 signaling modulates the fibrogenic activity and migration of hepatic stellate cells. Life Sci 2018;203:39-47.

31. **Li C**, **Yang G**, **Lin L**, Xuan Y, Yan S, Ji X, Song F, et al. Slit2 signaling contributes to cholestatic fibrosis in mice by activation of hepatic stellate cells. Exp Cell Res 2019;385:111626.

32. Coll M, Arino S, Martinez-Sanchez C, Garcia-Pras E, Gallego J, Moles A, Aguilar-Bravo B, et al. Ductular Reaction Promotes Intrahepatic Angiogenesis Via Slit2-Robo1 Signaling. Hepatology 2021.

33. Bedossa P, Consortium FP. Utility and appropriateness of the fatty liver inhibition of progression (FLIP) algorithm and steatosis, activity, and fibrosis (SAF) score in the evaluation of biopsies of nonalcoholic fatty liver disease. Hepatology 2014;60:565-575.

34. Pittenger MF, Mackay AM, Beck SC, Jaiswal RK, Douglas R, Mosca JD, Moorman MA, et al. Multilineage potential of adult human mesenchymal stem cells. Science 1999;284:143-147.

35. Crisan M, Yap S, Casteilla L, Chen CW, Corselli M, Park TS, Andriolo G, et al. A perivascular origin for mesenchymal stem cells in multiple human organs. Cell Stem Cell 2008;3:301-313.

36. **Sacchetti B**, **Funari A**, Remoli C, Giannicola G, Kogler G, Liedtke S, Cossu G, et al. No Identical "Mesenchymal Stem Cells" at Different Times and Sites: Human Committed Progenitors of Distinct Origin and Differentiation Potential Are Incorporated as Adventitial Cells in Microvessels. Stem Cell Reports 2016;6:897-913.

37. Knittel T, Kobold D, Piscaglia F, Saile B, Neubauer K, Mehde M, Timpl R, et al. Localization of liver myofibroblasts and hepatic stellate cells in normal and diseased rat livers: distinct roles of (myo-)fibroblast subpopulations in hepatic tissue repair. Histochem Cell Biol 1999;112:387-401.

38. Tateaki Y, Ogawa T, Kawada N, Kohashi T, Arihiro K, Tateno C, Obara M, et al. Typing of hepatic nonparenchymal cells using fibulin-2 and cytoglobin/STAP as liver fibrogenesis-related markers. Histochem Cell Biol 2004;122:41-49.

39. Dezso K, Jelnes P, Laszlo V, Baghy K, Bodor C, Paku S, Tygstrup N, et al. Thy-1 is expressed in hepatic myofibroblasts and not oval cells in stem cell-mediated liver regeneration. Am J Pathol 2007;171:1529-1537.

40. Lemoinne S, Thabut D, Housset C. Portal myofibroblasts connect angiogenesis and fibrosis in liver. Cell Tissue Res 2016;365:583-589.

41. Zhang DY, Goossens N, Guo J, Tsai MC, Chou HI, Altunkaynak C, Sangiovanni A, et al. A hepatic stellate cell gene expression signature associated with outcomes in hepatitis C cirrhosis and hepatocellular carcinoma after curative resection. Gut 2016;65:1754-1764.

Author names in bold designate shared co-first authorship

Figure legends

Fig. 1. ScRNAseq profiling of mesenchymal cells from the bilio-vascular tree. (A) Outline of the experimental procedure for preparation of Lin (EpCam,CD31,CD45,CD11b)-negative cells from the mouse bilio-vascular tree for scRNAseq analysis. (B) *t*-SNE projection of 4,976 single cells from one healthy liver, revealing 16 clusters (color-coded), identified by their expression profiles and ordered according to the number of cells they comprise. (C) Dendrogram showing the relationships of clusters. (D) Dot plot of two selective differentially expressed genes in each cluster.

Fig. 2. Characterization of PMSCs. (A) Single-cell entropy of all clusters. (B) Inference of sequenced mesenchymal cells by Monocle 2 reverse graph embedding (pseudotime along differentiation trajectory in inset). (C) Heatmap of GO enrichment related to development. (D) Dot plot of genes previously reported to demarcate progenitor fibroblasts (red frame) or portal (myo)fibroblasts (black frame). (E) Dot plot of genes encoding surface markers *Pdgfra*/*Cd34*/*Cd9* and *Cd200*. (F) FACS plot showing the gating strategy for Fib-3/Fib-4 cell sorting (Gate 4). (G) CFU-F formed by sorted cells from gates as defined in F (n=3-9). (H) Flow cytometry analysis of MSC surface markers in cells from gate 4 (n=4-10). (I) Trilineage differentiation of cells from gate 4 (PMSCs), towards adipocytes (Oil red O), osteoblasts (Alizarin red S) and chondrocytes (Alcian blue). (J) Immunofluorescence of Col15A1 and α-SMA in PMSC

spheroids (upper panel) or grown into PMSC-MFs on stiff substratum (lower panel). (K) *Col15a1*, *Acta2* and *Col1a1* expression in PMSCs (freshly isolated or cultured as in J) (n=3). Means ± SEM; ***p*<0.01; ****p*<0.001; *****p*<0.0001 (Wilcoxon test); Scale bars=50 µm.

Fig. 3. Transcriptomic features of PMSCs/PMSC-MFs compared to HSCs/HSC-MFs. (A,B) Bulk RNAseq analysis of PMSCs and HSCs, A) Volcano plot (upper panel) showing 3,273 and 3,122 DEGs (FDR ≤ 0.05, fold-difference ≥ 2) in PMSCs and HSCs, respectively. Top 10 DEGs are labeled and their average expression, projected on *t*-SNE plot of scRNAseq (lower panel); (B) Gene Set Enrichment Analysis (GSEA) of all genes overexpressed in PMSCs or HSCs. (C) Overview of cell preparations (n=4 per condition), analyzed by bulk RNAseq and PCA of variance of read counts (ellipses: 95% CI). (D) K-means clustering of 5,000 genes with highest variance showing enriched GO terms. (E) Venn diagram showing DEGs in PMSCs (or Fib-3/Fib-4) and in HSCs, both in bulk RNAseq and scRNAseq and maintaining high differential expression after myofibroblastic differentiation (-MFs-7d). (F-G) Heatmaps of PMSC and HSC oligogene expression signatures assessed by F) bulk RNAseq or G) RT-qPCR analyses of PMSCs, HSCs, derived myofibroblasts (-MFs-7d), and other liver cell types. KCs, Kupffer cells.

Fig. 4. *Slit2* marker in PMSCs/PMSC-MFs and its functional analysis. (A) *Slit2* RT-qPCR in PMSCs, HSCs, their derived myofibroblasts (-MFs-d7), and other liver cell types (n=3) (left panel); *Slit2* FISH and α-SMA immunofluorescence in PMSC-MFs-d7 and HSC-MFs-d7 (right panel). (B) *t*-SNE plot of *Slit2* and its *Robo* receptors in scRNAseq clusters. (C) PMSC-MFs that were transfected with *Slit2* or scramble (Scr)

siRNA, were examined for *Slit2* and *Acta2* expression by RT-qPCR, and their conditioned medium (CM) tested towards the cell viability, assessed by MTT, of LX-2 cells exposed to H2O2 (n=5-8). (D) Tube formation was evaluated in HUVECs incubated with PMSC-MF CM in the absence (n=6) or presence of ROBO1/Fc (n=5) or anti-ROBO1 antibody (n=5), or with control (CTL) serum-free medium (n=9); and in HUVECs incubated with the CM of PMSC-MFs infected with a lentivirus expressing Cas9 and a gRNA targeting the first exon of *Slit2* (LV*Slit2*, n=8) or a control lentivirus expressing Cas9 and a scramble gRNA (LV, n=8), or with CTL serum-free medium (n=3). After 6 hours, pictures were taken and the number of junctions, counted, using the Angiogenesis Analyzer tool Fiji. (E, F) *SLIT2* FISH and α-SMA or CD31 immunofluorescence in normal and cirrhotic human liver; E) In normal liver (left panel), a small number of *SLIT2*$^+$ PMSCs (arrowheads) are visible in portal tracts (perivascular *SLIT2*$^+$ PMSCs, distinct from α-SMA$^+$ VSMCs, shown in insets), representative of n=2 (CV, central vein; PV, portal vein). In cirrhosis (middle panel), *SLIT2*$^+$ are intermingled with *SLIT2*$^-$ myofibroblasts in fibrotic septa (FS) (*SLIT2*$^+$,α-SMA$^+$ PMSC-MF, shown in inset); right panel: quantification of labeled areas; F) SLIT2$^+$ PMSC-MFs (red arrowheads) line up along CD31$^+$ neo-vessels (white arrowheads), surrounded by several layers of α-SMA$^+$ myofibroblasts that populate the entire fibrotic septa (dashed green line) (merge shown in inset), representative of cirrhosis of alcoholic (n=3), NASH (n=1) or hepatitis C (n=1) origins (Scale bars=50 μm). Means ± SEM; **p*<0.05; ***p*<0.01; *****p*<0.0001 (One-way ANOVA in A, Wilcoxon test in C and D).

Fig. 5. Expression of *SLIT2*, PMSC/PMSC-MF and HSC/PMSC-MF oligogene signatures in liver fibrosis. Hepatic expression of *SLIT2*, *ACTA2*, *COL1A1*, *vWF*, PMSC/PMSC-MF or HSC/HSC-MF oligogene signatures assessed by (A,B) RT-qPCR,

A) in liver tissue from mice fed normal chow diet (NCD, n=12) or DDC (n= 8) for 4 weeks (upper panels), or fed CSAA (n=5) or CDAA (n=17) for 8 weeks (lower panels), B) in liver biopsy from patients with NAFLD, at stages of fibrosis F0 (n=26), F1 (n=15), F2 (n=12), F3-F4 (n=7). (C) by Affymetrix microarray analysis of normal human liver (n=5 patients) and of liver tissue samples from patients with NASH (n=7 patients), PSC (n=6 patients, 2 biopsies/patient) or other liver diseases (n=8 patients) (left panel); (D) PMSC/PMSC-MF and (E) HSC/HSC-MF oligogene signatures assessed by Affymetrix microarray analysis of human liver tissue samples as in C. Correlations between *SLIT2* or PMSC 7-gene signature and *ACTA2*, *COL1A1*, or *vWF* expression are shown in C and D right panels. Individual values and means ± SEM are shown; **p*<0.05; ***p*<0.01; ****p*<0.001; *****p*<0.0001; ns, non-significant (Wilcoxon test in A, C-E; one-way ANOVA in B); r values are Pearson correlation coefficients.

Figure 1

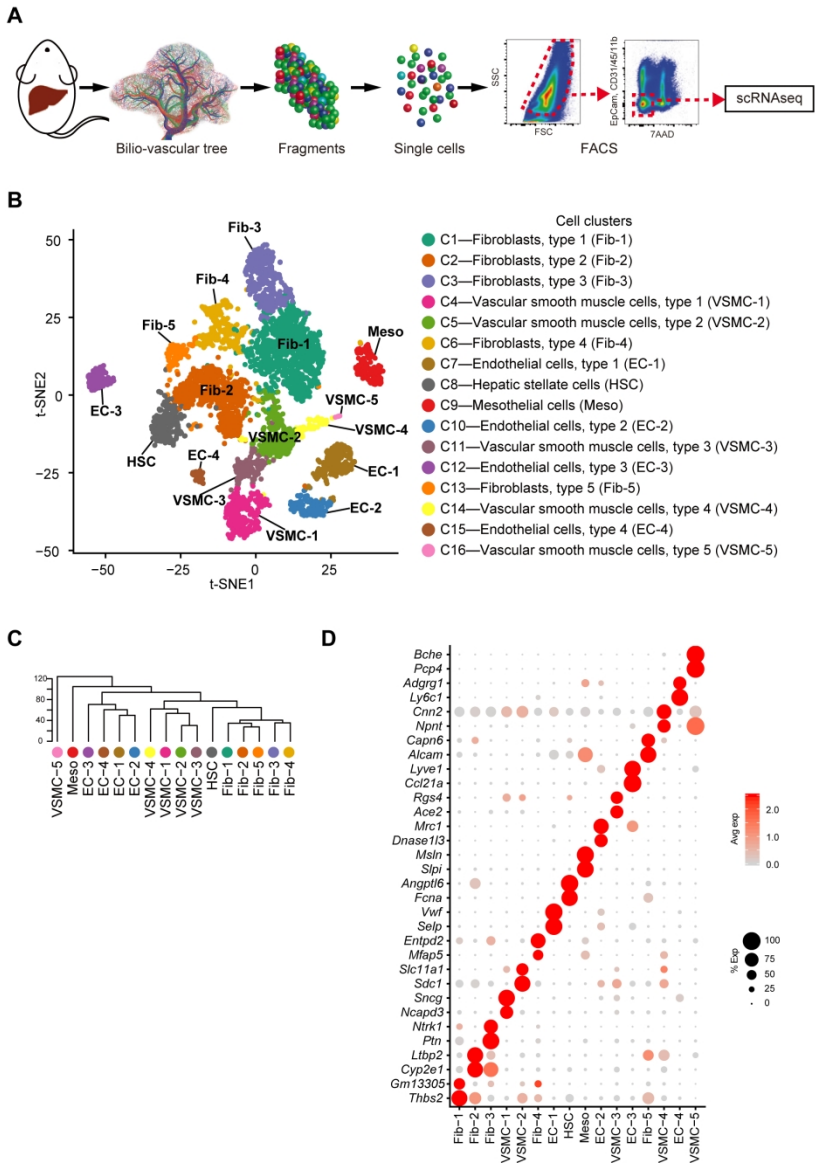

183x270mm (300 x 300 DPI)

Figure 2

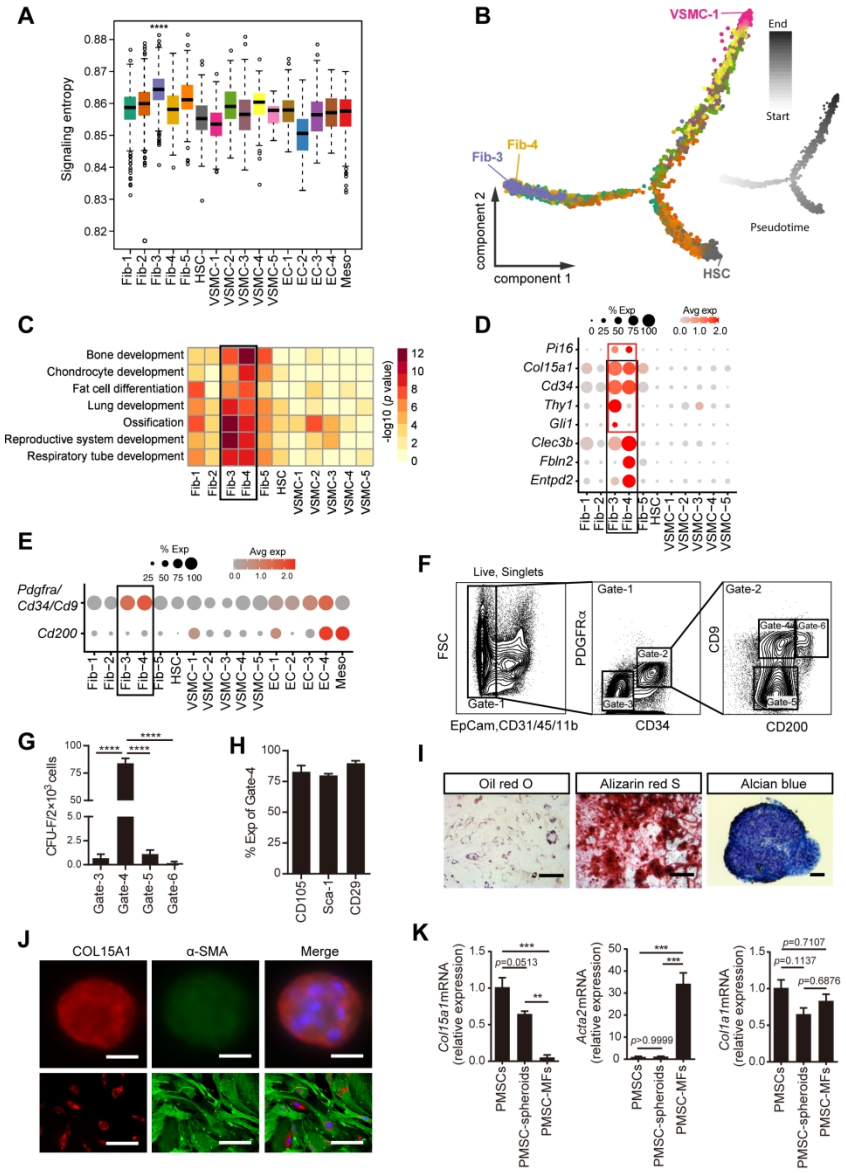

175x250mm (300 x 300 DPI)

Figure 3

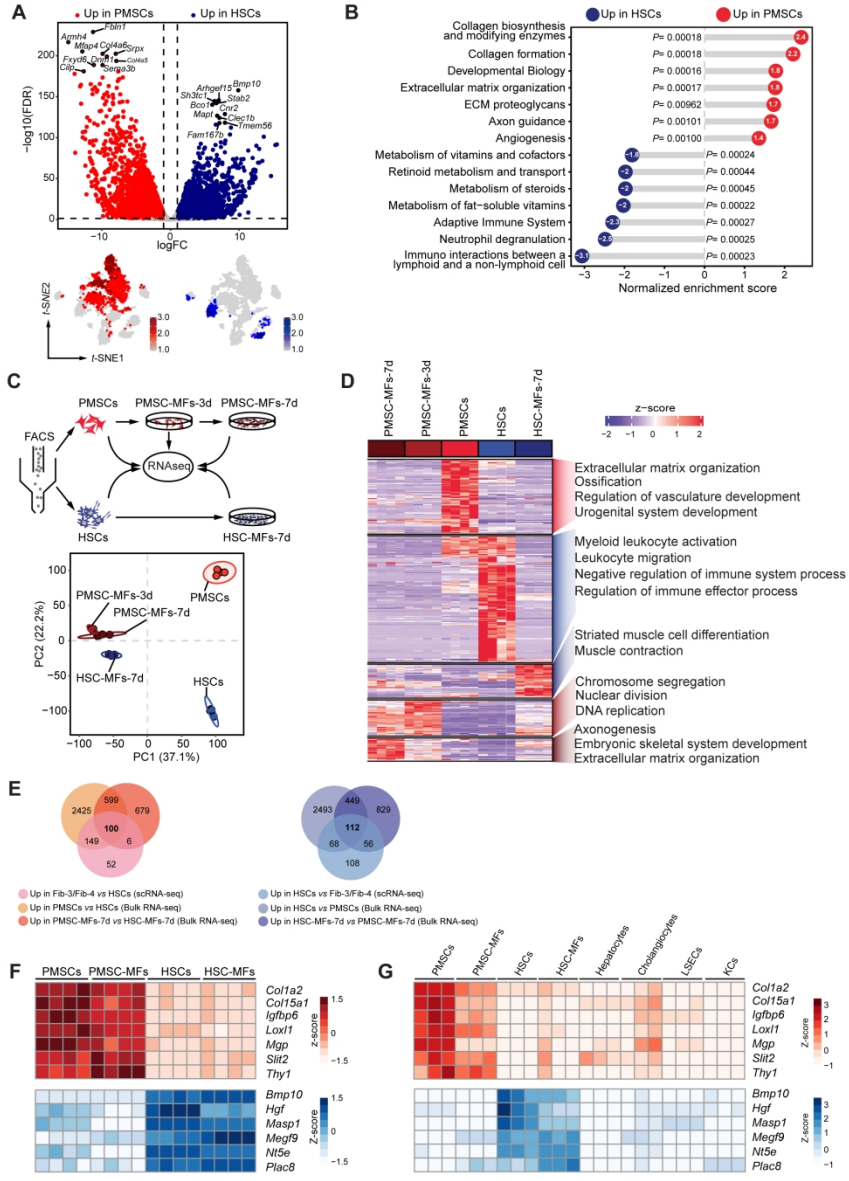

204x291mm (300 x 300 DPI)

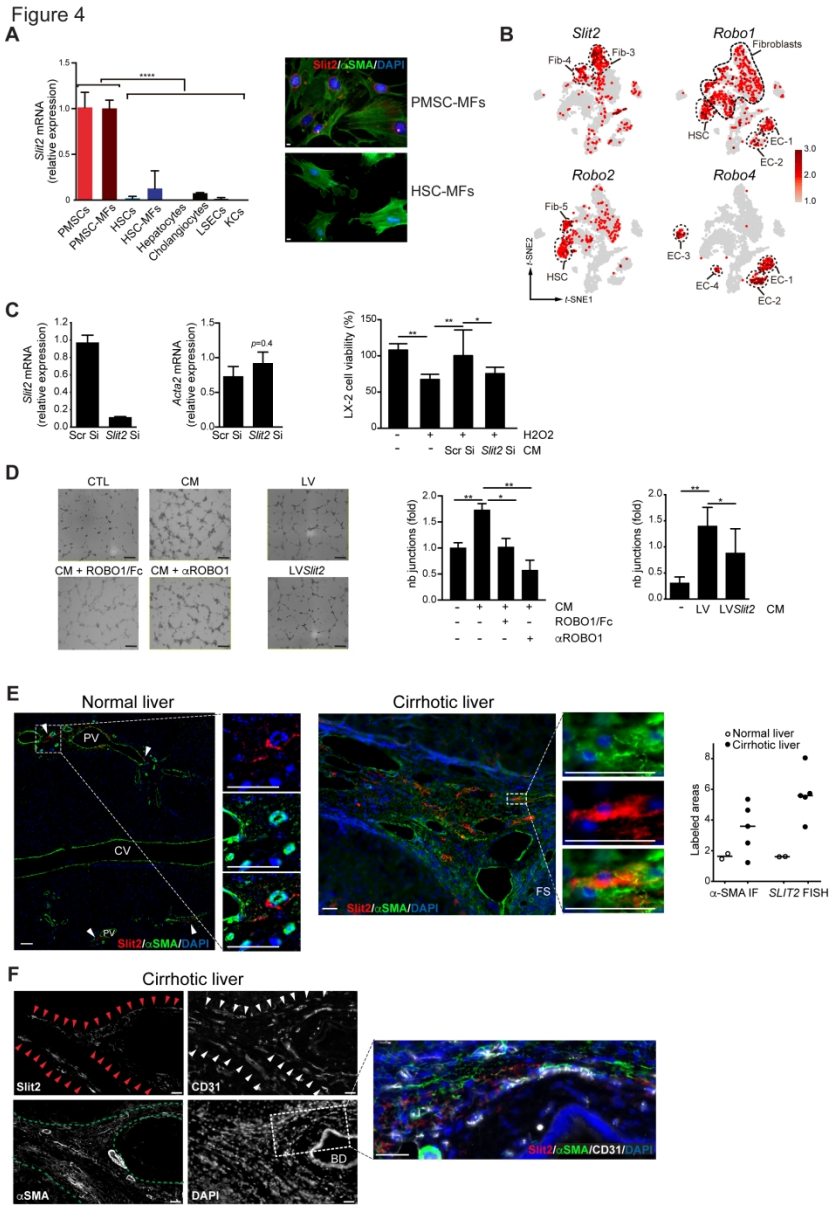

200x292mm (300 x 300 DPI)

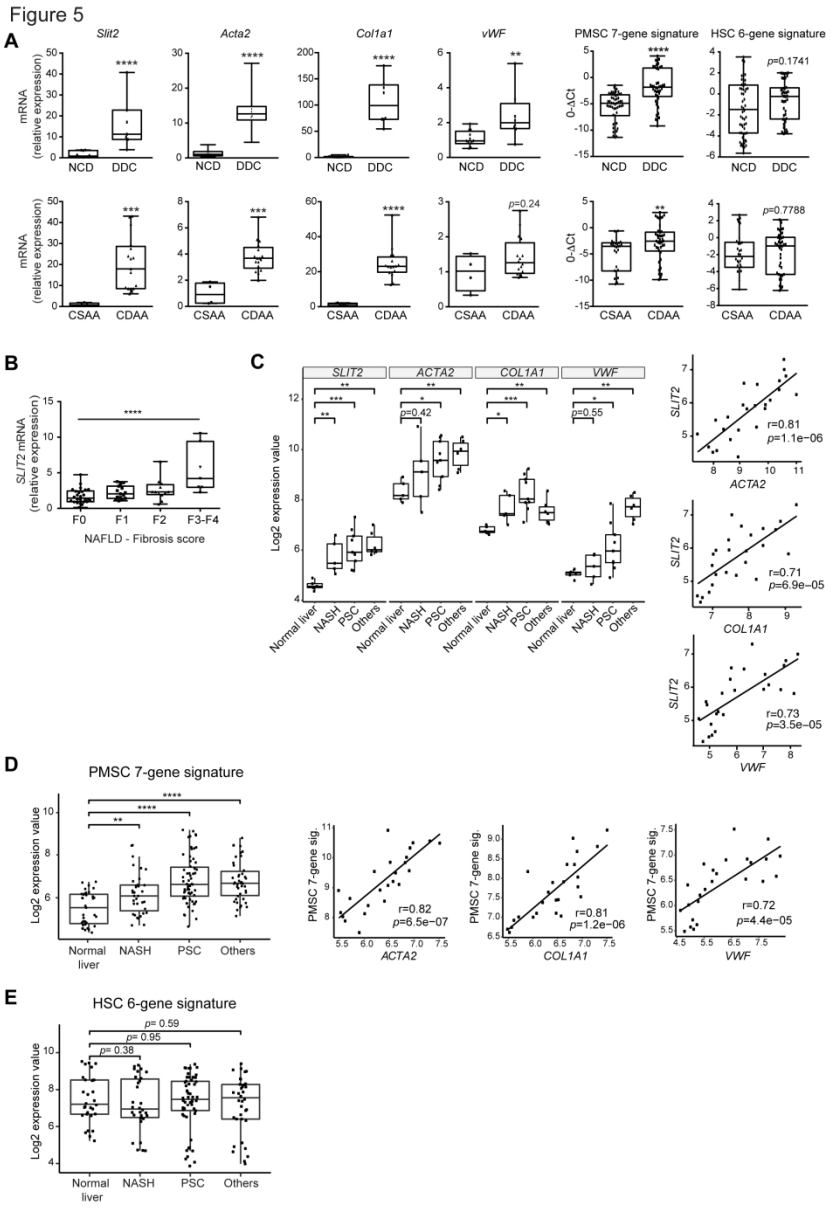

199x290mm (300 x 300 DPI)

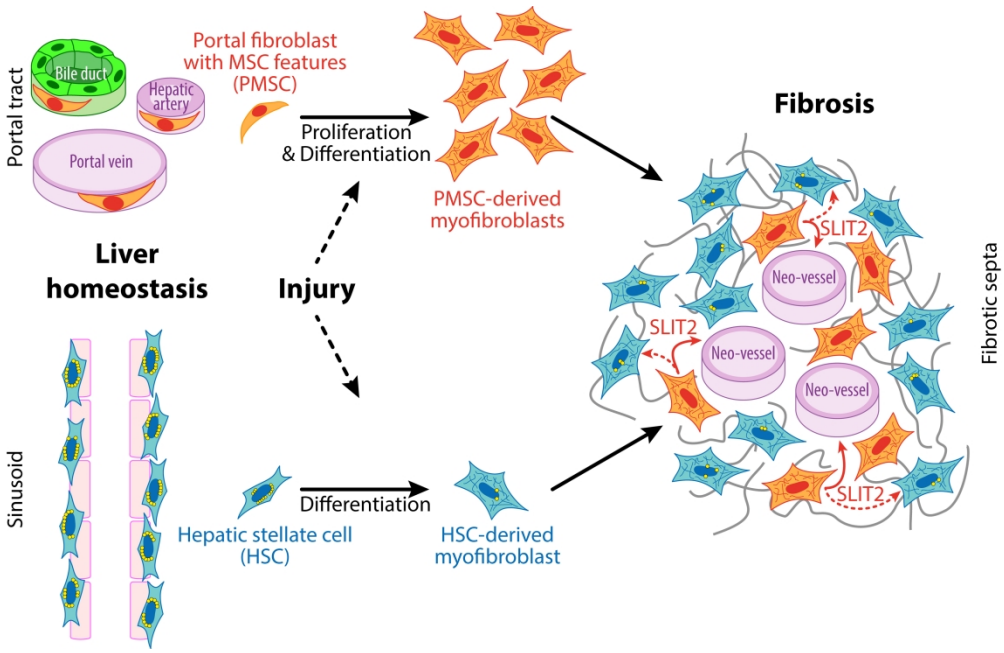

291x187mm (300 x 300 DPI)

Portal fibroblasts with mesenchymal stem cell features form a reservoir of proliferative myofibroblasts in liver fibrosis

Lin Lei, Alix Bruneau, Haquima El Mourabit, Justine Guégan, Trine Folseraas, Sara Lemoinne, Tom Hemming Karlsen, Bénédicte Hoareau, Romain Morichon, Ester Gonzalez-Sanchez, Claire Goumard, Vlad Ratziu, Pierre Charbord, Jérémie Gautheron, Frank Tacke, Thierry Jaffredo, Axelle Cadoret*, Chantal Housset* (*co-senior authorship).

Table of contents

Supplementary Experimental procedures

Animal experiments.

Animal experiments were conducted in the CRSA animal facility (DDPP agreement No. C 75-12-01) and were approved under Nos. 2018060418401070v2, 2018102211507258, 2019090307246392v3 and 2018072719352187v1 by the Ethics Committee of Animal Experiments, Charles Darwin No. 5, Paris. Animals, all males, were housed in a temperature-controlled, specific pathogen-free environment, on a 12-hour light-dark cycle, with free access to chow and water. *Abcb4*$^{-/-}$ mice and their wildtype *Abcb4*$^{+/+}$ littermates were bred, using *Abcb4*$^{+/-}$ heterozygous mice on an FVB/N genetic background (FVB.129P2-Abcb4tm1Bor/J) provided by Sanofi R&D (Chilly-Mazarin, France). Liver fibrosis was also induced in C57BL/6J male mice, by 3 methods: 1) 10-week-old mice were fed a diet containing 0.1% DDC (Sigma, 137030) or a normal control diet (NCD), for 4 weeks; 2) 8-week-old mice were fed a CDAA or CSAA diet (Ssniff spezialdiäten GmbH, Soest, Germany), for 8 weeks; 3) 8-week-old mice received i.p. injections of CCl4 (1 μL/g body weight) diluted at 50% (V/V) in mineral oil or mineral oil (vehicle), twice a week for 6 weeks.

Cell isolation.

Cell collection from the bilio-vascular tree. *In situ* retrograde perfusion of the liver was performed through the inferior vena cava with Ca^{2+},Mg^{2+}-free HBSS (Gibco, 14170-088)/1% EDTA (Sigma, 03690) for 5 minutes at 37°C, and then with HBSS containing Ca^{2+},Mg^{2+} (Gibco, 24020117)/0.15 mg/mL collagenase P (Sigma, 11213873001) for 20 minutes at 37°C. Next, the liver was collected and placed in L15 Leibovitz medium (Sigma, L5520) at 4°C. The liver parenchyma was mechanically detached and discarded. The remaining bilio-vascular tree was minced and incubated in MEM (Gibco, 21090-022) containing 0.075 mg/mL collagenase P, 0.02 mg/mL DNAse (Sigma, DN25), 3% FBS (FBS; Gibco, 10270-098), 1 mg/mL BSA (Sigma, A7030), 1% Hepes (Gibco, 15630) and 1% Penicillin-Streptomycin (Gibco, 15140-122), under agitation for 15 minutes at 37°C. The bilio-vascular fragments were collected on top of a 40-μm cell strainer and centrifuged at 1,500 rpm, for 5 minutes at 4°C. The cell pellet was resuspended in 0.05% Trypsin-EDTA (Invitrogen, 25300-054) with 0.02 mg/mL DNAse and incubated under agitation for 15 minutes at 37°C, and the dissociated cells were filtered three times through a 20-μm cell strainer. Following red blood cell lysis with ACK lysis buffer, the cell suspension was centrifuged at 1,500 rpm, for 5 minutes at 4°C, and the cell pellet was resuspended in a FACS buffer composed of PBS with 2% FBS, 1% Hepes and 1% Penicillin-Streptomycin, at a concentration of 1×10^7 cells/mL for cell sorting. For cholangiocyte isolation, cells were incubated with an anti-Epcam-FITC antibody (BioLegend, Clone: G8.8) for 30 minutes at 4°C and cells were sorted using a FACSAria II cell sorter (BD Biosciences).

Hepatocyte, Kupffer cell, LSEC and HSC collection. Hepatocytes, LSECs and Kupffer cells were isolated as previously described (1), with modifications. For

hepatocyte isolation, the liver was perfused *in situ* with HBSS containing 0.15 mg/mL collagenase P for 20 minutes at 37°C. The cell suspension was filtered through a 70-µm strainer and centrifuged twice at 400 rpm, for 5 minutes at 4°C, to eliminate non-parenchymal cells. LSEC and Kupffer cell isolation was performed by *ex situ* dissociation of the liver using a gentleMACs dissociator (Miltenyi) and magnetic selection using CD146 microbeads (Miltenyi, 130-092-007) and anti-F4/80 microbeads (Miltenyi, 130-110-443), respectively. For HSC isolation, the liver was perfused *in situ*, with HBSS containing 0.4 mg/mL pronase (Sigma, 10165921001) for 5 minutes at 37°C, and then with 0.05 mg/mL collagenase P for 15 min at 37°C. The liver was collected, minced and further digested in HBSS containing 0.044 mg/mL collagenase P, 0.5 mg/mL pronase and 0.02 mg/mL DNAse, under agitation for 15 minutes at 37°C. The resulting cell suspension was submitted to density gradient-centrifugation at 1,380 g for 17 minutes, in GBSS (Gibco)/Histodenz (Sigma, D2158) at 4°C. HSCs were collected from the interface and resuspended in FACS buffer for further purification by cell sorting based on retinoid autofluorescence, as previously described (2).

Cell sorting and flow cytometry analysis

Cells isolated from the bilio-vascular tree were incubated with 1% anti-mouse CD16/CD32 antibody (BD Pharmingen, 553141) for 10 minutes on ice, to block Fc receptors before incubation with anti-Epcam-FITC, anti-CD31-FITC, anti-CD45-FITC and anti-CD11b-FITC antibodies, all at concentrations of 1:100, for 30 minutes at 4°C. Dead cells were stained with 7-aminoactinomycin D (7-AAD; BD Biosciences, 559925) immediately before cell sorting was performed, using a FACSAria II cell sorter (BD Biosciences). Lin-negative cells, gated as $Epcam^{-}CD31^{-}CD45^{-}CD11b^{-}$ cells, were collected and subjected to scRNAseq analysis. To isolate PMSCs from the bilio-vascular tree, cells were labeled with anti-Epcam-, anti-CD31-, anti-CD45- and anti-CD11b-FITC antibodies as above, and anti-PDGFRα-PE, anti-CD34-APC, anti-CD9-BV421 and anti-CD200-APC-R700, all at concentrations of 1:100 except for anti-PDGFRα-PE (1:50). PMSCs were gated as $Lin^{-}PDGFR\alpha^{+}CD34^{+}CD9^{+}CD200^{low}$ cells. To sort $Thy1^{-}$, $Thy1^{low}$ and $Thy1^{high}$ PMSCs, cells from the bilio-vascular tree were labeled with anti-Epcam-FITC, anti-CD31-FITC, anti-CD45-FITC, anti-CD11b-FITC, anti-PDGFRα-PE, anti-CD34-APC, anti-CD9-BV421, anti-CD200-APC-R700 antibodies as above, and anti-Thy1-PE-Cy7 antibody at a concentration of 1:100. For flow cytometry analysis, freshly isolated PMSCs were labeled either with anti-CD105-BV510, anti-Sca1-BV510 or anti-CD29-PE/Cy7, all at concentrations of 1:100. Analyses were performed using BD FACSDiva™ and FlowJo (Tree Star) software. All antibodies are listed in Table S1.

Cell culture.

PMSCs and HSCs were seeded in 6-well plates at a density of 20,000 cells/cm^2 and cultured in DMEM containing 20% FBS, 1% Hepes and 1% Penicillin-Streptomycin to obtain PMSC-MFs and HSC-MFs, respectively. To maintain PMSCs in a resting state, cells were seeded in 96-well ultra-low attachment

(ULA) round-bottomed plates. The LX-2 human HSC cell line (provided by Human HepCell, IHU-ICAN) was cultured in DMEM containing 10% FBS, 1% Hepes and 1% Penicillin-Streptomycin. HUVECs were grown in EndoGRO™-VEGF complete medium (Millipore).

Cell clonogenicity and differentiation assays.

Cell clonogenicity was examined by CFU-F assay, as follows: 2,000 sorted cells were plated onto a 10-cm plastic dish and maintained in DMEM/20% FBS. The presence of more than 50 cells in a cluster after 14 days in culture, was counted as a colony. The capacity of PMSCs to differentiate towards adipogenic, osteogenic or chondrogenic lineages was analyzed using specific protocols. For adipogenic and osteogenic differentiation, sorted PMSCs were plated in 48-well plates coated with matrigel (Corning, 356231) at a density of 5,000 cells/cm^2 in DMEM/20% FBS until subconfluence. Then, the culture medium was changed for adipogenic (R&D Systems, CCM011) or osteogenic (R&D Systems**,** CCM009**)** differentiation medium. After 21 days, cells were fixed with 4% paraformaldehyde and stained using Oil Red O (Sigma) or Alizarin Red solution (Sigma), respectively. For chondrogenic differentiation, 50,000 sorted PMSCs were plated in ULA plate in chondrogenic differentiation medium (R&D Systems, CCM006) to form spheroids. After 21 days, the spheroids were fixed in 4% paraformaldehyde, embedded in OCT (Sakura Finetek) and cryosections (8 µm) were stained with Alcian blue (Santa Cruz Biotechnology) and counterstained with nuclear fast red (Vector).

Videomicroscopy.

PMSCs and HSCs were seeded in 24-well plates at densities of 5,000 and 50,000 per well, respectively, and cultured in standard conditions. Twenty-four hours after seeding, the cells were placed in the CellVivo Incubation System (Pecon GmbH, Ernah, Germany) driven by a high-end inverted microscope IX83 (Olympus Corporation, Tokyo, Japan). One picture has been taken every hour, using a 10X UPLFN 0.3NA PH1objective lens and ORCA-Flash 4 LT digital (Hamamastu Photonics KK, Tokyo, Japan) driven by Cellsens dimension 1.16 (Olympus). The movies have been built using the open source software Fiji (3).

ScRNAseq.

Cells were loaded onto a GemCode instrument (10x Genomics) to generate single-cell barcoded droplets, *i.e.*, gel beads in emulsion (GEMs). Sequencing libraries were constructed using the Chromium Single-cell 3' Library Kit (10x Genomics) according to the manufacturer's protocol and sequenced on a NextSeq 500 device (Illumina). Average read depth of the sample was 79,199 reads/cell. Reads were then aligned to the mouse genome mm10/Grcm38 using the CellRanger 3.0.2 software. Subsequent analysis was performed in R using the filtered barcode and count matrices produced by CellRanger. The data were analyzed using Seurat 3.6.1 (4). Genes expressed in less than 6 cells, as well as cells with less than 500 or more than 25,000 unique molecular identifiers (UMIs), were filtered out. Any single-cell with more than 10% UMIs

mapped to mitochondrial genes was also removed. Seurat SCTransform function (5) was used to normalize and scale the data (**https://www.ncbi.nlm.nih.gov/geo/query/acc.cgi?&acc=GSE163777**). Dimensionality reduction was performed through PCA on the gene expression matrix and using the first 30 PCs for clustering and visualization. Unsupervised shared nearest neighbor clustering was performed using Seurat FindClusters function at the resolution of 0.6 and visualization was achieved using spectral *t*-SNE of the principal components as implemented in Seurat. Cluster dendrogram was constructed using BuildClustertree built-in function of the R package Seurat which used cluster averaged PCs for calculating a PC distance matrix. The cell clusters identified were evaluated for differential genes expression (DGE), using Seurat FindAllMarkers function. All genes considered for cell-type classification were determined with p value < 0.01 and log (fold-change) > 0.25 as cutoff by performing DGE analysis between the clusters using Wilcoxon rank sum test and Benjamini and Hochberg procedure for p-values adjustment. Single-cell entropy was calculated using LandSCENT v. 0.99.3, as previously described. Doublet analysis was performed, using two methods, *i.e.*, DoubletFinder, R package v 2.0 and Scrublet, python library v0.1. Thereby, we identified 334 and 103 potential doublets, respectively. They included 66 doublets in common, that were plotted on *t*-SNE projection (Fig. S1B). The Monocle version 2.14.0 R package (6) was used to organize cells in pseudotime and infer cell trajectories from the Seurat dataset. We ran reduceDimension with *t*-SNE as the reduction method, num_dim=12, norm_method="log" and max_components = 2. Cells were clustered with the density peak clustering algorithm by setting P to 2 and Δ to 4 (and skip_rho_sigma = T to facilitate the computation). The top 1000 significantly differentially expressed genes between clusters were selected as the ordering genes and used in Monocle for clustering and ordering cells using the DDRTree method and reverse graph embedding.

Bulk RNAseq.

RNA was extracted using Rneasy Micro Kit (Qiagen). Libraries were generated from total RNA and paired-end sequencing was performed on a NextSeq 500 device (Illumina). Raw sequencing data were quality-controlled with the FastQC program. Paired reads were aligned to the mouse reference genome (mm10 build) with the STAR software v2.5.3a (option for no multihits). Mapping results were quality-checked using RNASeQC. Gene counts were obtained by using RSEM tools v1.2.28 (rsem-calculate-expression, option for paired-end and stranded). Expected gene counts were first normalized using TMM method in the edgeR R package and genes with a count per million (CPM) < 1 in 20% of samples, were removed (**https://www.ncbi.nlm.nih.gov/geo/query/acc.cgi?acc=GSE164037**).

Differential gene expression analysis was performed using DEseq2. A $\log_2$ of fold change of 1 and a Benjamini-Hochberg adjusted p value cutoff < 0.05 (FDR) was set to determine significant differentially expressed genes.

GO enrichment and Gene Set Enrichment Analysis.

Symbol gene IDs were first converted to Entrez gene IDs using the clusterProfiler R package (7). Functional enrichment in GO biological processes of differentially expressed genes was performed using EnrichGO built-in function of the clusterProfiler version 3.14 with default parameters. The comparison of enriched functional enrichment among mesenchymal cell populations was performed using clusterProfiler CompareCluster function (7). Heatmap of enriched term was generated in R. GSEA was implemented using the R package ReactomePA with default parameters (8).

Import of previously published data sets.

We downloaded the raw scRNAseq data of i) 23,291 Pdgfrb-GFP+ mesenchymal cells from uninjured and fibrotic (6 weeks CCl4) mouse livers published and deposited in the GEO by Dobie *et al.* (GSE137720), ii) 47,752 liver cells of all types from uninjured oil-treated (10,636) and fibrotic (CCl4 3 weeks, 18,185; BDL 10 days, 18,931) mouse livers published and deposited in the GEO by Yang *et al.* (GSE171904).

Slit2 silencing by siRNA and LX-2 survival.

Slit2 and scramble siRNA (SMARTpool: ON-TARGETplus Slit2 siRNA L-058235-00-0005, ON-TARGETplus Non-targeting Pool D-001810-10-05) were purchased from Dharmacon. PMSC-MFs at passage 1 in 6-well plates were transfected with siRNA (50 nmol/L) using Dharmafect1. Forty-eight hours after transfection, the cells were incubated with serum-free DMEM for 24 hours to generate conditioned medium. LX-2 cells were seeded in 96-well plates (7,000/well) and 24 hours later, were incubated in serum-free DMEM containing H2O2 (200 µmol/L) for 30 min. Thereafter, the medium was replaced by serum-free DMEM or conditioned medium from transfected PMSC-MFs and 24 hours later, cell viability was assessed using MMT assay. Absorbance was quantified at 540 nm (TECAN).

Slit2 deletion by CRISPR/Cas9.

The lentiviral plasmid plentiCRISPRv2, a gift from Zhang lab (Addgene, MA, USA; plasmid #52961), contains hSpCas9, a guide RNA (gRNA), and a puromycin resistance sequence. The gRNA targeting exon 1 of *Slit2* was designed using http://cistrome.org/SSC, that ensures specificity and high cleavage efficiency.

Its sequence was sense, 5' CTTGAACAAGGTGGCGCCGC 3', antisense, 5' GCGGCGCCACCTTGTTCAAG 3'. The web-based tool, CRISPOR (http://crispor.tefor.net) that predicts the risk of off-target sequences by providing a cutting frequency determination (CFD) specificity score ranging from 1 to 100, was used to avoid off-target sequences. Guides with a CFD specificity score > 50 are recommended by Doench JG et al. (9). The gRNA we used to target *Slit2* exon 1 has a CFD score of 98. This gRNA did not perfectly match any other genomic region. One off-target with three mismatches was found in an intronic region of *Mapk4* and 40 off-targets were found with four

mismatches, making unlikely that these off-targets were involved in the effect caused by *Slit2* ablation. Lentiviruses dedicated to *Slit2* knockout (LV*Slit2*) and a control lentivirus (LV) expressing Cas9 and a scramble gRNA were produced by the VVTG platform (Federative Research Institute, Necker, France). Sub-confluent PMSC-MFs at day 7 of primary culture, were infected with viral particles at a minimal titer of 10^8 units per mL. Forty-eight hours post-infection, the culture medium was discarded and conditioned medium was prepared by incubating the cells with serum-free medium for 24 hours.

Tube assay.

HUVECs (15,000 cells/well) were plated in 15-well µ-slide angiogenesis Ibidi plates (Clinisciences) previously coated with 50 µl of growth factor-reduced Matrigel (BD Biosciences) and incubated in the presence of PMSC-MF conditioned medium (harvested from cells incubated with serum-free medium for 24 hours) or serum-free medium as a control. To assess the contribution of SLIT2 secreted by PMSC-MFs in angiogenesis, HUVECs were incubated with PMSC-MF conditioned medium a) in the presence of 100 ng/mL of recombinant rat ROBO1/Fc chimera protein (R&D Systems, #1749B) (10), b) after they had been preincubated for 1 hour with 10 µg/mL of anti-human ROBO1 antibody (R&D Systems, #AF7118), or c) with the conditioned medium from PMSC-MFs infected with a lentivirus expressing Cas9 and a gRNA targeting the first exon of *Slit2*, dedicated to *Slit2* knockout (LV*Slit2*) or a control lentivirus (LV) expressing Cas9 and a scramble gRNA. HUVECs were placed in the CellVivo Incubation System as for videomicroscopy (described above) and tube formation was evaluated after 6 hours of incubation using the Angiogenesis Analyzer tool (Fiji software).

Human liver tissue samples.

Samples of normal liver from patients undergoing liver resections for focal lesions (n=2 patients), and of cirrhotic livers from patients with NASH (n=1), chronic hepatitis C (n=1) or alcoholic liver disease (n=3) undergoing liver resection or transplantation, were provided by Human HepCell platform (IHU-ICAN, Declaration No. AC-2020-3861) for FISH. Frozen samples of liver biopsy from subjects with a suspicion of non-alcoholic fatty liver disease at stages of fibrosis F0 (n=26), F1 (n=15), F2 (n=12), F3-F4 (n=7), were provided by the Biological Resource Center, BIO-ICAN, Paris, France, with ethical approval from the Persons Protection Committee (CPP Ile de France VI) for RT-qPCR analyses. The RNA used for microarray experiments was extracted from frozen tissue obtained from explanted livers or diagnostic liver biopsies from i) normal human liver tissue (tumor-free tissue from livers with colorectal cancer metastasis) (n=5 patients) and ii) liver tissue from patients with chronic liver diseases, including PSC (n=6 patients, 2 biopsies/patient), NASH (n=7 patients) and other liver diseases including autoimmune hepatitis (n=3), primary biliary cholangitis (n=2), alcoholic liver disease (n=1), haemochromatosis (n=1) and sarcoidosis (n=1). The liver specimens were provided by the Norwegian biobank for primary sclerosing cholangitis, Oslo, Norway with ethical approval

from the Regional Committee for Medical and Health Research ethics of South East Norway. All subjects gave written informed consent before to allow the use of the samples.

RT-qPCR.

Total RNA was extracted from frozen liver tissue samples or harvested cells using the RNeasy Mini Kit or Micro Kit (Qiagen), respectively. The cDNA was synthesized using the MMLV-RT (Invitrogen, 28025013) or SuperScript™ II (Invitrogen, 18064014) and real-time PCR was performed using the LightCycler 480 SYBR Green I Master Kit on an LC480 device (Roche Diagnostics). Target gene mRNA levels were normalized using HPRT or 18S as a reference gene and expressed as relative levels (2-ΔΔCt method). Normalized values (ΔCt) were used for oligogene signature analysis and presented as 0-ΔCt, so that higher values indicate higher expression levels. The primers (Table S2) were designed using the primer software from Roche Diagnostics.

Immunofluorescence and FISH.

For immunofluorescence, cell preparations were fixed in 4% paraformaldehyde at 4°C for 15 minutes, and incubated with primary antibodies against COL15A1 (Abcam, ab58717, 1:200) or α-SMA (Agilent, M085129-2, 1:100) at 4°C overnight. Nuclear staining was performed using Draq5 (Abcam). Cells were examined with a SP2 confocal microscope (Leica, Bannockburn, IL, USA).

For co-labeling by FISH and immunofluorescence, cell preparations and tissue samples were fixed in 4% paraformaldehyde at 4°C for 20 minutes and 4 hours, respectively. Tissue samples were then transferred to 30% sucrose in PBS at 4°C until sinking and then placed in a plastic mold filled with O.C.T. that was immersed in 2 methyl-butane maintained at -70°C, and stored at -80°C. Tissue sectioning was performed at -25°C and 10-µm cryosections were mounted on SuperFrostPlus™ slides that were kept on dry ice. Before processing, tissue sections were thawed in 100% ethanol for 5 minutes, followed by 1 minute in TBS buffer. Cell preparations or tissue sections were then transferred to pre-warmed hybridization buffer (5X SSC / 1% BSA / 10% Formamid / 0,1% (w/v) SDS) at 75°C for 20 minutes. The probes, directed at *SLIT2* or Scramble (Table S3), conjugated to Fam-6 or Atto-633, respectively, were diluted at 50 ng/µL and denatured at 85°C for 5 minutes while the samples were dried and denatured on a preheated plate at 85°C for 2 minutes. The probes (100µL) were added to tissue sections then covered with a coverslip and sealed with glue. In the following steps the samples were kept in the dark. They were incubated at 75°C overnight in a dark wet chamber. After removal of the coverslip, the slides were transferred to freshly prepared hybridization buffer at 75°C for 15 minutes. The slides were washed with TBS for 5 minutes, and then with TBS-Triton x100 0.3% for 15 minutes, at room temperature. After a 5-minute TBS wash at room temperature, the slides were blocked for 60 minutes with 2% Normal Goat Serum (Thermo Fisher) in TBS-T (0.1%). Tissue sections were incubated with anti-α-SMA (1:100, M085129-2, Agilent) in blocking buffer, overnight at 4°C. Slides were washed with TBS 3 times for 5 minutes at room temperature and

incubated with secondary antibody (Goat anti-mouse IgG Alexa Fluor 555 Conjugate, CellSignaling #4409, 1:500) and DAPI 2µg/mL (Sigma-Aldrich). Large field imaging acquisition was performed on a Zeiss Axio Observer 7. For image processing, the large field images were stitched and background was subtracted, using the default settings of ZEISS software ZEN 3.1 (blue edition). Exported single channel grayscale in .tiff were later processed in Fiji. The background due to FISH staining was assessed using the scramble probe and this autofluorescence was subtracted from the *SLIT2* channel using image calculator module. For quantification, binary masks of at least two independent experiments were generated using the trainable classification software Ilastik (v 1.3.3). Marked areas were then measured using Fiji. The plugin Color pixel counter was used to count the number of pixels on the image of a specific color. Results are expressed as a percentage of pixels in the Region of Interest.

Microarray analyses.

Pangenomic analysis of frozen liver tissue samples, was performed using the Affymetrix human gene 1.0 st microarray. Analysis was conducted using R. *oligo* bioconductor package to import raw data CEL files in an ExpressionSet object and *rma* function to normalize the data. After normalization, summarization was performed because transcripts are represented by multiple probes, on the Affymetrix platform. For each gene, the background-adjusted and normalized intensities of all probes were summarized into one estimated amount proportional to the amount of RNA transcripts. Summarized data have been annotated with hugene10sttranscriptcluster.db bioconductor package (**https://www.ncbi.nlm.nih.gov/geo/query/acc.cgi?acc=GSE159676**).
Statistical analysis was performed using non-parametric Wilcoxon test.

A

	nCounts (transcripts)	nFeatures (genes)	% mitochondrial genes
Mean per cell	10539	2951	3.14 %

B

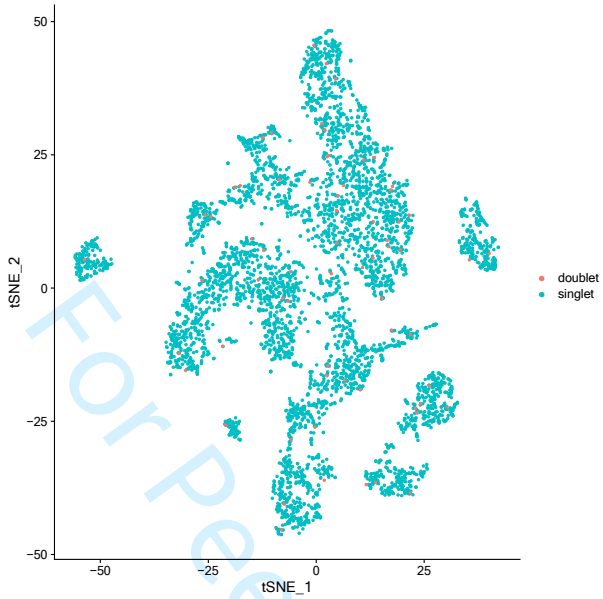

Fig. S1: scRNAseq (A) Quality control metrics; (B) Analysis of doublets (plotted on *t*-SNE).

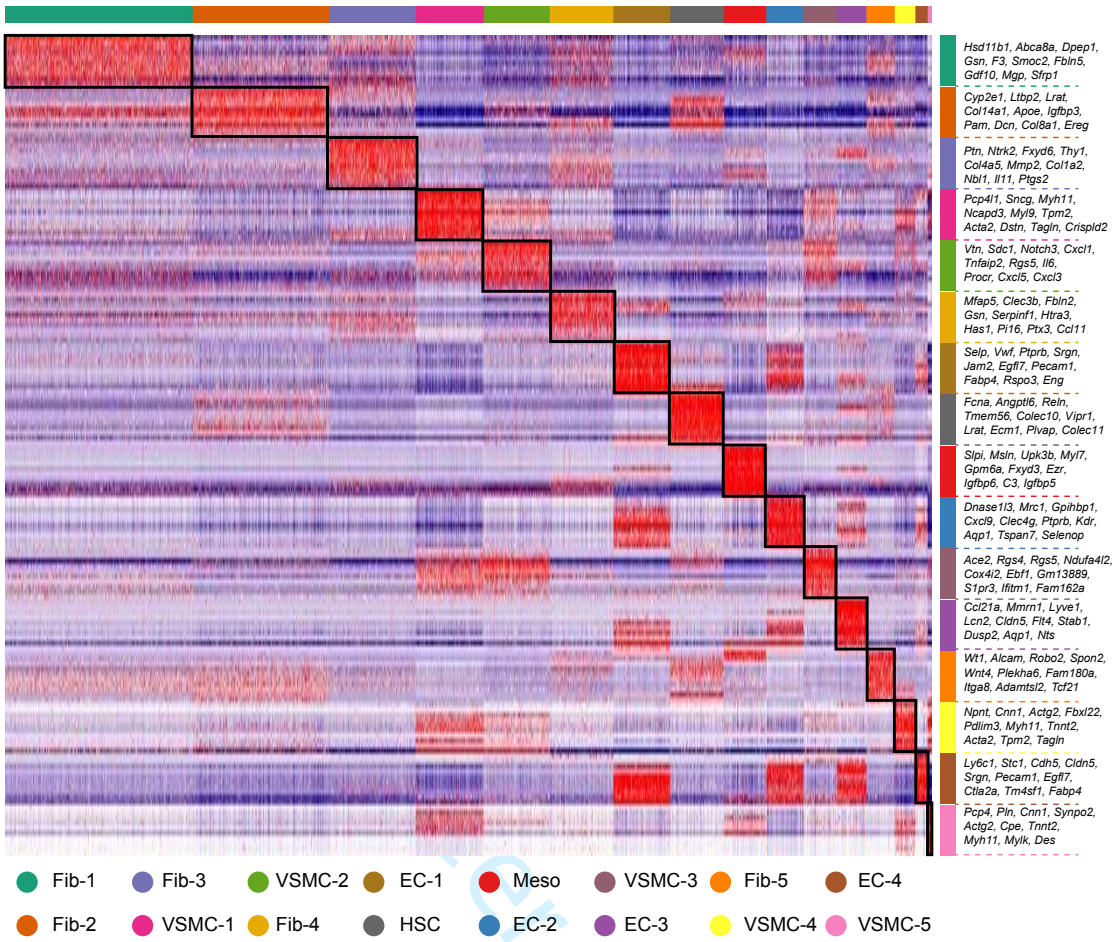

Fig. S2: Heatmap of the top 10 differentially expressed genes in scRNAseq clusters. (see also Table S4).

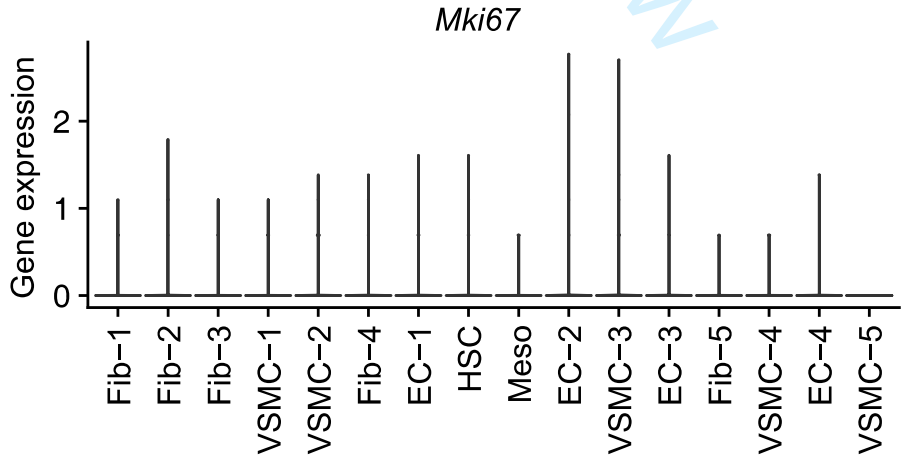

Fig. S3: Violin plots showing the expression of the proliferation marker Mki67 across all scRNAseq clusters.

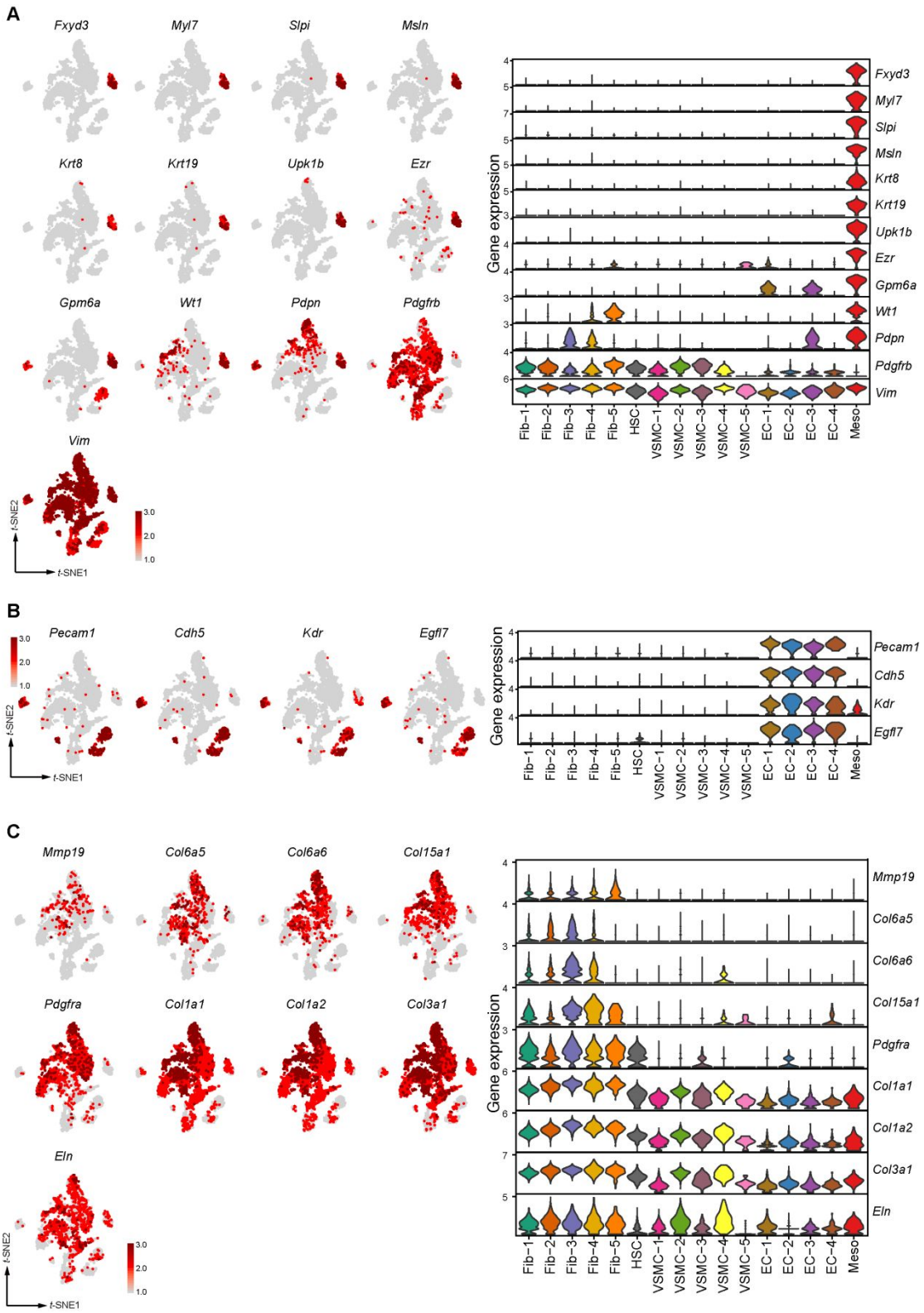
A
Fxyd3
Myl7
Slpi
Msln
Krt8
Krt19
Upk1b
Ezr
Gpm6a
Wt1
Pdpn
Pdgfrb
Vim
t-SNE2
t-SNE1
Gene expression
Fib−1
Fib−2
Fib−3
Fib−4
Fib−5
HSC
VSMC−1
VSMC−2
VSMC−3
VSMC−4
VSMC−5
EC−1
EC−2
EC−3
EC−4
Meso
B
Pecam1
Cdh5
Kdr
Egfl7
C
Mmp19
Col6a5
Col6a6
Col15a1
Pdgfra
Col1a1
Col1a2
Col3a1
Eln

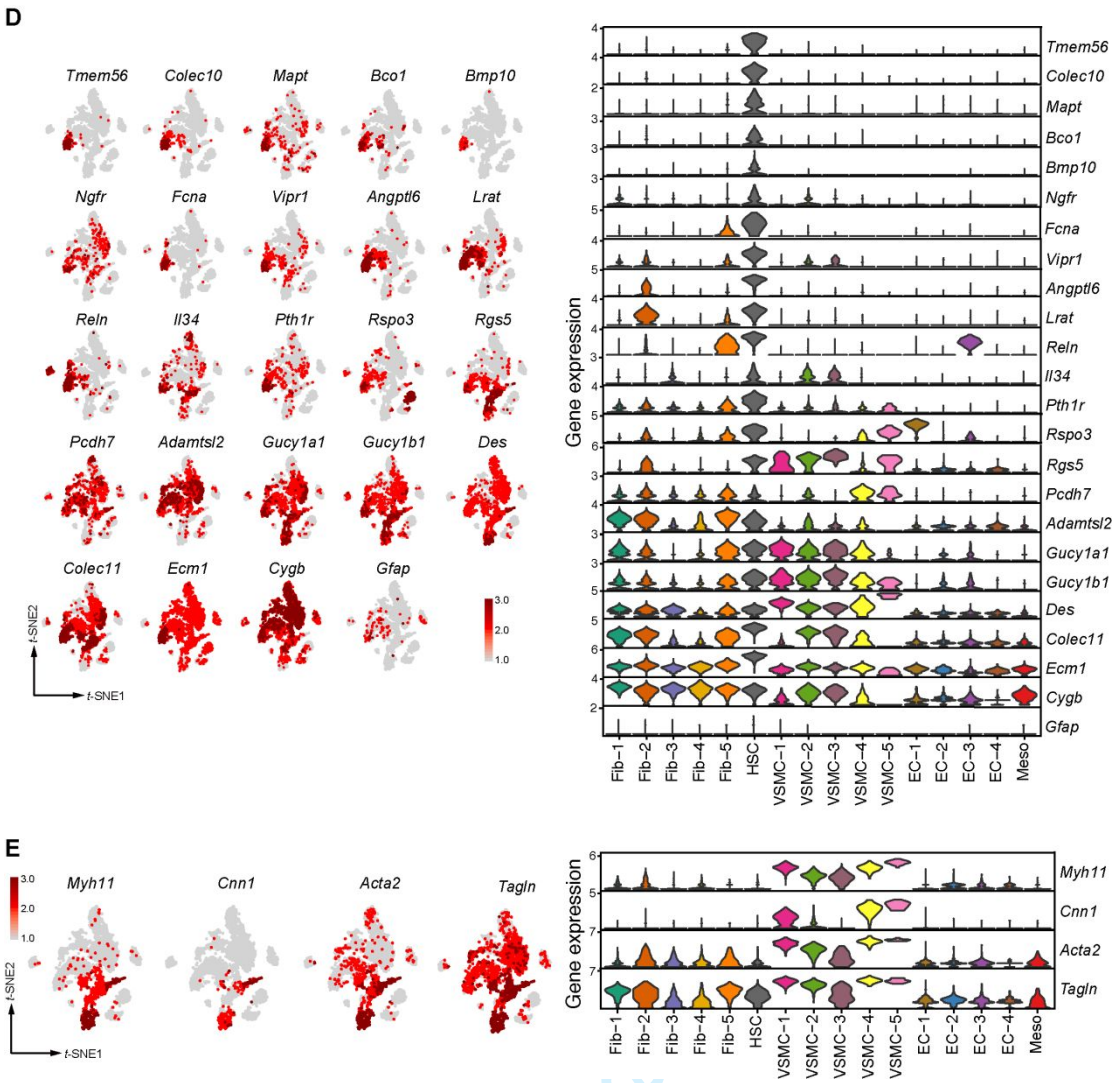

Fig. S4: *t*-SNE and Violin plots across all scRNAseq clusters of gene expressions, that were previously or herein reported to demarcate the following cell types: (A) mesothelial cells (Meso), (B) endothelial cells (EC), (C) fibroblasts (Fib), (D) hepatic stellate cells (HSC), (E) vascular smooth muscle cells (VSMC).

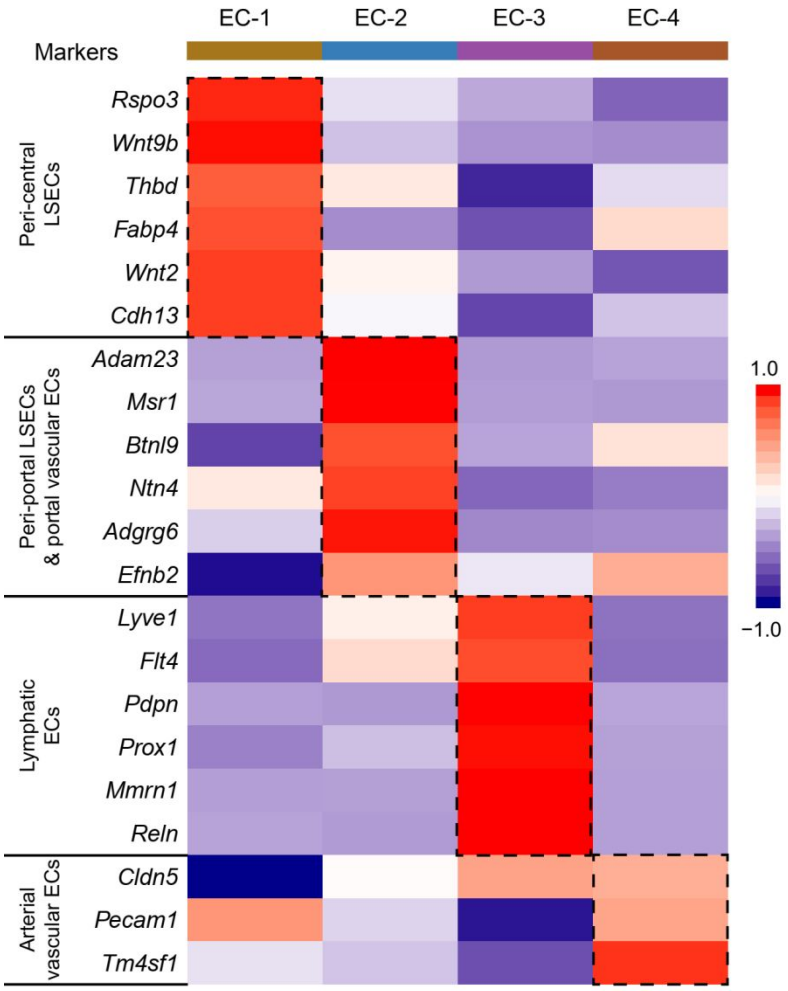

Fig. S5: Heatmap depicting representative genes expressed in the endothelial cell (EC) clusters of the scRNAseq.
Color scale represents the average expression level across all cells within each cluster. LSECs, liver sinusoidal endothelial cells.

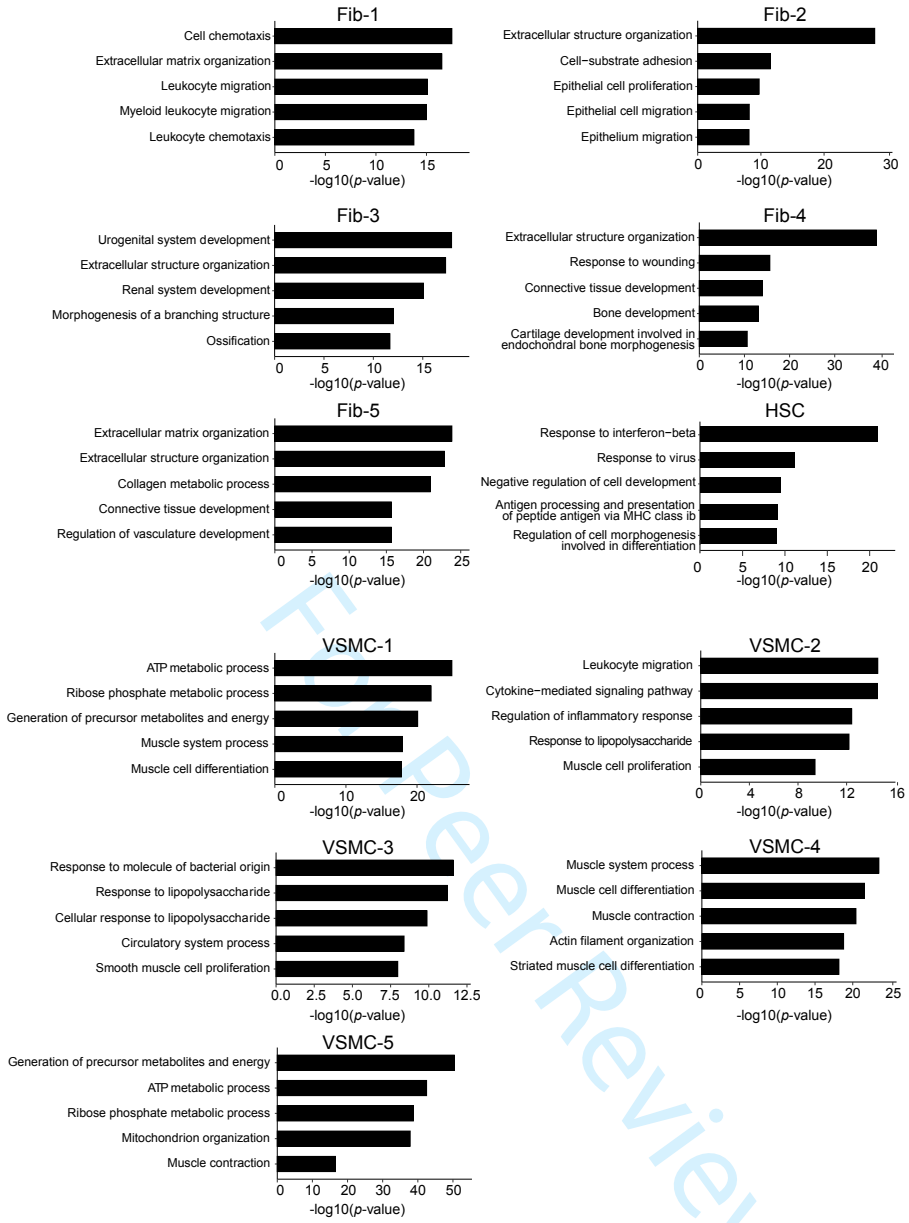

Fig. S6: GO enrichment of genes significantly overexpressed in the different mesenchymal cell clusters of the scRNAseq. (see also Table S5).

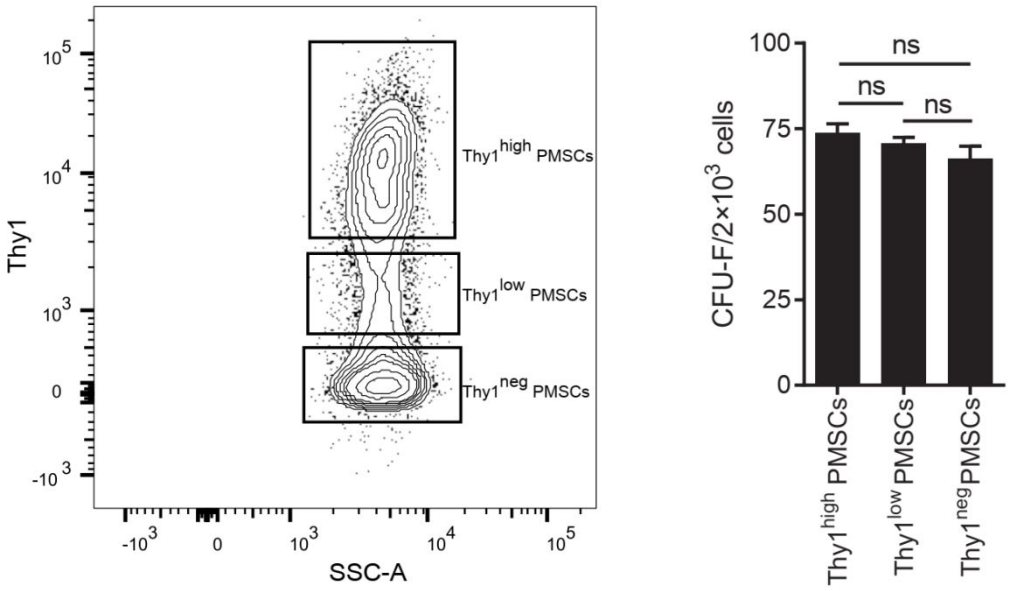

Fig. S7: Clonogenicity of PMSCs according to Thy1 expression.
Left panel: Representative flow cytogram of Thy1 expression on PMSCs. Right panel: CFU-F formed by Thy1^{neg}, Thy1^{low} and Thy1^{high} PMSCs. Data represent means ± SEM (n=3). Statistical significance was evaluated using one-way ANOVA; ns, non-significant.

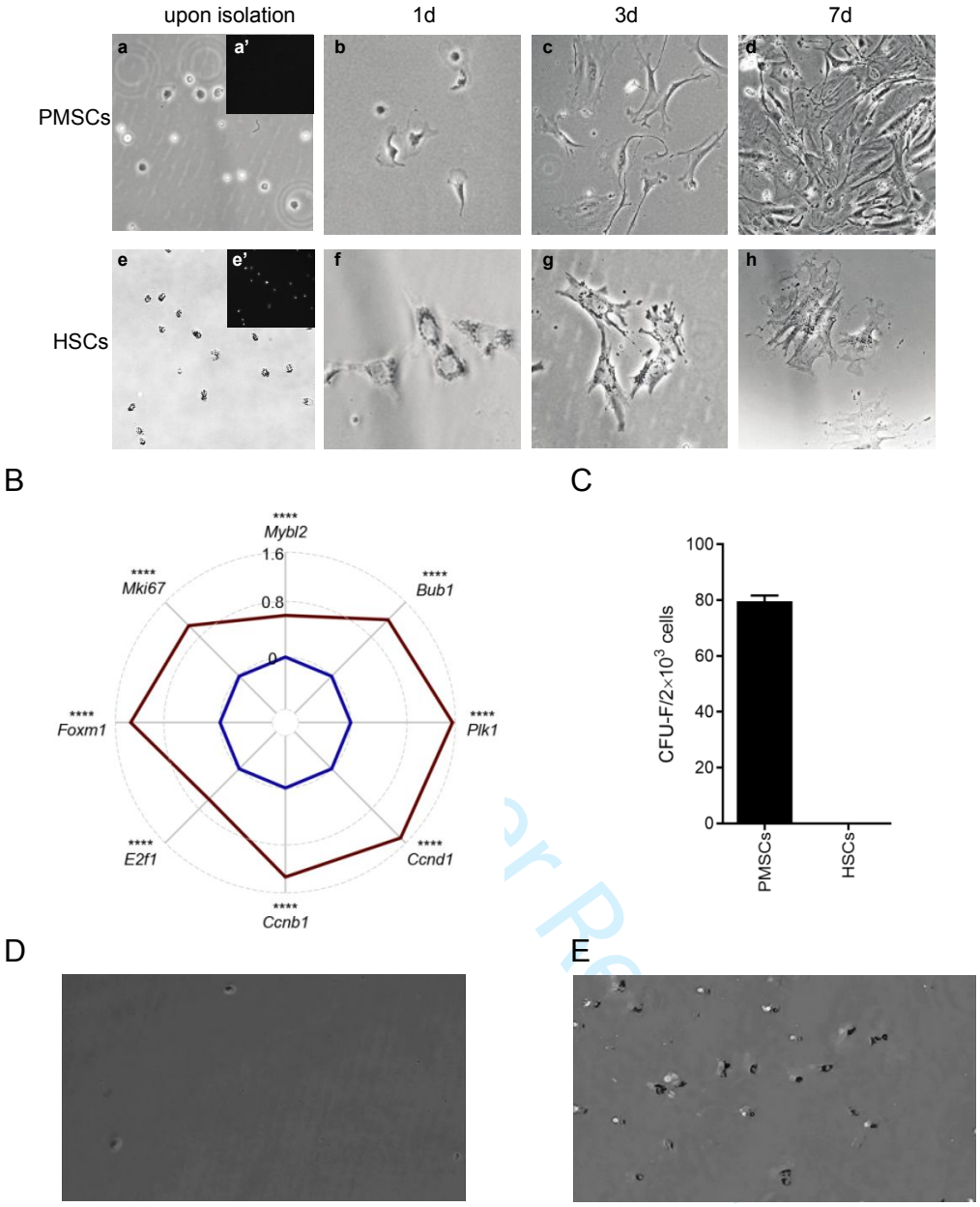

Fig. S8: Phenotypic comparison of PMSCs/PMSC-MFs and HSCs/HSC-MFs.

(A) Microscopic appearance: Cells were observed under phase-contrast microscopy (fluorescence microscopy under 328-nm ultraviolet excitation in insets) (a,e) immediately after cell sorting, (b-d, f-h) at the indicated days (d) of primary culture. (B-E) Proliferative properties: B) Proliferation-related gene expressions in PMSC-MFs *vs.* HSC-MFs. Radar plot showing the log2 fold-difference in the expression of cell proliferation-related genes in bulk RNAseq analysis of PMSC-MFs (red line) and HSC-MFs (blue line) after 7 days in culture. Statistical significance was evaluated using Wilcoxon test; ****p<0.0001; C) CFU-F formed by sorted PMSCs and HSCs (Means ± SEM, n=8); Videomicroscopy (provided separately) of D) PMSCs and E) HSCs between day 1 and day 5 of primary culture (representative of 2 random fields).

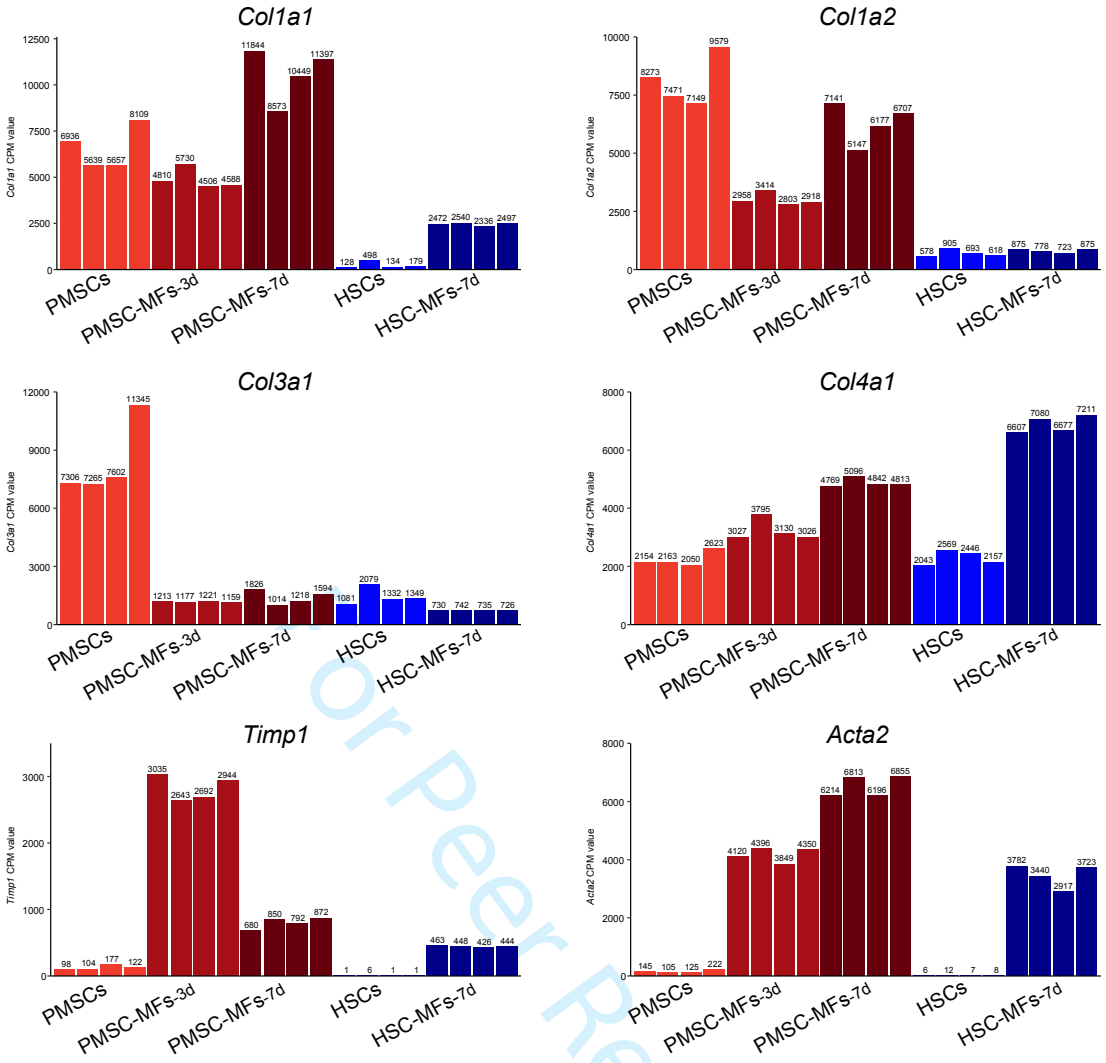

Fig. S9: Expression of pro-fibrotic genes in PMSCs and HSCs, in resting or myofibroblastic states after 3 days (-MFs-3d) or 7 days (-MFs-7d) in primary culture. CPM, counts per million.

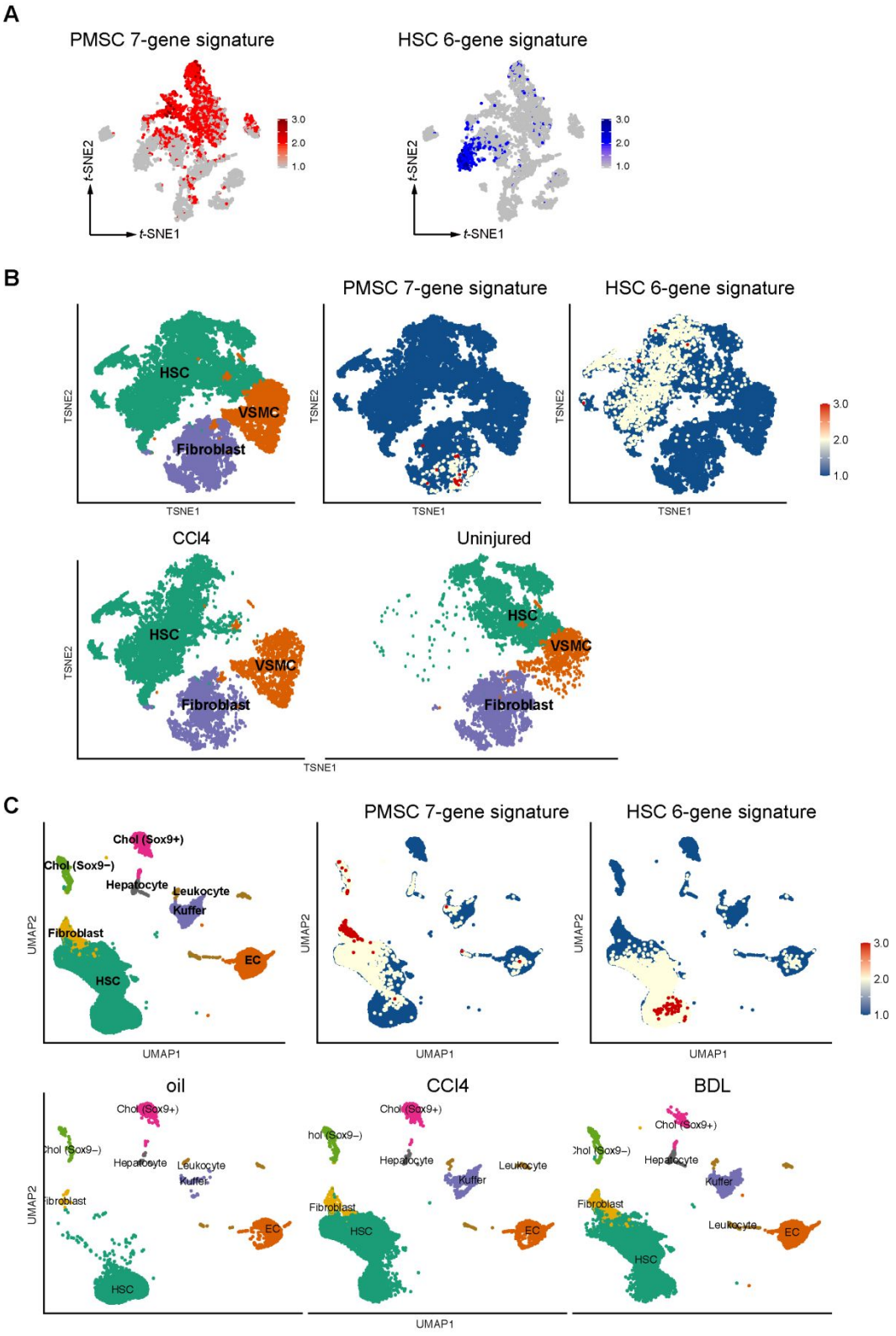

Fig. S10: PMSC/PMSC-MF and HSC/HSC-MF oligogene signatures projected onto (A) current and (B, C) previous scRNAseq data sets.
A) Clustering of portal mesenchymal cells from uninjured mouse liver as in Fig. 1B; B) Clustering of Pdgfrb-GFP+ mesenchymal cells from uninjured and fibrotic (6 weeks CCl4) mouse livers from Dobie *et al*. (GSE137720); C) Clustering of all liver cells from uninjured (oil) and fibrotic (3 weeks CCl4, 10 days BDL) mouse livers from Yang *et al*. (GSE171904). Chol, cholangiocytes.

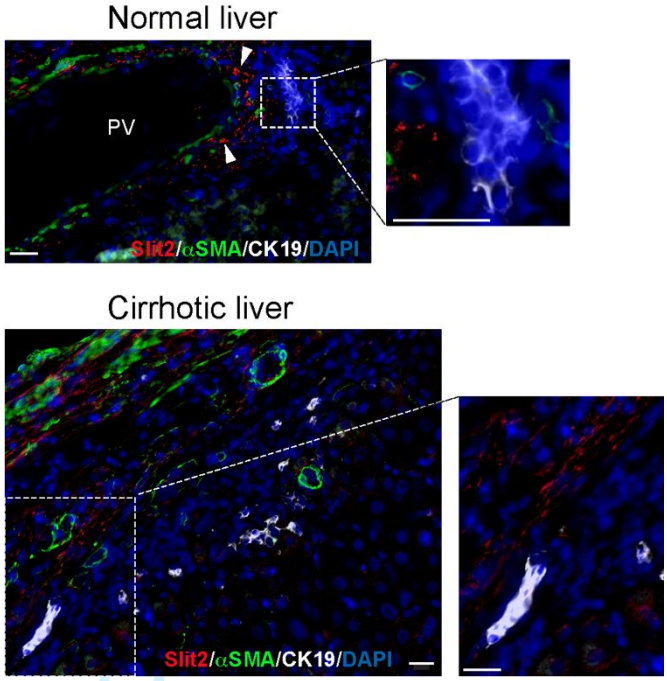

Fig. S11: Distinct localization of SLIT2⁺ cells and cholangiocytes.
SLIT2 FISH and α-SMA or CK19 immunofluorescence were performed on normal and cirrhotic human liver tissue sections. In normal liver (upper panel), perivascular *SLIT2*⁺ cells (arrowheads) in a large portal tract are distinct from α-SMA⁺ VSMCs and from CK19⁺ cholangiocytes (higher magnification in inset), representative of n=2 (PV, portal vein). In cirrhotic liver (lower panel), *SLIT2*⁺ intermingled with *SLIT2*⁻ myofibroblasts in fibrotic septa, are distinct from CK19⁺ cholangiocytes (higher magnification in inset), representative of cirrhosis of alcoholic (n=3), NASH (n=1) or hepatitis C (n=1) origins (Scale bars=50 μm).

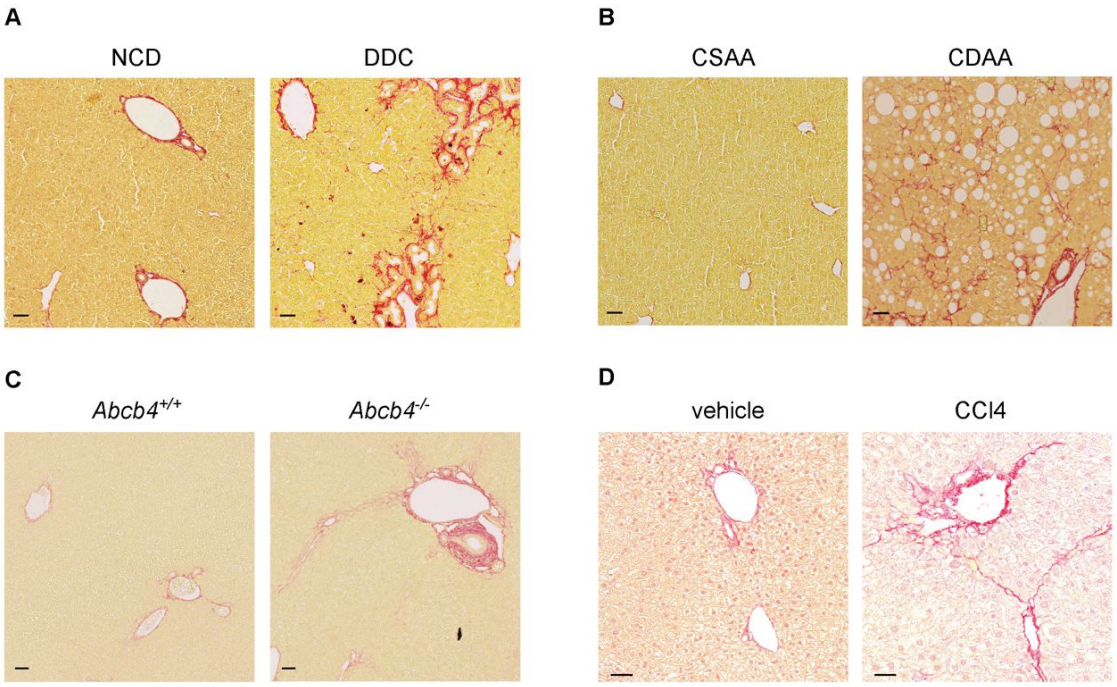

Fig. S12: Mouse models of liver fibrosis.
Sirius red staining of the liver from (A) mice fed NCD or DDC diet for 4 weeks; (B) mice fed CSAA or CDAA diet for 8 weeks; C) *Abcb4*$^{+/+}$ and *Abcb4*$^{-/-}$ mice at the age of 8 weeks; D) vehicle- or CCl4-i.p.-injected mice for 6 weeks. NCD, normal chow diet; DDC, 3,5-diethoxycarbonyl-1,4-dihydrocollidine; CSAA, choline-sufficient L-amino acid-defined; CDAA, choline-deficient L-amino acid-defined diet. Representative of 5 to 17 animals per group. Scale bars=50 µm.

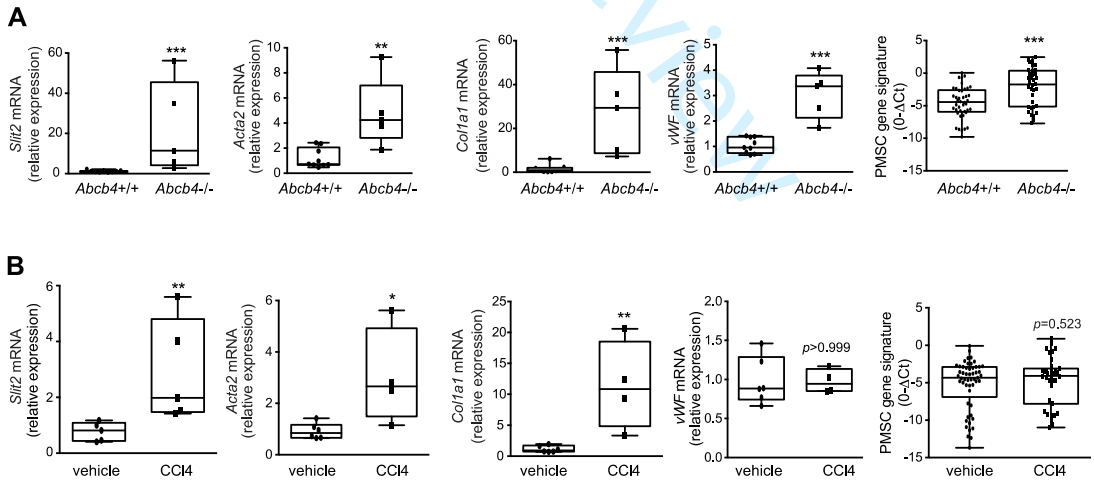

Fig. S13: Expression of SLIT2 and PMSC 7-gene signature in the Abcb4$^{-/-}$ and CCl4 mouse models of liver fibrosis.
Hepatic expression of *Slit2*, *Acta2*, *Col1a1*, *vWF* and of PMSC 7-gene signature was measured by RT-qPCR in liver tissue from (A) *Abcb4*$^{+/+}$ (n=9) and *Abcb4*$^{-/-}$ (n=5) mice at the age of 8 weeks, (B) vehicle- or CCl4-i.p.-injected mice for 6 weeks (n=5/group). Data represent individual values and means ± SEM. **p*<0.05; ***p*<0.01; ****p*<0.001 (Wilcoxon test).

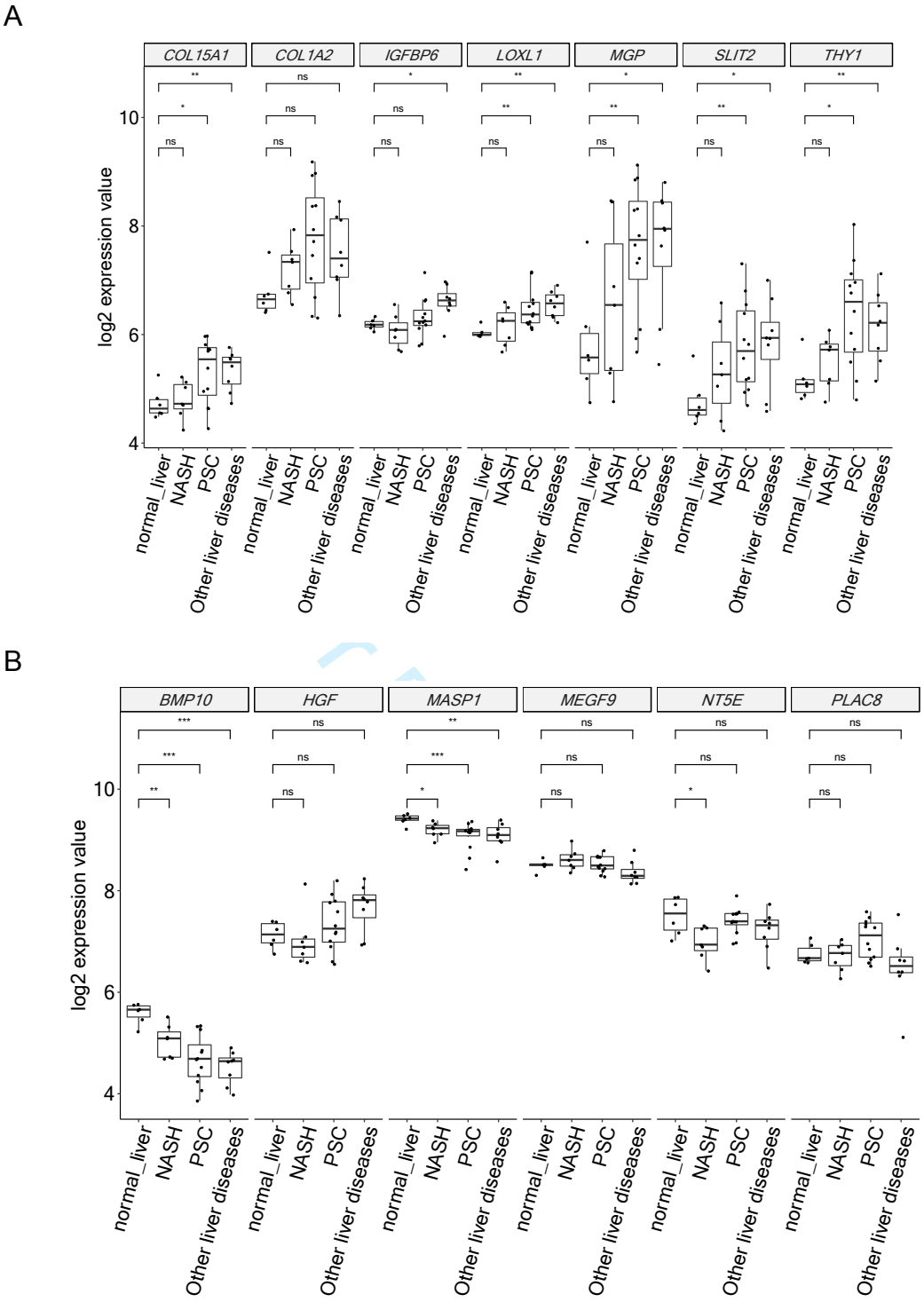

Fig. S14: Individual expression of the PMSC and HSC signature genes in human liver fibrosis.

Hepatic expression of the genes of (A) PMSC/PMSC-MF, and (B) HSC/HSC-MF signatures, was assessed by Affymetrix microarray analysis of normal human liver (n=5 patients) and of liver tissue samples from patients with NASH (n=7 patients), PSC (n=6 patients, 2 biopsies/patient) or other liver diseases (n=8 patients). Data represent individual values and means ± SEM. **p*<0.05; ***p*<0.01; ****p*<0.001; ns, non-significant; statistical significance was evaluated using non-parametric Wilcoxon test.

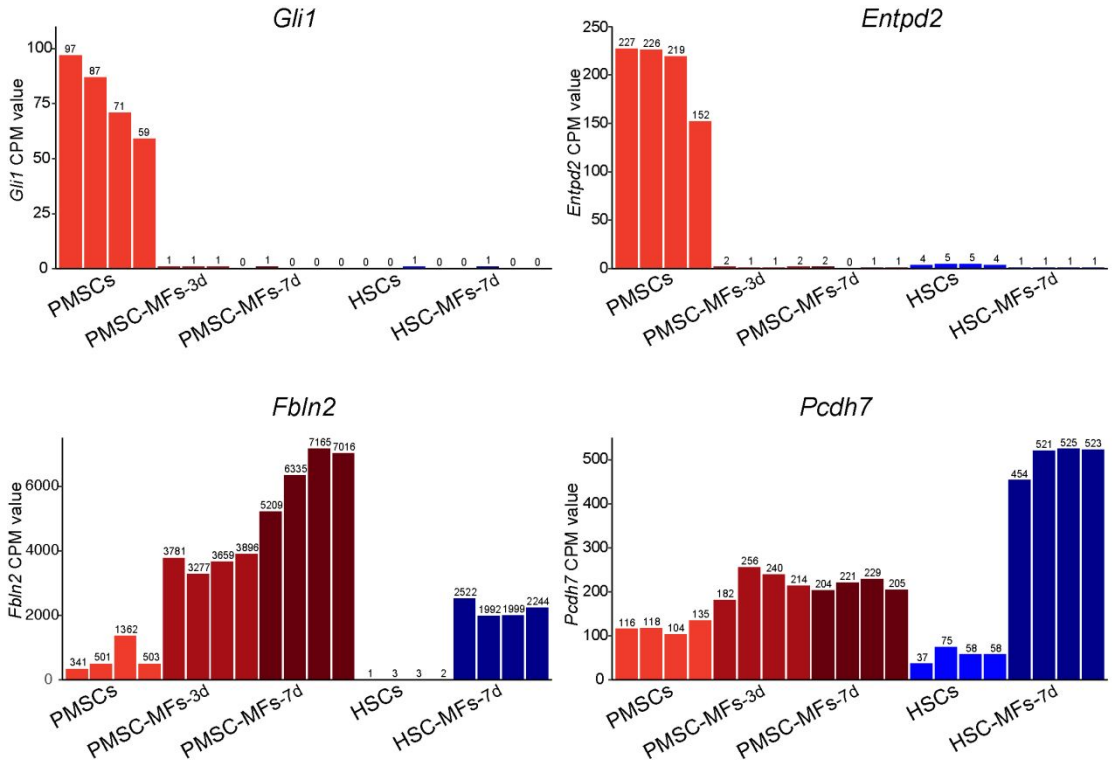

Fig. S15: *Gli1*, *Entpd2*, *Fbln2* and *Pcdh7* expression in the bulk RNAseq analysis of PMSCs and HSCs, in resting or myofibroblastic states after 3 days (-MFs-3d) or 7 days (-MFs-7d) in primary culture.
CPM, counts per million.

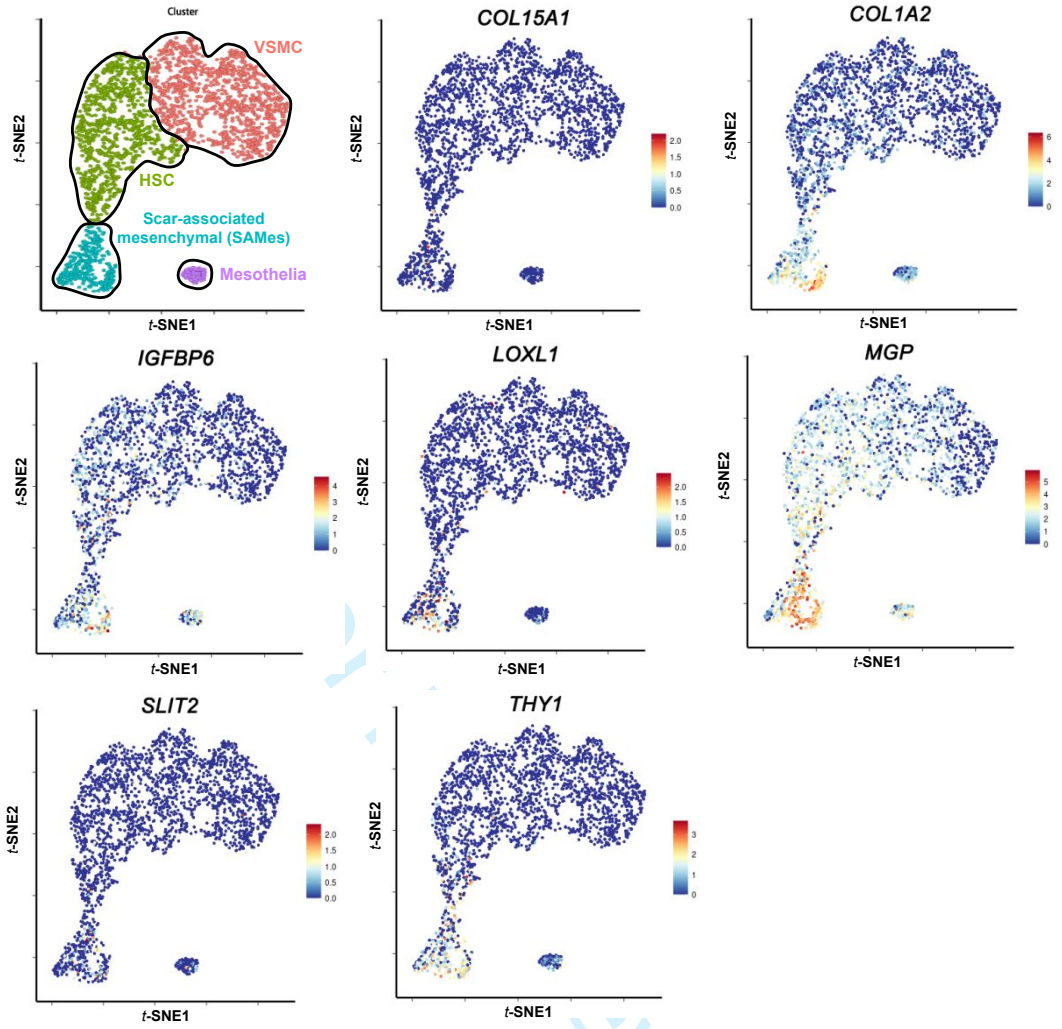

Fig. S16: Comparison of PMSCs/PMSC-MFs with the previously annotated scar-associated mesenchymal cells.
t-SNE plot of PMSC/PMSC-MF signature genes in human mesenchymal cells from Ramachandran et al. (https://www.livercellatlas.ed.ac.uk/).

Table S1: Antibodies used for cell sorting, flow cytometry and immunofluorescence.

Antibody	Company	Cat no.	Clone no.
Cell sorting & Flow cytometry			
rat anti-mouse CD9-BV421	BD Biosciences	564235	KMC8
rat anti-mouse CD11b-FITC	BioLegend	101245	M1/70
hamster anti-mouse CD29-PE/Cy7	BioLegend	102222	HMβ1-1
rat anti-mouse CD31-FITC	BD Biosciences	561813	MEC 13.3
rat anti-mouse CD34-APC	BioLegend	119310	MEC14.7
rat anti-mouse CD45-FITC	BioLegend	103137	30-F11
rat anti-mouse CD105-BV510	BD Biosciences	740188	MJ7/18
rat anti-mouse CD200-APC-R700	BD Biosciences	565546	OX-90
rat anti-mouse Epcam-FITC	BioLegend	118207	G8.8
rat anti-mouse PDGFRa-PE	eBioscience	12-1401-81	APA5
rat anti-mouse Sca1-BV510	BD Biosciences	565507	D7
rat anti-mouse Thy1-PE-Cy7	eBioscience	25-0902-81	53-2.1
Immunofluorescence			
mouse anti-human α-SMA	Agilent	M085129-2	1A4
rabbit anti-human Col15a1	Abcam	ab58717	N/A

Table S2: Primers used for qPCR.

Gene	GenBank	Forward primer	Reverse primer
Mouse			
Acta2	NM_007392.3	CTGTCAGGAACCCTGA	TACTCCCTGATGTCT
Bmp10	NM_009756.3	CGGAGCTTCAAGAACG	TGGTGAGGGATAGAC
Col1a1	NM_007742.4	GCTCCTCTTAGGGGCC	CCACGTCTCACCATT
Col1a2	NM_007743.3	CAAGCATGTCTGGTTA	AGGACACCCCTTCTA
Col15a1	NM_009928.3	AGATTTACGGGTTCCA	CAACGTGTGATTCTTT
Hgf	NM_001289458.1	CACCCCTTGGGAGTAT	GGGACATCAGTCTCA
Hprt	NM_013556.2	TCAAATCCCTGAAGTA	AGGACCTCTCGAAGT
Igfbp6	NM_008344.3	GGGCTCTATGTGCCAA	CCTGCGAGGAACGAC
Loxl1	NM_010729.3	TATGCCTGCACCTCTC	TGTCCGCATTGTATG
Masp1	NM_001359083.1	CCTACAGAGCGGCAG	GGCTCGATTTTCCCG
Megf9	NM_172694.2	ACAACCGGTCTGATAG	TTTGCATTCTTCACAG
Mgp	NM_008597.4	TCACGAAAGCATGGAG	GCTGAGGGGACATAA
Nt5e	NM_001204813	CCATTGATGAGAAGAA	GTCAAATGTCCCTCC
Plac8	NM_139198.3	TGTGTGCCAACTCAAG	GTTGAGCTTCTTCAG
Slit2	NM_178804.5	ATCTGCCTGAGACCAT	CGTCTAAGCTTTTTGT
Thy1	NM_009382.3	GAAAACTGCGGGCTTC	CCAAGAGTTCCGACT
vWf	NM_011708.4	CTACCTAGAACGCGAG	CATCGATTCTGGCCG
18S	NR_003278.3	GAGCGAAAGCATTTGC	GGCATCGTTTATGGT
Human			
ACTA2	NM_001613.4	GACAATGGCTCTGGGC	CTGTGCTTCGTCACC
COL1A	NM_000088.4	GTGCGATGACGTGATC	CGGTGGTTTCTTGGT
HPRT	NM_000194.3	TAATTGGTGGAGATGA	TGCCTGACCAAGGAA
SLIT2	NM_004787.4	GTGTTCGTGCCAGCTA	TTCCATCATTGATTGT
vWF	NM_000552.5	CTCCCACGCCTACATC	GCGGTCGATCTTGCT

Table S3: Probes used for FISH.

Probe name	Sequence
Scrambled	5' TAGCGAATCTCAGGCAAG – AT 633 3'
SLIT2-1	5' GGACCACGTCTCGCAGCGGTTCCTGCGGC – 6 Fam 3'
SLIT2-2	5' CACGGGTCCTTATAGGGGGCGTTGTGGC – 6 Fam 3'
SLIT2-3	5' CTTACGGTTGTTCTATTTGACGGAAGC – 6 Fam 3'
SLIT2-4	5' CACCTGCTCCAACTCTTTCACCACTTCACGC – 6 Fam 3'

Table S4: Differentially expressed genes in each scRNAseq cluster compared to all others.

Tab 1: All differentially expressed genes classified according to Seurat R toolkit;
Tab 2: Top 10 differentially expressed genes classified according to average log Fold-Change (avg_logFC).
(Provided separately).

Table S5: GO enrichment of differentially expressed genes in the scRNAseq clusters of Fibroblasts (Fib), Hepatic stellate cells (HSCs), and Vascular smooth muscle cells (VSMCs).

(Provided separately).

Table S6: Differential gene expressions in bulk RNAseq analyses, between PMSCs or HSCs and their myofibroblastic progenies after 3 days (-MFs-3d) or 7 days (-MFs-7d) in primary culture.

Genes (ID) are classified according to average log Fold-Change (logFC) from 4 replicates per condition.
(Provided separately)

Supplementary references

1. Gonzalez-Sanchez E, Firrincieli D, Housset C, Chignard N. Expression patterns of nuclear receptors in parenchymal and non-parenchymal mouse liver cells and their modulation in cholestasis. Biochim Biophys Acta Mol Basis Dis 2017;1863:1699-1708.

2. Mederacke I, Dapito DH, Affo S, Uchinami H, Schwabe RF. High-yield and high-purity isolation of hepatic stellate cells from normal and fibrotic mouse livers. Nat Protoc 2015;10:305-315.

3. Schindelin J, Arganda-Carreras I, Frise E, Kaynig V, Longair M, Pietzsch T, Preibisch S, et al. Fiji: an open-source platform for biological-image analysis. Nat Methods 2012;9:676-682.

4. Stuart T, Butler A, Hoffman P, Hafemeister C, Papalexi E, Mauck WM, 3rd, Hao Y, et al. Comprehensive Integration of Single-Cell Data. Cell 2019;177:1888-1902 e1821.

5. Hafemeister C, Satija R. Normalization and variance stabilization of single-cell RNA-seq data using regularized negative binomial regression. Genome Biol 2019;20:296.

6. Trapnell C, Cacchiarelli D, Grimsby J, Pokharel P, Li S, Morse M, Lennon NJ, et al. The dynamics and regulators of cell fate decisions are revealed by pseudotemporal ordering of single cells. Nat Biotechnol 2014;32:381-386.

7. Yu G, Wang LG, Han Y, He QY. clusterProfiler: an R package for comparing biological themes among gene clusters. OMICS 2012;16:284-287.

8. Yu G, He QY. ReactomePA: an R/Bioconductor package for reactome pathway analysis and visualization. Mol Biosyst 2016;12:477-479.

9. Doench JG, Fusi N, Sullender M, Hegde M, Vaimberg EW, Donovan KF, Smith I, et al. Optimized sgRNA design to maximize activity and minimize off-target effects of CRISPR-Cas9. Nat Biotechnol 2016;34:184-191.

10. Ricano-Cornejo I, Altick AL, Garcia-Pena CM, Nural HF, Echevarria D, Miquelajauregui A, Mastick GS, et al. Slit-Robo signals regulate pioneer axon pathfinding of the tract of the postoptic commissure in the mammalian forebrain. J Neurosci Res 2011;89:1531-1541.

Portal fibroblasts with mesenchymal stem cell features form a reservoir of proliferative myofibroblasts in liver fibrosis

Lin Lei,[1] Alix Bruneau,[2] Haquima El Mourabit,[1] Justine Guégan,[3] Trine Folseraas,[4] Sara Lemoinne,[1,5] Tom Hemming Karlsen,[4] Bénédicte Hoareau,[6] Romain Morichon,[1] Ester Gonzalez-Sanchez,[1] Claire Goumard,[1,7] Vlad Ratziu,[7] Pierre Charbord,[8] Jérémie Gautheron,[1] Frank Tacke,[2] Thierry Jaffredo,[8] Axelle Cadoret,[1]* Chantal Housset[1,5]*

[1]Sorbonne Université, INSERM, Centre de Recherche Saint-Antoine (CRSA), Institute of Cardiometabolism and Nutrition (ICAN), Paris, France;
[2]Charité University Medicine Berlin, Department of Hepatology and Gastroenterology, Berlin, Germany;
[3]Sorbonne Université, INSERM, Institut du Cerveau (ICM), Bioinformatics/Biostatistics iCONICS Facility, Paris, France;
[4]Oslo University Hospital Rikshospitalet, Norwegian PSC Research Center, Research Institute of Internal Medicine, Division of Surgery, Inflammatory Medicine and Transplantation, Oslo, Norway;
[5]Assistance Publique-Hôpitaux de Paris (AP-HP), Department of Hepatology, Reference Center for Inflammatory Biliary Diseases and Autoimmune Hepatitis (CRMR MIVB-H, ERN RARE-LIVER), Saint-Antoine Hospital, Paris, France;
[6]Sorbonne Université, INSERM, UMS Production et Analyse de Données en Sciences de la Vie et en Santé (PASS), Cytométrie Pitié-Salpêtrière (CyPS), Paris, France ;
[7]AP-HP, Sorbonne Université, ICAN, Departments of Hepatology, Hepatobiliary surgery and liver transplantation, Pitié-Salpêtrière Hospital, Paris, France ;
[8]Sorbonne Université, CNRS, INSERM, Institut de Biologie Paris Seine (IBPS), Laboratoire de Biologie du Développement, Paris, France.

*These authors share senior authorship

Keywords: Angiogenesis; Cirrhosis; Hepatic stellate cell; Single-cell RNA-sequencing; SLIT2.

Corresponding authors:
Chantal Housset, M.D., Ph.D.
Sorbonne Université, Faculté de Médecine, Site Saint-Antoine, 27 rue Chaligny, 75571 Paris cedex 12, France.
E-mail: chantal.housset@inserm.fr; Phone: (33) 1-40-01-13-59

Axelle Cadoret, Ph.D.
Sorbonne Université, Faculté de Médecine, Site Saint-Antoine, 27 rue Chaligny, 75571 Paris cedex 12, France.
E-mail: axelle.cadoret@inserm.fr; Phone: (33) 1-40-01-13-53

Abbreviations: ABCB4, ATP-binding cassette B4; α-SMA, alpha-smooth muscle actin; CK19, cytokeratin 19; CCl4, carbon tetrachloride; CDAA, choline-deficient, L-amino acid-defined; CFU-F, colony forming unit-fibroblast; CSAA, choline-sufficient, L-amino acid-defined; DDC, 3,5-diethoxycarbonyl-1,4-dihydrocollidine; DEG, differentially expressed gene; EC, endothelial cell; ECM, extracellular matrix; FISH, fluorescent *in situ* hybridization; GO, gene ontology; HSC, hepatic stellate cell; HUVEC, human umbilical vein endothelial cell; LSEC, liver sinusoidal endothelial cell; MSC, mesenchymal stem cell; NAFLD, non-alcoholic fatty liver disease; NASH, non-alcoholic steatohepatitis; NCD, normal chow diet; PCA, principal component analysis; PMSC, portal fibroblast with mesenchymal stem cell features; PSC, primary sclerosing cholangitis; ROBO, Roundabout; RT-qPCR, Reverse transcription-quantitative PCR; scRNAseq, single-cell RNA-sequencing; *t*-SNE, *t*-distributed stochastic neighbor embedding; VSMC, vascular smooth muscle cell.

Electronic word count: / 6037 words; 5 Figures

Conflict of interest: The authors have no conflict of interest to declare.

Financial support: This work was supported by funding from ANRS (ECTZ35217), FRM (EQU202003010517) and the Microbiome Foundation. Lin Lei received a fellowship from the China Scholarship Council (CSC).

Authors contributions: L.L., T.J., A.C., C.H. designed the study; L.L., A.B., H.E.M., J.Gu., T.F., T.H.K., B.H., R.M., E.G-S., C.G., V.R., J.Ga., T.J. acquired experimental and clinical data; L.L., A.B., H.E.M., J.Gu., S.L., P.C., F.T., T.J., C.H., A.C. analyzed and interpreted the data; L.L., S.L., A.C., C.H. drafted the manuscript, with critical revision from all authors.

Abstract

Background & Aims: In liver fibrosis, myofibroblasts derive from hepatic stellate cells (HSCs) and as yet undefined mesenchymal cells. We aimed to identify portal mesenchymal progenitors of myofibroblasts. **Approach & Results:** Portal mesenchymal cells were isolated from mouse bilio-vascular tree and analyzed by scRNAseq. Thereby, we uncovered the landscape of portal mesenchymal cells in homeostatic mouse liver. Trajectory analysis enabled inferring a small cell population further defined by surface markers used to isolate it. This population consisted of portal fibroblasts with mesenchymal stem cell features (PMSCs), *i.e.*, high clonogenicity and tri-lineage differentiation potential, that generated proliferative myofibroblasts, contrasting with non-proliferative HSC-derived myofibroblasts (-MFs). Using bulk RNAseq, we built oligogene signatures of the two cell populations, that remained discriminant across myofibroblastic differentiation. *SLIT2*, a prototypical gene of PMSC/PMSC-MF signature, mediated pro-fibrotic and angiogenic effects of these cells, whose conditioned medium promoted HSC survival and endothelial cell tubulogenesis. Using PMSC/PMSC-MF 7-gene signature and *SLIT2* FISH, we showed that PMSCs display a perivascular portal distribution in homeostatic liver and largely expand with fibrosis progression, contributing to the myofibroblast populations that form fibrotic septa, preferentially along neo-vessels, in murine and human liver disorders, irrespective of aetiology. We also unraveled a 6-gene expression signature of HSCs/HSC-MFs that did not vary in these disorders, consistent with their low proliferation rate. **Conclusions:** PMSCs form a small reservoir of expansive myofibroblasts, which in interaction with neo-vessels and HSC-MFs that mainly arise *via* differentiation from a preexisting pool, underlie the formation of fibrotic septa in all types of liver diseases.

Mesenchymal cells are key players in tissue homeostasis and wound healing. In the liver, mesenchymal cells comprise hepatic stellate cells (HSCs), that reside in sinusoids, and perivascular cells including vascular smooth muscle cells (VSMCs) and fibroblasts, that reside in the portal tracts and around central veins. Genetic-based lineage-tracing analyses have demonstrated that HSCs and perivascular mesenchymal cells as well as mesothelial cells all derive from the septum transversum during liver development (1). Over the past 30 years, HSCs have been extensively investigated for their capacity to undergo myofibroblastic differentiation, and have been identified as a major source of myofibroblasts in liver fibrosis (2). However, the other liver mesenchymal cells, particularly portal mesenchymal cells have gained increasing interest as evidence has accumulated that indicates they could also generate myofibroblasts (3-6). The portal tracts contain three main structures referred to as the portal triad, *i.e.*, the portal vein, hepatic artery and bile duct, surrounded by a mesenchyme, which has remained poorly defined so far. Little is known regarding the identity, spatial distribution or functions of portal mesenchymal cells and how they contribute to fibrosis. A major limitation has been the lack of markers, especially surface markers that would allow to isolate portal mesenchymal cells or track them *in vivo*. Using a model of outgrowth from fragments of the bilio-vascular tree isolated from rat liver, we previously showed that portal cells distinct from HSCs could generate myofibroblasts, that we referred to as portal myofibroblasts, characterized by COL15A1 expression, a high proliferation rate and pro-angiogenic properties (4, 7, 8). However, the precursors of portal myofibroblasts have not been truly identified in these studies. In the present study, we isolated portal mesenchymal cells from mouse liver as a single-cell preparation and analyzed their diversity using single-cell RNA-

sequencing (scRNAseq). A minimal set of surface markers enabled us to isolate a subset of portal fibroblasts with mesenchymal stem cell features (PMSCs) and the ability to generate myofibroblasts. Markers of PMSCs were discovered and used to examine the expansion potential of these cells in murine and human liver fibrosis.

Experimental procedures

Details are provided in Supplementary material.

Animals. Male mice of C57BL/6J or FVB.129 genetic background, were used at the age of 8-12 weeks for cell isolation and liver fibrosis models, in compliance with ARRIVE guidelines.

Cell isolation and culture. The bilio-vascular tree was isolated from mouse liver, by adapting a procedure we previously described in rat (7), and further processed using cell sorting and flow cytometry analysis to collect and analyze mesenchymal cells. Ultrapure HSCs and other liver cell types were isolated using established methods. Cell clonogenicity, trilineage and myofibroblastic differentiation were examined in cell culture.

RNAseq. ScRNAseq of the bilio-vascular tree Lin-negative cells (gated as $Epcam^-$ $CD31^-CD45^-CD11b^-$ cells), was performed using the 10X Genomics 3' v3 kit (10× Genomics). NextSeq500 (Illumina) device was used for single-cell and bulk RNAseq. ScRNAseq analyses were performed using CellRanger, Seurat and Monocle, and bulk RNAseq analyses, using STAR, RSEM and edgeR R package.

Human liver samples. Fresh and frozen samples of normal and pathological liver tissue were collected with the approval of ethical committees, from patients who gave written informed consent.

Reverse transcription-quantitative PCR (RT-qPCR), Immunofluorescence and fluorescent *in situ* hybridization (FISH). Primers, antibodies and probes are listed in Table S1-3.

Microarray analyses. Pangenomic analysis of frozen liver tissue samples, was performed using the Affymetrix human gene 1.0 st microarray.

SLIT2-mediated functions analyses. The conditioned medium of PMSC-derived myofibroblasts (PMSC-MFs) was tested for potential effects on the viability of the LX-2 HSC cells, and the tubulogenesis of human umbilical vein endothelial cells (HUVECs). In these experiments, SLIT2 signaling was blocked using siRNA, CRISPR/Cas9, anti-ROBO1 antibody or a recombinant ROBO1/Fc chimera.

Statistical analyses. Unless otherwise stated, statistical analyses were performed using Graphpad Prism v6.0 and R. Unpaired two-sided Wilcoxon test and ANOVA with a Scheffe post-hoc test were used to compare differences between two groups, and more than two groups, respectively. A significant difference was defined as $p<0.05$.

Results

Landscape of the portal mesenchyme revealed by scRNAseq

Portal mesenchymal cells represent a small cell population. They are tightly bound to the portal triad, relying on basement membranes. This makes them more difficult to isolate than hepatocytes or sinusoidal cells, which reside in a loose, basement membrane-free, extracellular matrix (ECM). In the present study, we set up a specific procedure to isolate portal mesenchymal cells, for scRNAseq analysis. We adapted a method we previously established for the culture of rat portal myofibroblasts (7), to isolate fragments of the bilio-vascular tree from mouse liver. The bilio-vascular tree fragments were submitted to enzymatic digestion, resulting in a single-cell suspension,

which was depleted in cells expressing the lineage (Lin) markers of cholangiocytes (EpCAM), endothelial cells (CD31), and hematopoietic cells (CD45 and CD11b) using cell sorting. Lin-negative single-cell suspension was then processed to generate a scRNAseq cDNA library (Fig. 1A). We captured 4,976 sequenced cells that met quality control metrics (Fig. S1A) from healthy mouse liver. Unsupervised clustering identified 16 distinct clusters that were assigned to fibroblast (5 clusters), VSMC (5 clusters), endothelial (4 clusters), HSC (1 cluster) and mesothelial (1 cluster) identities (Fig. 1B). The hierarchical clustering of gene expression profiles supported this classification except for the very small cluster of VSMC-5 (Fig. 1C). The most selective expressed genes that allowed to segregate cell clusters are shown in Fig. 1D, Fig. S2 and Table S4. In all clusters, the expression of cell cycle-related genes, *e.g.*, *Mki67*, was at the limit of detection, as expected from resting cells in homeostatic liver (Fig. S3).

The non-mesenchymal components: mesothelial and endothelial cells

Mesothelial cells display an intermediate phenotype between epithelial and mesenchymal cells and form a single layer that covers the liver surface (9). The liver capsule also covers the intrahepatic parenchyma surrounding the Glissonean pedicles including bile ducts (10), which can explain the presence of mesothelial cells in our cell suspension. Genes expressed in these cells included previously reported mesothelial markers, among which the most specific were *Msln* and *Upk1b* as well as epithelial markers, such as *Krt8* and *Krt19*, and mesenchymal markers, such as *Vim* but almost no *Pdgfrb.* Additional putative markers restricted to this cluster included *Fxyd3, Myl7* and *Slpi* (Fig. S4A).

We identified four clusters of endothelial cells (ECs), enriched in markers such as *Pecam1*, *Cdh5*, *Kdr* and *Egfl7* (Fig. S4B). The PECAM1 protein (alias CD31) has been

shown to be intracellular in liver sinusoidal endothelial cells (LSECs) (11), which explains, at least partly, why ECs escaped our negative selection according to the membrane antigen CD31. Moreover, even though cells from the bilio-vascular tree were preferentially retrieved by our method, basement membrane-free LSECs adhere to other cell types and are prone to be collected during isolation procedures, as previously reported (12). As shown in Fig. S5, we found markers of EC zonation in the liver, *i.e.*, of peri-central LSECs in EC-1, of peri-portal LSECs and/or portal vascular ECs in EC-2, of lymphatic ECs in EC-3, and of hepatic arterial ECs in EC-4 (12, 13).

The mesenchymal components: fibroblasts, HSCs and VSMCs

Our single-cell analysis revealed five clusters of fibroblasts (Fig. 1B-D), which predominantly expressed genes involved in vascular ECM such as *Mmp19*, *Col6a5*, *Col6a6* or *Col15a1*, and also expressed genes of interstitial collagens such as *Col1a1*, *Col1a2*, *Col3a1* at higher levels than other clusters. Both fibroblasts and HSCs expressed *Pdgfra*, whereas *Eln* previously reported as a marker of portal fibroblasts (5), was expressed in many other clusters (Fig. S4C). Fib-3 highly expressed *Ptn* (Fig. 1D), a pericyte-derived trophic factor for ECs (14), suggesting a particular interaction of this cluster with portal vessels, whereas Fib-5 was enriched in HSC markers, such as *Lrat* (2) and *Reln* (5) (Fig. S4D), which was not driven by doublets (Fig. S1B), and may thus represent an intermediate population between fibroblasts and HSCs. All five fibroblast clusters were enriched in the gene ontology (GO) terms “ECM organization” and “Wound healing” (Fig. S6, Table S5). Individual clusters were also enriched in terms related to cell (including leucocyte) chemotaxis (Fib-1), epithelial cell proliferation and migration (Fib-2), tissue development or morphogenesis (Fib-3, Fib-4, Fib-5).

Cells of cluster 8 were recognized as HSCs. They were enriched in GO terms related to immunity and cell differentiation (Fig. S6). Among classical markers of HSCs, *Lrat* and *Reln* (2, 5) appeared to be not fully specific, being expressed notably in Fib-2 and Fib-5 (Fig. S4D). Like others (2, 15), we found virtually no expression of *Gfap*, whereas *Des* and *Cygb* (2, 3), were expressed at variable levels in virtually all clusters. Among HSC markers newly identified by scRNAseq (15-18) or bulk RNAseq (19), our analysis confirmed that some of them were restricted to HSCs, such as *Tmem56*, *Colec10, Mapt* or *Bco1*. Others such as *Fcna* or *Angptl6*, although not fully specific, were largely overexpressed in HSCs, whereas yet others such as *Rgs5*, *Pcdh7*, *Adamtsl2*, *Gucy1a1/b1* or *Colec11* were expressed at relatively high levels in several other mesenchymal cells, in addition to HSCs. Both *Ngfr* and *Il34* on one hand, *Vipr1* and *Pth1r* on the other one, previously reported to preferentially mark peri-portal and peri-central HSCs, respectively (15), were expressed in the HSC cluster, indicating that this cluster was representative of all HSCs (Fig. S4D).

We identified 5 clusters of VSMCs that expressed at highest levels markers such as *Myh11, Cnn1, Acta2* or *Tagln* (13, 15) (Fig. S4E). VSMC clusters were enriched in GO terms related to muscle functions but also to “Inflammatory response” (Fig. S6).

Identification of PMSCs

As a first approach to assess differentiation potency of the different clusters, we computed single-cell entropy, an approximation of single-cell differentiation potency based on predicted signalling promiscuity (20). Of all clusters, Fib-3 displayed the highest differentiation potency as suggested by the highest entropy value (Fig. 2A). We also examined the differentiation dynamics among mesenchymal cells, and analyzed all cells except mesothelial and endothelial cells, using Monocle 2 (21). This

analysis showed a common trajectory of mesenchymal cells with one bifurcation and three branches defining states (Fig. 2B). On the basis of entropy analysis, the branch containing Fib-3 was defined as the root state. As shown in Fig. 2B, the root state was mainly populated by Fib-3 and Fib-4 cells, which were consequently assumed to be progenitor cells, contrasting with the two other states populated by VSMCs, notably VSMC-1, and HSCs, both well-differentiated cell types with high pseudotime values. Consistent with this assumption, GO terms related to development were concentrated in Fib-3 and Fib-4, suggesting multilineage potential of these two clusters (Fig. 2C). Genes previously reported to demarcate universal fibroblasts in mouse tissues, *i.e. Pi16* and *Col15a1* (22), or portal fibroblasts/myofibroblasts, *i.e.*, *Col15a1* (4), *Cd34* (6, 15), *Thy1* alias CD90 (6, 23, 24), *Gli1* (19, 25), *Clec3b* (15), *Fbln2* (26) and *Entpd2* (27), were mainly expressed in these two clusters (Fig. 2D). *Pi16*$^{+}$ cells, were recently shown to serve as resource fibroblasts that would pass through *Col15a1*$^{+}$ fibroblasts able to secrete basement membrane proteins, before developing into specialized fibroblasts, in all steady-state mouse tissues (22). In addition, CD34, Thy1 and Gli1 are all considered as stem cell markers. To further analyze Fib-3 and Fib-4 clusters, we defined a minimal set of surface markers enabling to isolate them together. As shown in Fig. 2E, a high expression of *Pdgfra*, *Cd34* and *Cd9* combined with a low expression of *Cd200* appeared to discriminate Fib-3 and Fib-4 from other Lin-negative cells. We FACS-sorted Lin (Epcam/CD31/CD45/CD11b)-negative, PDGFRα/CD34/CD9-positive, and CD200-low cells (Gate 4 in Fig. 2F) and examined this population for stem cell features. The percentage of cells recovered was approximately 0.03 % of total liver cells. The cells of this population were highly clonogenic (80 colony forming unit-fibroblast (CFU-F) per 2,000 cells) (Fig. 2G) irrespective of whether they were Thy1-positive or negative (Fig. S7). They also

displayed the expression of classical mesenchymal stem cell (MSC) markers, *i.e.*, CD105, Sca-1, CD29 (Fig. 2H), and the ability to undergo trilineage (adipogenic, osteogenic and chondrogenic) differentiation, in culture (Fig. 2I). Taken together, the cells isolated by our gating strategy displayed MSC attributes and were designated PMSCs. When cultured on a stiff substratum (Fig. 2J, bottom panels), PMSCs proliferated and gave rise to cells phenotypically similar to portal myofibroblasts expressing COL15A1 (4), here referred to as PMSC-MFs. This phenotypic change was accompanied by the expected up-regulation of *Acta2*, the gene encoding alpha-smooth muscle actin (α-SMA), no change in *Col1a1* expression, and a down-regulation of *Col15a1* (Fig. 2K). Despite such down-regulation, *Col15a1* demarcates both PMSCs and portal myofibroblasts (4). It was possible to maintain PMSCs in a resting state by cultivating them in spheroids, on ultra-low attachment plates, in which case the expression of α-SMA was not induced and that of Col15a1, less reduced (Fig. 2J-K). Overall, these data indicate that our screening strategy and isolation procedure enabled identifying portal fibroblasts with MSC properties and high collagen expression as precursors of portal myofibroblasts.

Specific phenotypes and molecular profiles of PMSCs, HSCs and derived myofibroblasts

The isolation of PMSCs provided a unique opportunity to compare them with HSCs, and uncover specific markers of the two cell populations and of their myofibroblastic progenies. We performed transcriptomic analyses using bulk RNAseq, to compare PMSCs with ultrapure HSCs (28), as ascertained by vitamin A fluorescence (Fig. S8A). We identified 3,273 genes expressed at higher levels in PMSCs, and 3,122, in HSCs (Fig. 3A, upper panel). Projections onto *t*-SNE plot (Fig. 3A, lower panel), showed that

the top 10 differentially expressed genes in PMSCs included common markers of portal fibroblasts, as expected from a comparison with HSCs, but were expressed at highest levels in Fib-3/Fib-4, indicating that PMSCs comprised mainly if not exclusively Fib-3/Fib-4 fibroblasts. The top 10 differentially expressed genes of HSCs included common markers with ECs, but none with the other mesenchymal cells. Consistent with the GO analyses of scRNAseq (Fig. S6, Table S5), bulk RNAseq analysis showed enrichment in pathways related to “Extracellular matrix organization” in PMSCs and “Immunity” in HSCs, and further highlighted pathways related to “Angiogenesis” in PMSCs and to “Metabolism of fat-soluble vitamins” in HSCs (Fig. 3B).

Both PMSCs (Fig. 2J-K), and HSCs (3, 4), undergo phenotypic changes into myofibroblasts in primary culture. Phenotypically, the major difference we observed between the two cell populations, was an intense proliferation in PMSCs as they became myofibroblastic, whereas HSCs differentiated into myofibroblasts without dividing (Fig. S8A, D-E including videomicroscopy). We extended bulk RNAseq analyses to the myofibroblasts derived from both cell populations in culture, including an early and late stage of differentiation for PMSC-MFs (Table S6). Principal component analysis (PCA) showed a clear discrimination of PMSCs and HSCs from their myofibroblastic progenies according to PC1, while PMSC-MFs were discriminated from HSC-derived myofibroblasts (HSC-MFs) according to PC2 (Fig. 3C). The molecular profiles of PMSCs and HSCs became more similar as they differentiated into myofibroblasts. Yet, they retained specificities at the stage of myofibroblasts as confirmed by GO analysis (Fig. 3D). When fully differentiated into myofibroblasts, *i.e.*, after 7 days of culture, both cell populations were enriched in themes related to muscle differentiation, whereas additionally, PMSC-MFs were enriched in themes related to axonogenesis and ECM organization. To a large extent,

PMSCs/PMSC-MFs overexpressed genes encoding fibrillar collagens (*Col1a1*, *Col1a2*, *Col3a1*), *Timp1* and *Acta2*, the hallmarks of liver fibrosis, whereas *Col4a1*, a major component of sinusoidal ECM was overexpressed in HSC-MFs (Fig. S9). At an early stage of myofibroblastic differentiation, *i.e.*, after 3 days of culture, PMSC transcriptome was highly enriched in pathways related to cell proliferation (Fig. 3D). At a later stage of myofibroblastic differentiation, *i.e.*, after 7 days of culture, PMSC-MFs compared to HSC-MFs still markedly overexpressed genes involved in cell proliferation, consistent with videomicroscopy and CFU-F assays, showing that only PMSCs as opposed to HSCs were clonogenic and divided in culture (Fig. S8B-E).

Next, we looked for gene expressions that would demarcate the two cell populations both in their resting and myofibroblastic states, and that could thus be used in fibrotic liver tissue analyses to assess if PMSCs/PMSC-MFs were more expansive than HSCs/HSC-MFs, also *in vivo*. Altogether, comparative analyses of gene expressions indicated that 100 genes in PMSCs (or Fib-3/Fib-4) and 112 genes in HSCs, i) were overexpressed according to both scRNAseq and bulk RNAseq analyses, and ii) remained differentially expressed in these cells throughout myofibroblastic differentiation (Fig. 3E). Among such genes, we selected those that combined the highest differential expression (>3.5-fold), a relatively high expression (CPM>40) in the demarcated cell population, limited variation with myofibroblastic differentiation, and no or little expression in the other liver cell types, to build an oligogene expression signature of PMSCs/PMSC-MFs (7 genes) and HSCs/HSC-MFs (6 genes) (Fig. 3F-G). Projection of the two signatures onto current (Fig. 1B) and previous scRNAseq datasets (15, 18) showed that the PMSC/PMSC-MF signature demarcated liver fibroblasts, with highest intensity in Fib-3/Fib-4 (Fig. S10A) and in liver fibroblasts accumulating in liver fibrosis induced either by carbon tetrachloride (CCl4) or bile duct

ligation (BDL) (Fig. S10B-C), with little or no signal in other liver cell types. The HSC/HSC-MF signature demarcated the HSC cluster (Fig. S10A), as well as the vast majority of HSCs in mouse liver, including in CCl4- and BDL-induced liver fibrosis, and virtually no other liver cell populations except a small portion of ECs (Fig. S10B-C).

Implication of PMSCs and PMSC-MFs in liver fibrosis

Our transcriptome analyses highlighted *Slit2* as a prototypical gene of PMSC/PMSC-MF signature. Its expression was particularly stable in PMSCs throughout their myofibroblastic differentiation and virtually absent from all other liver cell types including HSCs/HSC-MFs (Fig. 4A, left panel). Using FISH, we confirmed that PMSC-MFs in culture were distinguishable from HSC-MFs by *Slit2* expression (Fig. 4A, right panel). SLIT2 is an axon guidance molecule, which was previously shown to trigger HSC activation and fibrosis (29-31) as well as angiogenesis, in the liver (32). However, so far, the endogenous source of SLIT2 in the liver, had not been accurately identified. Our scRNAseq data showed that *Slit2* expression was concentrated in Fib-3/Fib-4, whereas its roundabout (ROBO) receptors were mainly expressed in the HSC and EC clusters, and to a lesser extent in the fibroblast clusters (Fig. 4B). Therefore, previous and current findings suggested that PMSCs had the potential to signal towards HSCs and ECs via *Slit2*, to promote their pro-fibrotic and pro-angiogenic activity, respectively. Supporting such mechanisms, PMSC-MF conditioned medium prevented the decrease in cell viability induced by an oxidative stress in the LX-2 HSC cell line and this effect was abolished by silencing *Slit2 via* SiRNA in PMSC-MFs (Fig. 4C). PMSC-MF conditioned medium also increased tubulogenesis in HUVECs and this effect was largely SLIT2-dependent. It was prevented in the presence of anti-ROBO1 antibody or recombinant ROBO1/Fc chimera that entraps soluble SLIT2 and it was reduced by

Slit2 depletion *via* CRISPR/Cas9 in PMSC-MFs (Fig. 4D). We used *SLIT2* FISH to demarcate PMSCs/PMSC-MFs and address their connections with other cell types in normal and cirrhotic human liver. In normal liver, *SLIT2*$^+$ cells were scarce, although more abundant in large portal tracts than in the small ones. They were virtually restricted to portal tracts and displayed a perivascular distribution (Fig. 4E, left panel, Fig. S11, upper panel). In cirrhotic liver, irrespective of aetiology (*i.e.*, alcoholic liver disease, non-alcoholic steatohepatitis (NASH) or chronic hepatitis C), *SLIT2*$^+$ cells were much more abundant than in normal liver (Fig. 4E, middle and right panels). They were mainly located in the fibrotic septa, displayed α-SMA expression and were thus identified as PMSC-MFs. Within fibrotic septa, SLIT2$^+$/α-SMA$^+$ PMSC-MFs were intermingled with, and outnumbered by SLIT2$^-$/α-SMA$^+$ myofibroblasts, and were frequently located in the surrounding of vascular lumens (Fig. 4E, middle panel). Consistent with PMSC/PMSC-MF interacting with HSCs/HSC-MFs and ECs, we found that in cirrhosis, SLIT2$^+$ PMSC-MFs often lined up along CD31$^+$ neo-vessels, and thus appeared as a scaffold for the accumulation of abundant SLIT2$^-$/α-SMA$^+$ myofibroblasts, most likely largely derived from HSCs (Fig. 4F). Both in normal and cirrhotic human livers, *SLIT2*$^+$ cells were clearly distinct from cytokeratin 19 (CK19)-labeled cholangiocytes (Fig. S11).

To further ascertain that PMSCs/PMSC-MFs accumulated in liver fibrosis, we measured SLIT2 mRNA levels in mouse and human injured livers. We found that the hepatic expression of *Slit2* increased in mouse models of either cholestatic diseases, *i.e.*, 3,5-diethoxycarbonyl-1,4-dihydrocollidine (DDC), *Abcb4*$^{-/-}$, or NASH, *i.e.*, choline-deficient, L-amino acid-defined (CDAA) and cytotoxic injury, *i.e.*, CCl4 (Fig. S12), along with those of fibrosis markers (*Acta2*, *Col1a1*) in all models, and of an angiogenesis marker (*vWF*) in the cholestatic models (Fig. 5A and S13). The complete

PMSC/PMSC-MF 7-gene signature was increased in the DDC, *Abcb4*$^{-/-}$ and CDAA models, whereas the HSC/HSC-MF 6-gene signature that was tested in the DDC and CDAA models, was not (Fig. 5A and S13). The analysis of a cohort of patients with non-alcoholic fatty liver disease (NAFLD) showed that the expression of *SLIT2* was increased in the group with advanced fibrosis, *i.e.* F3-F4 according to the SAF score (33) (Fig. 5B). We also examined the microarray data of liver tissue samples from patients with NASH, primary sclerosing cholangitis (PSC) and other chronic liver diseases (alcoholic liver disease, haemochromatosis, primary biliary cholangitis, autoimmune hepatitis), for *SLIT2* expression and the oligogene expression signatures of PMSCs/PMSC-MFs and of HSCs/HSC-MFs. This analysis showed that *SLIT2* expression and the 7-gene expression signature of PMSCs/PMSC-MFs were both significantly increased in the liver of patients with all types of chronic liver diseases, as compared to normal liver (Fig. 5C-D, left panels and S14A). *SLIT2* expression and the 7-gene expression signature were both similarly correlated with *ACTA2*, *COL1A1* and *vWF* expression in these samples (Fig. 5C-D). The analysis of the microarray data also indicated that in contrast to the PMSC/PMSC-MF 7-gene signature, the 6-gene expression signature of HSCs/HSC-MFs was not significantly different between any group of diseased livers and normal livers (Fig. 5E and S14B). This finding is consistent with a low proliferation rate of HSCs and further supports the assumption that HSC-MFs would primarily derive from myofibroblastic differentiation of the HSC preexisting pool. We concluded from these results that PMSCs give rise to a highly expansive population of myofibroblasts in liver fibrosis irrespective of the cause.

Discussion

In the present study, we provide a detailed atlas of portal mesenchymal cells, that were obtained *via* dissociation of the bilio-vascular tree. While being consistent with previous scRNAseq studies of the liver, notably from a *Pdgfrb*-GFP reporter mouse (15), our analysis revealed the existence of several clusters of fibroblasts. Among them, the Fib-3 and Fib-4 clusters, displayed relatively low levels of *Pdgfrb* expression compared to the other clusters of liver mesenchymal cells (Fig. S4A), and thus may have been underestimated in the study of PDGFRβ^{+} cells (15). Fib-3 and Fib-4 were highlighted as potential progenitor cells on the basis of entropy, GO and trajectory analyses as well as the expression of stem cell markers. Thus, Fib-3 and Fib-4 appeared as the most primitive of liver mesenchymal cells, which form a continuum of cells with overlapping markers, along a gradient of differentiation that bifurcates towards mature VSMCs on one hand and HSCs on the other one. In this context, PMSCs were isolated as a cell population, that primarily comprised Fib-3 and Fib-4. MSCs were first identified in the bone marrow as clonogenic, multipotent cells, able to differentiate into lineages of mesenchymal tissues including osteoblasts, chondrocytes and adipocytes in culture (34). Subsequently, cells with similar properties were identified in multiple organs and also referred to as MSCs (35), although a controversy over the MSC terminology has been fueled by studies showing that MSCs from different tissues exhibited different differentiation capacities (36). Yet, MSCs from different tissues share common features including a small cell population, clonogenicity, the ability to differentiate into the afore-mentioned mesenchymal cell lineages *in vitro* and a frequent perivascular distribution (35, 36). PMSCs displayed all these characteristics. Thy1 and Gli1, two stem cell markers predominantly expressed in Fib-3, as well as fibulin-2 and ENTPD2, predominantly expressed in Fib-4, were previously immunolocalized in the portal tracts of homeostatic liver, with a perivascular or periductal distribution (19, 23-

25, 27, 37-39). We found that the sub-populations of Thy1^{+} and Thy1^{-} PMSCs were equally clonogenic (Fig. S7), implying that both Fib-3 and Fib-4 are resource fibroblasts in the liver. COL15A1 (4) and SLIT2, that we identified as PMSC markers, are expressed in both clusters, and also display a perivascular or periductal distribution in the homeostatic liver. As formerly proposed for other MSCs, *e.g.,* in the skeletal muscle (36), we suggest that Fib3 and Fib4 represent subsets of the same original population, recruited to the surface of nascent portal blood vessels or later, of developing bile ducts.

The lack of markers that would enable to differentiate HSC-derived from non-HSC-derived myofibroblasts has been a major hurdle so far, to gain insight into the specificities of the different types of liver myofibroblasts and their contributions to liver fibrosis. The isolation of PMSCs allowed us to gain such insight and seek invaluable markers of the two populations. The comparison of transcriptional profiles indicated that in their resting state, PMSCs primarily ensure ECM organization and vasculature integrity whereas HSCs are mainly involved in immunity and the metabolism of vitamin A. A striking difference between the two cell populations as they transform into myofibroblasts *in vitro*, is that PMSCs intensely proliferate whereas HSCs do not divide. In addition, whereas the expression of α-SMA is induced in both cell types, that of ECM genes such as *Col1a1*, is up-regulated in HSCs but not in PMSCs, so that they both converge towards more similar phenotypes. As a result, most of gene expressions that could demarcate the two cell populations in their resting state are lost or no longer discriminant between their myofibroblastic progenies. Thus, among markers of PMSCs, the expression of *Gli1* or *Entpd2* is totally suppressed in PMSC-MFs, whereas that of *Fbln2* expression is induced in HSC-MFs (Fig. S15). Our strategy was to build

oligogene expression signatures, which included only markers of the two cell populations that maintained high differential expression, with limited variation (average fold-change of approximately one), throughout their myofibroblastic differentiation. Specificity of the cell signatures for liver fibroblasts and HSCs *in vivo*, was attested by their projection onto previous scRNAseq datasets of mouse liver fibrosis (15, 18). PMSC gene signature was predominantly expressed in Fib-3/Fib-4, but also to a lesser extent in other fibroblast clusters (Fig. S10A), which therefore could also proliferate in liver injury.

Slit2, known as a profibrotic and proangiogenic factor in the liver (29-32), is a prototypical gene of PMSC/PMSC-MF signature. From the present data, we may postulate that following liver injury, SLIT2, produced by proliferating PMSCs/PMSC-MFs, promotes the formation of new vessels and the survival of HSC-MFs. Supporting this view, FISH analyses showed that *SLIT2*$^{+}$ PMSCs/PMSC-MFs accumulated along neo-vessels in the fibrotic septa of cirrhotic livers, surrounded by *SLIT2*$^{-}$ myofibroblasts, likely mostly HSC-derived. As we previously showed for *COL15A1* (4), the hepatic expression of *SLIT2* increased in injured liver in correlation with that of *COL1A1* and *vWF*, in all types of liver fibrosis. Akin to *SLIT2*, the complete PMSC/PMSC-MF 7-gene signature increased, indicating that this cell population expanded in mouse and human liver fibrosis of multiple causes. As they expand, PMSCs/PMSC-MFs may promote liver fibrosis *via* several mechanisms including the SLIT2/ROBO axis, but also the production of COL15A1, a multiplexin that anchors interstitial collagen to basement membranes forming a scaffold for fibrosis progression (4, 40), the overproduction of COL1A1 and COL1A2, that form the major interstitial collagen in liver fibrosis, and of LOXL1, which promotes elastin cross-linking, among

others. ScRNAseq analysis of human liver mesenchymal cells in cirrhosis (13), previously identified a cluster distinguished by PDGFRA expression that expanded in cirrhotic livers and was annotated scar-associated mesenchymal cells. We found that the expression of all PMSC/PMSC-MF signature genes is largely predominant in this population (Fig. S16), supporting the clinical relevance of our findings and our conclusion regarding the expansion of PMSC-MFs in liver fibrosis. In a previous study, a 122-gene HSC signature was shown to be increased in experimental and human liver fibrosis (41). However, this latter signature was designed in comparison with other liver cell types that did not include other liver mesenchymal cells, and highlighted genes such as *Pcdh7* that were herein found to be expressed not only in HSCs/HSC-MFs but also in PMSCs/PMSC-MFs (Fig. S4D and S15). Our HSC/HSC-MF 6-gene expression signature did not increase in human fibrosis, which is consistent with a low proliferation rate of HSCs/HSC-MFs *in vitro*, as shown here and *in vivo*, in recent scRNAseq analysis of HSCs/HSC-MFs in mouse models of liver fibrosis (17, 18). Despite little or no proliferation, HSC-MFs that derive from the large preexisting pool of HSCs, likely form the major part of liver myofibroblasts. However, as they proliferate and expand within the lobule, PMSC-MFs may develop interactions with ECs and HSCs anticipated to play crucial roles in fibrosis progression.

Acknowledgements: The authors acknowledge Tatiana Ledent (CRSA Animal Facility), Yannick Marie and Delphine Bouteiller (ICM Sequencing Facility), Pierre-Antoine Soret (CRSA), Filomena Conti, Lynda Aoudjehane (Human HepCell) and Pierre-Emmanuel Rautou (CRI, Université de Paris) for their contributions.

Data availability: All sequencing data are deposited in the Gene Expression Omnibus (GEO) with the accession numbers GSE163777 (scRNAseq), GSE164037 (bulk RNAseq) and GSE159676 (microarrays).

References

1. Asahina K, Zhou B, Pu WT, Tsukamoto H. Septum transversum-derived mesothelium gives rise to hepatic stellate cells and perivascular mesenchymal cells in developing mouse liver. Hepatology 2011;53:983-995.

2. Mederacke I, Hsu CC, Troeger JS, Huebener P, Mu X, Dapito DH, Pradere JP, et al. Fate tracing reveals hepatic stellate cells as dominant contributors to liver fibrosis independent of its aetiology. Nat Commun 2013;4:2823.

3. Bosselut N, Housset C, Marcelo P, Rey C, Burmester T, Vinh J, Vaubourdolle M, et al. Distinct proteomic features of two fibrogenic liver cell populations: hepatic stellate cells and portal myofibroblasts. Proteomics 2010;10:1017-1028.

4. Lemoinne S, Cadoret A, Rautou PE, El Mourabit H, Ratziu V, Corpechot C, Rey C, et al. Portal myofibroblasts promote vascular remodeling underlying cirrhosis formation through the release of microparticles. Hepatology 2015;61:1041-1055.

5. Lua I, Li Y, Zagory JA, Wang KS, French SW, Sevigny J, Asahina K. Characterization of hepatic stellate cells, portal fibroblasts, and mesothelial cells in normal and fibrotic livers. J Hepatol 2016;64:1137-1146.

6. Nishio T, Hu R, Koyama Y, Liang S, Rosenthal SB, Yamamoto G, Karin D, et al. Activated hepatic stellate cells and portal fibroblasts contribute to cholestatic liver fibrosis in MDR2 knockout mice. J Hepatol 2019;71:573-585.

7. El Mourabit H, Loeuillard E, Lemoinne S, Cadoret A, Housset C. Culture Model of Rat Portal Myofibroblasts. Front Physiol 2016;7:120.

8. Loeuillard E, El Mourabit H, Lei L, Lemoinne S, Housset C, Cadoret A. Endoplasmic reticulum stress induces inverse regulations of major functions in portal myofibroblasts during liver fibrosis progression. Biochim Biophys Acta Mol Basis Dis 2018;1864:3688-3696.

9. Lua I, Asahina K. The Role of Mesothelial Cells in Liver Development, Injury, and Regeneration. Gut Liver 2016;10:166-176.

10. Sugioka A, Kato Y, Tanahashi Y. Systematic extrahepatic Glissonean pedicle isolation for anatomical liver resection based on Laennec's capsule: proposal of a novel comprehensive surgical anatomy of the liver. J Hepatobiliary Pancreat Sci 2017;24:17-23.

11. **Poisson J**, **Lemoinne S**, Boulanger C, Durand F, Moreau R, Valla D, Rautou PE. Liver sinusoidal endothelial cells: Physiology and role in liver diseases. J Hepatol 2017;66:212-227.

12. **Halpern KB**, **Shenhav R**, Massalha H, Toth B, Egozi A, Massasa EE, Medgalia C, et al. Paired-cell sequencing enables spatial gene expression mapping of liver endothelial cells. Nat Biotechnol 2018;36:962-970.

13. Ramachandran P, Dobie R, Wilson-Kanamori JR, Dora EF, Henderson BEP, Luu NT, Portman JR, et al. Resolving the fibrotic niche of human liver cirrhosis at single-cell level. Nature 2019;575:512-518.

14. Copes F, Ramella M, Fusaro L, Mantovani D, Cannas M, Boccafoschi F. Pleiotrophin: Analysis of the endothelialisation potential. Adv Med Sci 2019;64:144-151.

15. Dobie R, Wilson-Kanamori JR, Henderson BEP, Smith JR, Matchett KP, Portman JR, Wallenborg K, et al. Single-Cell Transcriptomics Uncovers Zonation of Function in the Mesenchyme during Liver Fibrosis. Cell Rep 2019;29:1832-1847 e1838.

16. Krenkel O, Hundertmark J, Ritz TP, Weiskirchen R, Tacke F. Single Cell RNA Sequencing Identifies Subsets of Hepatic Stellate Cells and Myofibroblasts in Liver Fibrosis. Cells 2019;8:503.

17. Rosenthal SB, Liu X, Ganguly S, Dhar D, Pasillas MP, Ricciardelli E, Li RZ, et al. Heterogeneity of HSCs in a Mouse Model of NASH. Hepatology 2021;74:667-685.

18. **Yang W**, **He H**, Wang T, Su N, Zhang F, Jiang K, Zhu J, et al. Single-Cell Transcriptomic Analysis Reveals a Hepatic Stellate Cell-Activation Roadmap and Myofibroblast Origin During Liver Fibrosis in Mice. Hepatology 2021;74:2774-2790.

19. Gupta V, Gupta I, Park J, Bram Y, Schwartz RE. Hedgehog Signaling Demarcates a Niche of Fibrogenic Peribiliary Mesenchymal Cells. Gastroenterology 2020;159:624-638 e629.

20. Chen W, Teschendorff AE. Estimating Differentiation Potency of Single Cells Using Single-Cell Entropy (SCENT). Methods Mol Biol 2019;1935:125-139.

21. Trapnell C, Cacchiarelli D, Grimsby J, Pokharel P, Li S, Morse M, Lennon NJ, et al. The dynamics and regulators of cell fate decisions are revealed by pseudotemporal ordering of single cells. Nat Biotechnol 2014;32:381-386.

22. **Buechler MB**, **Pradhan RN**, Krishnamurty AT, Cox C, Calviello AK, Wang AW, Yang YA, et al. Cross-tissue organization of the fibroblast lineage. Nature 2021;593:575-579.

23. Dudas J, Mansuroglu T, Batusic D, Ramadori G. Thy-1 is expressed in myofibroblasts but not found in hepatic stellate cells following liver injury. Histochemistry and cell biology 2009;131:115-127.

24. Katsumata LW, Miyajima A, Itoh T. Portal fibroblasts marked by the surface antigen Thy1 contribute to fibrosis in mouse models of cholestatic liver injury. Hepatol Commun 2017;1:198-214.

25. Kramann R, Schneider RK, DiRocco DP, Machado F, Fleig S, Bondzie PA, Henderson JM, et al. Perivascular Gli1+ progenitors are key contributors to injury-induced organ fibrosis. Cell Stem Cell 2015;16:51-66.

26. Knittel T, Kobold D, Saile B, Grundmann A, Neubauer K, Piscaglia F, Ramadori G. Rat liver myofibroblasts and hepatic stellate cells: different cell populations of the fibroblast lineage with fibrogenic potential. Gastroenterology 1999;117:1205-1221.

27. Dranoff JA, Kruglov EA, Robson SC, Braun N, Zimmermann H, Sevigny J. The ecto-nucleoside triphosphate diphosphohydrolase NTPDase2/CD39L1 is expressed in a novel functional compartment within the liver. Hepatology 2002;36:1135-1144.

28. **Mederacke I**, **Dapito DH**, Affo S, Uchinami H, Schwabe RF. High-yield and high-purity isolation of hepatic stellate cells from normal and fibrotic mouse livers. Nat Protoc 2015;10:305-315.

29. **Chang J**, **Lan T**, Li C, Ji X, Zheng L, Gou H, Ou Y, et al. Activation of Slit2-Robo1 signaling promotes liver fibrosis. J Hepatol 2015;63:1413-1420.

30. Zeng Z, Wu Y, Cao Y, Yuan Z, Zhang Y, Zhang DY, Hasegawa D, et al. Slit2-Robo2 signaling modulates the fibrogenic activity and migration of hepatic stellate cells. Life Sci 2018;203:39-47.

31. **Li C**, **Yang G**, **Lin L**, Xuan Y, Yan S, Ji X, Song F, et al. Slit2 signaling contributes to cholestatic fibrosis in mice by activation of hepatic stellate cells. Exp Cell Res 2019;385:111626.

32. Coll M, Arino S, Martinez-Sanchez C, Garcia-Pras E, Gallego J, Moles A, Aguilar-Bravo B, et al. Ductular Reaction Promotes Intrahepatic Angiogenesis Via Slit2-Robo1 Signaling. Hepatology 2021.

33. Bedossa P, Consortium FP. Utility and appropriateness of the fatty liver inhibition of progression (FLIP) algorithm and steatosis, activity, and fibrosis (SAF) score in the evaluation of biopsies of nonalcoholic fatty liver disease. Hepatology 2014;60:565-575.

34. Pittenger MF, Mackay AM, Beck SC, Jaiswal RK, Douglas R, Mosca JD, Moorman MA, et al. Multilineage potential of adult human mesenchymal stem cells. Science 1999;284:143-147.

35. Crisan M, Yap S, Casteilla L, Chen CW, Corselli M, Park TS, Andriolo G, et al. A perivascular origin for mesenchymal stem cells in multiple human organs. Cell Stem Cell 2008;3:301-313.

36. **Sacchetti B**, **Funari A**, Remoli C, Giannicola G, Kogler G, Liedtke S, Cossu G, et al. No Identical "Mesenchymal Stem Cells" at Different Times and Sites: Human Committed Progenitors of Distinct Origin and Differentiation Potential Are Incorporated as Adventitial Cells in Microvessels. Stem Cell Reports 2016;6:897-913.

37. Knittel T, Kobold D, Piscaglia F, Saile B, Neubauer K, Mehde M, Timpl R, et al. Localization of liver myofibroblasts and hepatic stellate cells in normal and diseased rat livers: distinct roles of (myo-)fibroblast subpopulations in hepatic tissue repair. Histochem Cell Biol 1999;112:387-401.

38. Tateaki Y, Ogawa T, Kawada N, Kohashi T, Arihiro K, Tateno C, Obara M, et al. Typing of hepatic nonparenchymal cells using fibulin-2 and cytoglobin/STAP as liver fibrogenesis-related markers. Histochem Cell Biol 2004;122:41-49.

39. Dezso K, Jelnes P, Laszlo V, Baghy K, Bodor C, Paku S, Tygstrup N, et al. Thy-1 is expressed in hepatic myofibroblasts and not oval cells in stem cell-mediated liver regeneration. Am J Pathol 2007;171:1529-1537.

40. Lemoinne S, Thabut D, Housset C. Portal myofibroblasts connect angiogenesis and fibrosis in liver. Cell Tissue Res 2016;365:583-589.

41. Zhang DY, Goossens N, Guo J, Tsai MC, Chou HI, Altunkaynak C, Sangiovanni A, et al. A hepatic stellate cell gene expression signature associated with outcomes in hepatitis C cirrhosis and hepatocellular carcinoma after curative resection. Gut 2016;65:1754-1764.

Author names in bold designate shared co-first authorship

Figure legends

Fig. 1. ScRNAseq profiling of mesenchymal cells from the bilio-vascular tree. (A) Outline of the experimental procedure for preparation of Lin (EpCam,CD31,CD45,CD11b)-negative cells from the mouse bilio-vascular tree for scRNAseq analysis. (B) *t*-SNE projection of 4,976 single cells from one healthy liver, revealing 16 clusters (color-coded), identified by their expression profiles and ordered according to the number of cells they comprise. (C) Dendrogram showing the relationships of clusters. (D) Dot plot of two selective differentially expressed genes in each cluster.

Fig. 2. Characterization of PMSCs. (A) Single-cell entropy of all clusters. (B) Inference of sequenced mesenchymal cells by Monocle 2 reverse graph embedding (pseudotime along differentiation trajectory in inset). (C) Heatmap of GO enrichment related to development. (D) Dot plot of genes previously reported to demarcate progenitor fibroblasts (red frame) or portal (myo)fibroblasts (black frame). (E) Dot plot of genes encoding surface markers *Pdgfra*/*Cd34*/*Cd9* and *Cd200*. (F) FACS plot showing the gating strategy for Fib-3/Fib-4 cell sorting (Gate 4). (G) CFU-F formed by sorted cells from gates as defined in F (n=3-9). (H) Flow cytometry analysis of MSC surface markers in cells from gate 4 (n=4-10). (I) Trilineage differentiation of cells from gate 4 (PMSCs), towards adipocytes (Oil red O), osteoblasts (Alizarin red S) and chondrocytes (Alcian blue). (J) Immunofluorescence of Col15A1 and α-SMA in PMSC

spheroids (upper panel) or grown into PMSC-MFs on stiff substratum (lower panel). (K) *Col15a1*, *Acta2* and *Col1a1* expression in PMSCs (freshly isolated or cultured as in J) (n=3). Means ± SEM; ***p*<0.01; ****p*<0.001; *****p*<0.0001 (Wilcoxon test); Scale bars=50 µm.

Fig. 3. Transcriptomic features of PMSCs/PMSC-MFs compared to HSCs/HSC-MFs. (A,B) Bulk RNAseq analysis of PMSCs and HSCs, A) Volcano plot (upper panel) showing 3,273 and 3,122 DEGs (FDR ≤ 0.05, fold-difference ≥ 2) in PMSCs and HSCs, respectively. Top 10 DEGs are labeled and their average expression, projected on *t*-SNE plot of scRNAseq (lower panel); (B) Gene Set Enrichment Analysis (GSEA) of all genes overexpressed in PMSCs or HSCs. (C) Overview of cell preparations (n=4 per condition), analyzed by bulk RNAseq and PCA of variance of read counts (ellipses: 95% CI). (D) K-means clustering of 5,000 genes with highest variance showing enriched GO terms. (E) Venn diagram showing DEGs in PMSCs (or Fib-3/Fib-4) and in HSCs, both in bulk RNAseq and scRNAseq and maintaining high differential expression after myofibroblastic differentiation (-MFs-7d). (F-G) Heatmaps of PMSC and HSC oligogene expression signatures assessed by F) bulk RNAseq or G) RT-qPCR analyses of PMSCs, HSCs, derived myofibroblasts (-MFs-7d), and other liver cell types. KCs, Kupffer cells.

Fig. 4. *Slit2* marker in PMSCs/PMSC-MFs and its functional analysis. (A) *Slit2* RT-qPCR in PMSCs, HSCs, their derived myofibroblasts (-MFs-d7), and other liver cell types (n=3) (left panel); *Slit2* FISH and α-SMA immunofluorescence in PMSC-MFs-d7 and HSC-MFs-d7 (right panel). (B) *t*-SNE plot of *Slit2* and its *Robo* receptors in scRNAseq clusters. (C) PMSC-MFs that were transfected with *Slit2* or scramble (Scr)

siRNA, were examined for *Slit2* and *Acta2* expression by RT-qPCR, and their conditioned medium (CM) tested towards the cell viability, assessed by MTT, of LX-2 cells exposed to H2O2 (n=5-8). (D) Tube formation was evaluated in HUVECs incubated with PMSC-MF CM in the absence (n=6) or presence of ROBO1/Fc (n=5) or anti-ROBO1 antibody (n=5), or with control (CTL) serum-free medium (n=9); and in HUVECs incubated with the CM of PMSC-MFs infected with a lentivirus expressing Cas9 and a gRNA targeting the first exon of *Slit2* (LV*Slit2*, n=8) or a control lentivirus expressing Cas9 and a scramble gRNA (LV, n=8), or with CTL serum-free medium (n=3). After 6 hours, pictures were taken and the number of junctions, counted, using the Angiogenesis Analyzer tool Fiji. (E, F) *SLIT2* FISH and α-SMA or CD31 immunofluorescence in normal and cirrhotic human liver; E) In normal liver (left panel), a small number of *SLIT2*$^+$ PMSCs (arrowheads) are visible in portal tracts (perivascular *SLIT2*$^+$ PMSCs, distinct from α-SMA$^+$ VSMCs, shown in insets), representative of n=2 (CV, central vein; PV, portal vein). In cirrhosis (middle panel), *SLIT2*$^+$ are intermingled with *SLIT2*$^-$ myofibroblasts in fibrotic septa (FS) (*SLIT2*$^+$,α-SMA$^+$ PMSC-MF, shown in inset); right panel: quantification of labeled areas; F) SLIT2$^+$ PMSC-MFs (red arrowheads) line up along CD31$^+$ neo-vessels (white arrowheads), surrounded by several layers of α-SMA$^+$ myofibroblasts that populate the entire fibrotic septa (dashed green line) (merge shown in inset), representative of cirrhosis of alcoholic (n=3), NASH (n=1) or hepatitis C (n=1) origins (Scale bars=50 μm). Means ± SEM; **p*<0.05; ***p*<0.01; *****p*<0.0001 (One-way ANOVA in A, Wilcoxon test in C and D).

Fig. 5. Expression of *SLIT2*, PMSC/PMSC-MF and HSC/PMSC-MF oligogene signatures in liver fibrosis. Hepatic expression of *SLIT2*, *ACTA2*, *COL1A1*, *vWF*, PMSC/PMSC-MF or HSC/HSC-MF oligogene signatures assessed by (A,B) RT-qPCR,

A) in liver tissue from mice fed normal chow diet (NCD, n=12) or DDC (n= 8) for 4 weeks (upper panels), or fed CSAA (n=5) or CDAA (n=17) for 8 weeks (lower panels), B) in liver biopsy from patients with NAFLD, at stages of fibrosis F0 (n=26), F1 (n=15), F2 (n=12), F3-F4 (n=7). (C) by Affymetrix microarray analysis of normal human liver (n=5 patients) and of liver tissue samples from patients with NASH (n=7 patients), PSC (n=6 patients, 2 biopsies/patient) or other liver diseases (n=8 patients) (left panel); (D) PMSC/PMSC-MF and (E) HSC/HSC-MF oligogene signatures assessed by Affymetrix microarray analysis of human liver tissue samples as in C. Correlations between *SLIT2* or PMSC 7-gene signature and *ACTA2*, *COL1A1*, or *vWF* expression are shown in C and D right panels. Individual values and means ± SEM are shown; **p*<0.05; ***p*<0.01; ****p*<0.001; *****p*<0.0001; ns, non-significant (Wilcoxon test in A, C-E; one-way ANOVA in B); r values are Pearson correlation coefficients.

Portal fibroblasts with mesenchymal stem cell features form a reservoir of proliferative myofibroblasts in liver fibrosis

Lin Lei, Alix Bruneau, Haquima El Mourabit, Justine Guégan, Trine Folseraas, Sara Lemoinne, Tom Hemming Karlsen, Bénédicte Hoareau, Romain Morichon, Ester Gonzalez-Sanchez, Claire Goumard, Vlad Ratziu, Pierre Charbord, Jérémie Gautheron, Frank Tacke, Thierry Jaffredo, Axelle Cadoret*, Chantal Housset* (*co-senior authorship).

Table of contents

Supplementary Experimental procedures

Animal experiments.

Animal experiments were conducted in the CRSA animal facility (DDPP agreement No. C 75-12-01) and were approved under Nos. 2018060418401070v2, 2018102211507258, 2019090307246392v3 and 2018072719352187v1 by the Ethics Committee of Animal Experiments, Charles Darwin No. 5, Paris. Animals, all males, were housed in a temperature-controlled, specific pathogen-free environment, on a 12-hour light-dark cycle, with free access to chow and water. *Abcb4*$^{-/-}$ mice and their wildtype *Abcb4*$^{+/+}$ littermates were bred, using *Abcb4*$^{+/-}$ heterozygous mice on an FVB/N genetic background (FVB.129P2-Abcb4tm1Bor/J) provided by Sanofi R&D (Chilly-Mazarin, France). Liver fibrosis was also induced in C57BL/6J male mice, by 3 methods: 1) 10-week-old mice were fed a diet containing 0.1% DDC (Sigma, 137030) or a normal control diet (NCD), for 4 weeks; 2) 8-week-old mice were fed a CDAA or CSAA diet (Ssniff spezialdiäten GmbH, Soest, Germany), for 8 weeks; 3) 8-week-old mice received i.p. injections of CCl4 (1 μL/g body weight) diluted at 50% (V/V) in mineral oil or mineral oil (vehicle), twice a week for 6 weeks.

Cell isolation.

Cell collection from the bilio-vascular tree. *In situ* retrograde perfusion of the liver was performed through the inferior vena cava with Ca^{2+},Mg^{2+}-free HBSS (Gibco, 14170-088)/1% EDTA (Sigma, 03690) for 5 minutes at 37°C, and then with HBSS containing Ca^{2+},Mg^{2+} (Gibco, 24020117)/0.15 mg/mL collagenase P (Sigma, 11213873001) for 20 minutes at 37°C. Next, the liver was collected and placed in L15 Leibovitz medium (Sigma, L5520) at 4°C. The liver parenchyma was mechanically detached and discarded. The remaining bilio-vascular tree was minced and incubated in MEM (Gibco, 21090-022) containing 0.075 mg/mL collagenase P, 0.02 mg/mL DNAse (Sigma, DN25), 3% FBS (FBS; Gibco, 10270-098), 1 mg/mL BSA (Sigma, A7030), 1% Hepes (Gibco, 15630) and 1% Penicillin-Streptomycin (Gibco, 15140-122), under agitation for 15 minutes at 37°C. The bilio-vascular fragments were collected on top of a 40-μm cell strainer and centrifuged at 1,500 rpm, for 5 minutes at 4°C. The cell pellet was resuspended in 0.05% Trypsin-EDTA (Invitrogen, 25300-054) with 0.02 mg/mL DNAse and incubated under agitation for 15 minutes at 37°C, and the dissociated cells were filtered three times through a 20-μm cell strainer. Following red blood cell lysis with ACK lysis buffer, the cell suspension was centrifuged at 1,500 rpm, for 5 minutes at 4°C, and the cell pellet was resuspended in a FACS buffer composed of PBS with 2% FBS, 1% Hepes and 1% Penicillin-Streptomycin, at a concentration of 1×10^7 cells/mL for cell sorting. For cholangiocyte isolation, cells were incubated with an anti-Epcam-FITC antibody (BioLegend, Clone: G8.8) for 30 minutes at 4°C and cells were sorted using a FACSAria II cell sorter (BD Biosciences).

Hepatocyte, Kupffer cell, LSEC and HSC collection. Hepatocytes, LSECs and Kupffer cells were isolated as previously described (1), with modifications. For

hepatocyte isolation, the liver was perfused *in situ* with HBSS containing 0.15 mg/mL collagenase P for 20 minutes at 37°C. The cell suspension was filtered through a 70-µm strainer and centrifuged twice at 400 rpm, for 5 minutes at 4°C, to eliminate non-parenchymal cells. LSEC and Kupffer cell isolation was performed by *ex situ* dissociation of the liver using a gentleMACs dissociator (Miltenyi) and magnetic selection using CD146 microbeads (Miltenyi, 130-092-007) and anti-F4/80 microbeads (Miltenyi, 130-110-443), respectively. For HSC isolation, the liver was perfused *in situ*, with HBSS containing 0.4 mg/mL pronase (Sigma, 10165921001) for 5 minutes at 37°C, and then with 0.05 mg/mL collagenase P for 15 min at 37°C. The liver was collected, minced and further digested in HBSS containing 0.044 mg/mL collagenase P, 0.5 mg/mL pronase and 0.02 mg/mL DNAse, under agitation for 15 minutes at 37°C. The resulting cell suspension was submitted to density gradient-centrifugation at 1,380 g for 17 minutes, in GBSS (Gibco)/Histodenz (Sigma, D2158) at 4°C. HSCs were collected from the interface and resuspended in FACS buffer for further purification by cell sorting based on retinoid autofluorescence, as previously described (2).

Cell sorting and flow cytometry analysis

Cells isolated from the bilio-vascular tree were incubated with 1% anti-mouse CD16/CD32 antibody (BD Pharmingen, 553141) for 10 minutes on ice, to block Fc receptors before incubation with anti-Epcam-FITC, anti-CD31-FITC, anti-CD45-FITC and anti-CD11b-FITC antibodies, all at concentrations of 1:100, for 30 minutes at 4°C. Dead cells were stained with 7-aminoactinomycin D (7-AAD; BD Biosciences, 559925) immediately before cell sorting was performed, using a FACSAria II cell sorter (BD Biosciences). Lin-negative cells, gated as $Epcam^{-}CD31^{-}CD45^{-}CD11b^{-}$ cells, were collected and subjected to scRNAseq analysis. To isolate PMSCs from the bilio-vascular tree, cells were labeled with anti-Epcam-, anti-CD31-, anti-CD45- and anti-CD11b-FITC antibodies as above, and anti-PDGFRα-PE, anti-CD34-APC, anti-CD9-BV421 and anti-CD200-APC-R700, all at concentrations of 1:100 except for anti-PDGFRα-PE (1:50). PMSCs were gated as $Lin^{-}PDGFR\alpha^{+}CD34^{+}CD9^{+}CD200^{low}$ cells. To sort $Thy1^{-}$, $Thy1^{low}$ and $Thy1^{high}$ PMSCs, cells from the bilio-vascular tree were labeled with anti-Epcam-FITC, anti-CD31-FITC, anti-CD45-FITC, anti-CD11b-FITC, anti-PDGFRα-PE, anti-CD34-APC, anti-CD9-BV421, anti-CD200-APC-R700 antibodies as above, and anti-Thy1-PE-Cy7 antibody at a concentration of 1:100. For flow cytometry analysis, freshly isolated PMSCs were labeled either with anti-CD105-BV510, anti-Sca1-BV510 or anti-CD29-PE/Cy7, all at concentrations of 1:100. Analyses were performed using BD FACSDiva™ and FlowJo (Tree Star) software. All antibodies are listed in Table S1.

Cell culture.

PMSCs and HSCs were seeded in 6-well plates at a density of 20,000 cells/cm^2 and cultured in DMEM containing 20% FBS, 1% Hepes and 1% Penicillin-Streptomycin to obtain PMSC-MFs and HSC-MFs, respectively. To maintain PMSCs in a resting state, cells were seeded in 96-well ultra-low attachment

(ULA) round-bottomed plates. The LX-2 human HSC cell line (provided by Human HepCell, IHU-ICAN) was cultured in DMEM containing 10% FBS, 1% Hepes and 1% Penicillin-Streptomycin. HUVECs were grown in EndoGRO™-VEGF complete medium (Millipore).

Cell clonogenicity and differentiation assays.

Cell clonogenicity was examined by CFU-F assay, as follows: 2,000 sorted cells were plated onto a 10-cm plastic dish and maintained in DMEM/20% FBS. The presence of more than 50 cells in a cluster after 14 days in culture, was counted as a colony. The capacity of PMSCs to differentiate towards adipogenic, osteogenic or chondrogenic lineages was analyzed using specific protocols. For adipogenic and osteogenic differentiation, sorted PMSCs were plated in 48-well plates coated with matrigel (Corning, 356231) at a density of 5,000 cells/cm^2 in DMEM/20% FBS until subconfluence. Then, the culture medium was changed for adipogenic (R&D Systems, CCM011) or osteogenic (R&D Systems**,** CCM009**)** differentiation medium. After 21 days, cells were fixed with 4% paraformaldehyde and stained using Oil Red O (Sigma) or Alizarin Red solution (Sigma), respectively. For chondrogenic differentiation, 50,000 sorted PMSCs were plated in ULA plate in chondrogenic differentiation medium (R&D Systems, CCM006) to form spheroids. After 21 days, the spheroids were fixed in 4% paraformaldehyde, embedded in OCT (Sakura Finetek) and cryosections (8 µm) were stained with Alcian blue (Santa Cruz Biotechnology) and counterstained with nuclear fast red (Vector).

Videomicroscopy.

PMSCs and HSCs were seeded in 24-well plates at densities of 5,000 and 50,000 per well, respectively, and cultured in standard conditions. Twenty-four hours after seeding, the cells were placed in the CellVivo Incubation System (Pecon GmbH, Ernah, Germany) driven by a high-end inverted microscope IX83 (Olympus Corporation, Tokyo, Japan). One picture has been taken every hour, using a 10X UPLFN 0.3NA PH1objective lens and ORCA-Flash 4 LT digital (Hamamastu Photonics KK, Tokyo, Japan) driven by Cellsens dimension 1.16 (Olympus). The movies have been built using the open source software Fiji (3).

ScRNAseq.

Cells were loaded onto a GemCode instrument (10x Genomics) to generate single-cell barcoded droplets, *i.e.*, gel beads in emulsion (GEMs). Sequencing libraries were constructed using the Chromium Single-cell 3' Library Kit (10x Genomics) according to the manufacturer's protocol and sequenced on a NextSeq 500 device (Illumina). Average read depth of the sample was 79,199 reads/cell. Reads were then aligned to the mouse genome mm10/Grcm38 using the CellRanger 3.0.2 software. Subsequent analysis was performed in R using the filtered barcode and count matrices produced by CellRanger. The data were analyzed using Seurat 3.6.1 (4). Genes expressed in less than 6 cells, as well as cells with less than 500 or more than 25,000 unique molecular identifiers (UMIs), were filtered out. Any single-cell with more than 10% UMIs

mapped to mitochondrial genes was also removed. Seurat SCTransform function (5) was used to normalize and scale the data (**https://www.ncbi.nlm.nih.gov/geo/query/acc.cgi?&acc=GSE163777**). Dimensionality reduction was performed through PCA on the gene expression matrix and using the first 30 PCs for clustering and visualization. Unsupervised shared nearest neighbor clustering was performed using Seurat FindClusters function at the resolution of 0.6 and visualization was achieved using spectral *t*-SNE of the principal components as implemented in Seurat. Cluster dendrogram was constructed using BuildClustertree built-in function of the R package Seurat which used cluster averaged PCs for calculating a PC distance matrix. The cell clusters identified were evaluated for differential genes expression (DGE), using Seurat FindAllMarkers function. All genes considered for cell-type classification were determined with p value < 0.01 and log (fold-change) > 0.25 as cutoff by performing DGE analysis between the clusters using Wilcoxon rank sum test and Benjamini and Hochberg procedure for p-values adjustment. Single-cell entropy was calculated using LandSCENT v. 0.99.3, as previously described. Doublet analysis was performed, using two methods, *i.e.*, DoubletFinder, R package v 2.0 and Scrublet, python library v0.1. Thereby, we identified 334 and 103 potential doublets, respectively. They included 66 doublets in common, that were plotted on *t*-SNE projection (Fig. S1B). The Monocle version 2.14.0 R package (6) was used to organize cells in pseudotime and infer cell trajectories from the Seurat dataset. We ran reduceDimension with *t*-SNE as the reduction method, num_dim=12, norm_method="log" and max_components = 2. Cells were clustered with the density peak clustering algorithm by setting P to 2 and Δ to 4 (and skip_rho_sigma = T to facilitate the computation). The top 1000 significantly differentially expressed genes between clusters were selected as the ordering genes and used in Monocle for clustering and ordering cells using the DDRTree method and reverse graph embedding.

Bulk RNAseq.

RNA was extracted using Rneasy Micro Kit (Qiagen). Libraries were generated from total RNA and paired-end sequencing was performed on a NextSeq 500 device (Illumina). Raw sequencing data were quality-controlled with the FastQC program. Paired reads were aligned to the mouse reference genome (mm10 build) with the STAR software v2.5.3a (option for no multihits). Mapping results were quality-checked using RNASeQC. Gene counts were obtained by using RSEM tools v1.2.28 (rsem-calculate-expression, option for paired-end and stranded). Expected gene counts were first normalized using TMM method in the edgeR R package and genes with a count per million (CPM) < 1 in 20% of samples, were removed (**https://www.ncbi.nlm.nih.gov/geo/query/acc.cgi?acc=GSE164037**).

Differential gene expression analysis was performed using DEseq2. A $\log_2$ of fold change of 1 and a Benjamini-Hochberg adjusted p value cutoff < 0.05 (FDR) was set to determine significant differentially expressed genes.

GO enrichment and Gene Set Enrichment Analysis.

Symbol gene IDs were first converted to Entrez gene IDs using the clusterProfiler R package (7). Functional enrichment in GO biological processes of differentially expressed genes was performed using EnrichGO built-in function of the clusterProfiler version 3.14 with default parameters. The comparison of enriched functional enrichment among mesenchymal cell populations was performed using clusterProfiler CompareCluster function (7). Heatmap of enriched term was generated in R. GSEA was implemented using the R package ReactomePA with default parameters (8).

Import of previously published data sets.

We downloaded the raw scRNAseq data of i) 23,291 Pdgfrb-GFP+ mesenchymal cells from uninjured and fibrotic (6 weeks CCl4) mouse livers published and deposited in the GEO by Dobie *et al.* (GSE137720), ii) 47,752 liver cells of all types from uninjured oil-treated (10,636) and fibrotic (CCl4 3 weeks, 18,185; BDL 10 days, 18,931) mouse livers published and deposited in the GEO by Yang *et al.* (GSE171904).

Slit2 silencing by siRNA and LX-2 survival.

Slit2 and scramble siRNA (SMARTpool: ON-TARGETplus Slit2 siRNA L-058235-00-0005, ON-TARGETplus Non-targeting Pool D-001810-10-05) were purchased from Dharmacon. PMSC-MFs at passage 1 in 6-well plates were transfected with siRNA (50 nmol/L) using Dharmafect1. Forty-eight hours after transfection, the cells were incubated with serum-free DMEM for 24 hours to generate conditioned medium. LX-2 cells were seeded in 96-well plates (7,000/well) and 24 hours later, were incubated in serum-free DMEM containing H2O2 (200 µmol/L) for 30 min. Thereafter, the medium was replaced by serum-free DMEM or conditioned medium from transfected PMSC-MFs and 24 hours later, cell viability was assessed using MMT assay. Absorbance was quantified at 540 nm (TECAN).

Slit2 deletion by CRISPR/Cas9.

The lentiviral plasmid plentiCRISPRv2, a gift from Zhang lab (Addgene, MA, USA; plasmid #52961), contains hSpCas9, a guide RNA (gRNA), and a puromycin resistance sequence. The gRNA targeting exon 1 of *Slit2* was designed using http://cistrome.org/SSC**,** that ensures specificity and high cleavage efficiency.

Its sequence was sense, 5’ CTTGAACAAGGTGGCGCCGC 3’, antisense, 5’ GCGGCGCCACCTTGTTCAAG 3’. The web-based tool, CRISPOR (http://crispor.tefor.net) that predicts the risk of off-target sequences by providing a cutting frequency determination (CFD) specificity score ranging from 1 to 100, was used to avoid off-target sequences. Guides with a CFD specificity score > 50 are recommended by Doench JG et al. (9). The gRNA we used to target *Slit2* exon 1 has a CFD score of 98. This gRNA did not perfectly match any other genomic region. One off-target with three mismatches was found in an intronic region of *Mapk4* and 40 off-targets were found with four

mismatches, making unlikely that these off-targets were involved in the effect caused by *Slit2* ablation. Lentiviruses dedicated to *Slit2* knockout (LV*Slit2*) and a control lentivirus (LV) expressing Cas9 and a scramble gRNA were produced by the VVTG platform (Federative Research Institute, Necker, France). Sub-confluent PMSC-MFs at day 7 of primary culture, were infected with viral particles at a minimal titer of 10^8 units per mL. Forty-eight hours post-infection, the culture medium was discarded and conditioned medium was prepared by incubating the cells with serum-free medium for 24 hours.

Tube assay.

HUVECs (15,000 cells/well) were plated in 15-well µ-slide angiogenesis Ibidi plates (Clinisciences) previously coated with 50 µl of growth factor-reduced Matrigel (BD Biosciences) and incubated in the presence of PMSC-MF conditioned medium (harvested from cells incubated with serum-free medium for 24 hours) or serum-free medium as a control. To assess the contribution of SLIT2 secreted by PMSC-MFs in angiogenesis, HUVECs were incubated with PMSC-MF conditioned medium a) in the presence of 100 ng/mL of recombinant rat ROBO1/Fc chimera protein (R&D Systems, #1749B) (10), b) after they had been preincubated for 1 hour with 10 µg/mL of anti-human ROBO1 antibody (R&D Systems, #AF7118), or c) with the conditioned medium from PMSC-MFs infected with a lentivirus expressing Cas9 and a gRNA targeting the first exon of *Slit2*, dedicated to *Slit2* knockout (LV*Slit2*) or a control lentivirus (LV) expressing Cas9 and a scramble gRNA. HUVECs were placed in the CellVivo Incubation System as for videomicroscopy (described above) and tube formation was evaluated after 6 hours of incubation using the Angiogenesis Analyzer tool (Fiji software).

Human liver tissue samples.

Samples of normal liver from patients undergoing liver resections for focal lesions (n=2 patients), and of cirrhotic livers from patients with NASH (n=1), chronic hepatitis C (n=1) or alcoholic liver disease (n=3) undergoing liver resection or transplantation, were provided by Human HepCell platform (IHU-ICAN, Declaration No. AC-2020-3861) for FISH. Frozen samples of liver biopsy from subjects with a suspicion of non-alcoholic fatty liver disease at stages of fibrosis F0 (n=26), F1 (n=15), F2 (n=12), F3-F4 (n=7), were provided by the Biological Resource Center, BIO-ICAN, Paris, France, with ethical approval from the Persons Protection Committee (CPP Ile de France VI) for RT-qPCR analyses. The RNA used for microarray experiments was extracted from frozen tissue obtained from explanted livers or diagnostic liver biopsies from i) normal human liver tissue (tumor-free tissue from livers with colorectal cancer metastasis) (n=5 patients) and ii) liver tissue from patients with chronic liver diseases, including PSC (n=6 patients, 2 biopsies/patient), NASH (n=7 patients) and other liver diseases including autoimmune hepatitis (n=3), primary biliary cholangitis (n=2), alcoholic liver disease (n=1), haemochromatosis (n=1) and sarcoidosis (n=1). The liver specimens were provided by the Norwegian biobank for primary sclerosing cholangitis, Oslo, Norway with ethical approval

from the Regional Committee for Medical and Health Research ethics of South East Norway. All subjects gave written informed consent before to allow the use of the samples.

RT-qPCR.

Total RNA was extracted from frozen liver tissue samples or harvested cells using the RNeasy Mini Kit or Micro Kit (Qiagen), respectively. The cDNA was synthesized using the MMLV-RT (Invitrogen, 28025013) or SuperScript™ II (Invitrogen, 18064014) and real-time PCR was performed using the LightCycler 480 SYBR Green I Master Kit on an LC480 device (Roche Diagnostics). Target gene mRNA levels were normalized using HPRT or 18S as a reference gene and expressed as relative levels (2-ΔΔCt method). Normalized values (ΔCt) were used for oligogene signature analysis and presented as 0-ΔCt, so that higher values indicate higher expression levels. The primers (Table S2) were designed using the primer software from Roche Diagnostics.

Immunofluorescence and FISH.

For immunofluorescence, cell preparations were fixed in 4% paraformaldehyde at 4°C for 15 minutes, and incubated with primary antibodies against COL15A1 (Abcam, ab58717, 1:200) or α-SMA (Agilent, M085129-2, 1:100) at 4°C overnight. Nuclear staining was performed using Draq5 (Abcam). Cells were examined with a SP2 confocal microscope (Leica, Bannockburn, IL, USA).

For co-labeling by FISH and immunofluorescence, cell preparations and tissue samples were fixed in 4% paraformaldehyde at 4°C for 20 minutes and 4 hours, respectively. Tissue samples were then transferred to 30% sucrose in PBS at 4°C until sinking and then placed in a plastic mold filled with O.C.T. that was immersed in 2 methyl-butane maintained at -70°C, and stored at -80°C. Tissue sectioning was performed at -25°C and 10-µm cryosections were mounted on SuperFrostPlus™ slides that were kept on dry ice. Before processing, tissue sections were thawed in 100% ethanol for 5 minutes, followed by 1 minute in TBS buffer. Cell preparations or tissue sections were then transferred to pre-warmed hybridization buffer (5X SSC / 1% BSA / 10% Formamid / 0,1% (w/v) SDS) at 75°C for 20 minutes. The probes, directed at *SLIT2* or Scramble (Table S3), conjugated to Fam-6 or Atto-633, respectively, were diluted at 50 ng/µL and denatured at 85°C for 5 minutes while the samples were dried and denatured on a preheated plate at 85°C for 2 minutes. The probes (100µL) were added to tissue sections then covered with a coverslip and sealed with glue. In the following steps the samples were kept in the dark. They were incubated at 75°C overnight in a dark wet chamber. After removal of the coverslip, the slides were transferred to freshly prepared hybridization buffer at 75°C for 15 minutes. The slides were washed with TBS for 5 minutes, and then with TBS-Triton x100 0.3% for 15 minutes, at room temperature. After a 5-minute TBS wash at room temperature, the slides were blocked for 60 minutes with 2% Normal Goat Serum (Thermo Fisher) in TBS-T (0.1%). Tissue sections were incubated with anti-α-SMA (1:100, M085129-2, Agilent) in blocking buffer, overnight at 4°C. Slides were washed with TBS 3 times for 5 minutes at room temperature and

incubated with secondary antibody (Goat anti-mouse IgG Alexa Fluor 555 Conjugate, CellSignaling #4409, 1:500) and DAPI 2µg/mL (Sigma-Aldrich). Large field imaging acquisition was performed on a Zeiss Axio Observer 7. For image processing, the large field images were stitched and background was subtracted, using the default settings of ZEISS software ZEN 3.1 (blue edition). Exported single channel grayscale in .tiff were later processed in Fiji. The background due to FISH staining was assessed using the scramble probe and this autofluorescence was subtracted from the *SLIT2* channel using image calculator module. For quantification, binary masks of at least two independent experiments were generated using the trainable classification software Ilastik (v 1.3.3). Marked areas were then measured using Fiji. The plugin Color pixel counter was used to count the number of pixels on the image of a specific color. Results are expressed as a percentage of pixels in the Region of Interest.

Microarray analyses.

Pangenomic analysis of frozen liver tissue samples, was performed using the Affymetrix human gene 1.0 st microarray. Analysis was conducted using R. *oligo* bioconductor package to import raw data CEL files in an ExpressionSet object and *rma* function to normalize the data. After normalization, summarization was performed because transcripts are represented by multiple probes, on the Affymetrix platform. For each gene, the background-adjusted and normalized intensities of all probes were summarized into one estimated amount proportional to the amount of RNA transcripts. Summarized data have been annotated with hugene10sttranscriptcluster.db bioconductor package (**https://www.ncbi.nlm.nih.gov/geo/query/acc.cgi?acc=GSE159676**).
Statistical analysis was performed using non-parametric Wilcoxon test.

A

	nCounts (transcripts)	nFeatures (genes)	% mitochondrial genes
Mean per cell	10539	2951	3.14 %

B

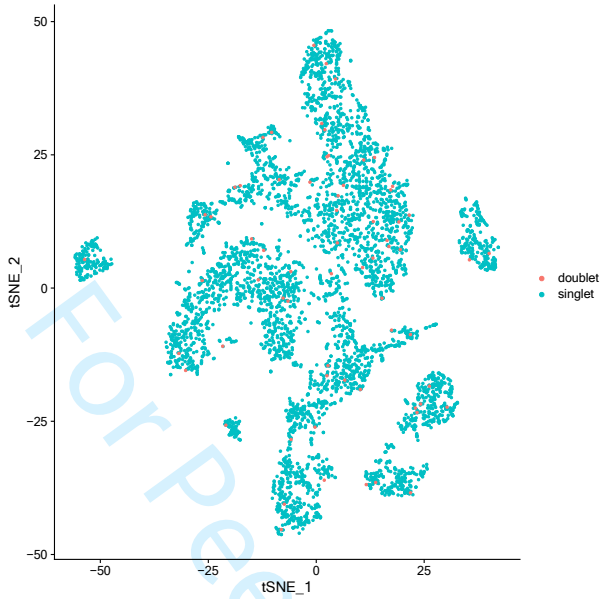

Fig. S1: scRNAseq (A) Quality control metrics; (B) Analysis of doublets (plotted on *t*-SNE).

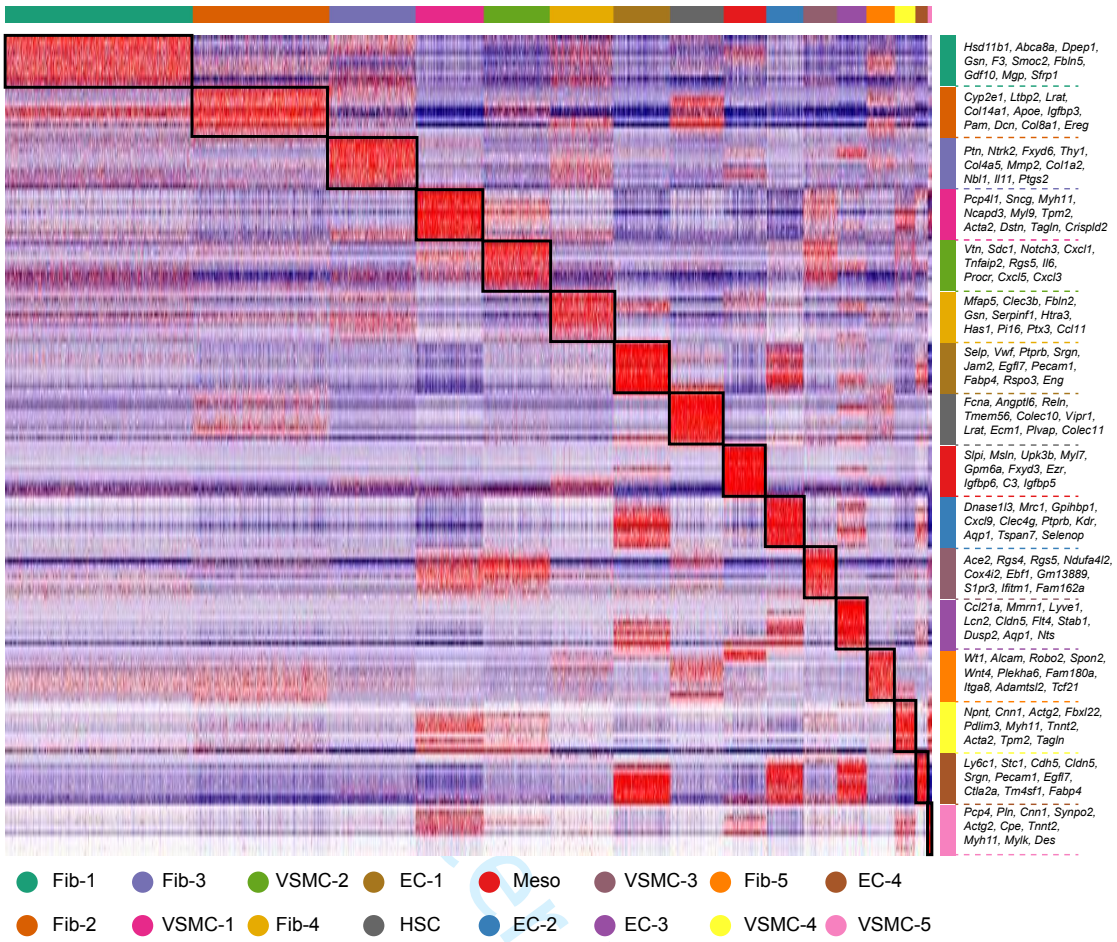

Fig. S2: Heatmap of the top 10 differentially expressed genes in scRNAseq clusters. (see also Table S4).

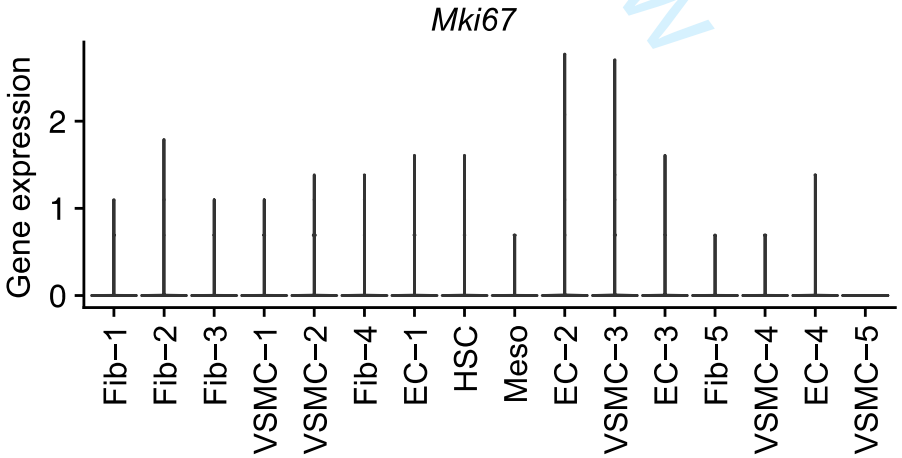

Fig. S3: Violin plots showing the expression of the proliferation marker Mki67 across all scRNAseq clusters.

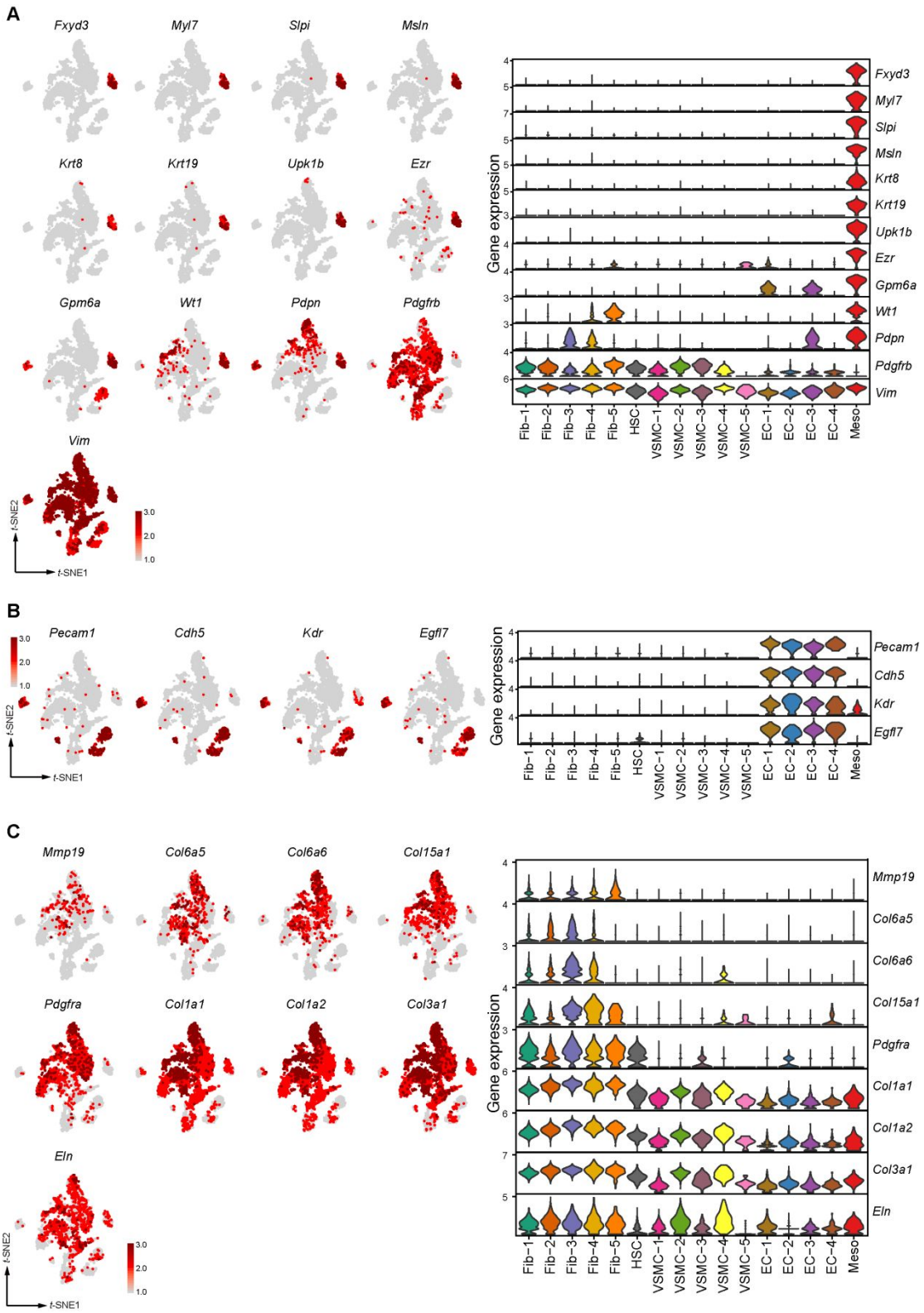
A
Fxyd3
Myl7
Slpi
Msln
Krt8
Krt19
Upk1b
Ezr
Gpm6a
Wt1
Pdpn
Pdgfrb
Vim
t-SNE2
t-SNE1
Gene expression
Fib−1
Fib−2
Fib−3
Fib−4
Fib−5
HSC
VSMC−1
VSMC−2
VSMC−3
VSMC−4
VSMC−5
EC−1
EC−2
EC−3
EC−4
Meso
B
Pecam1
Cdh5
Kdr
Egfl7
C
Mmp19
Col6a5
Col6a6
Col15a1
Pdgfra
Col1a1
Col1a2
Col3a1
Eln

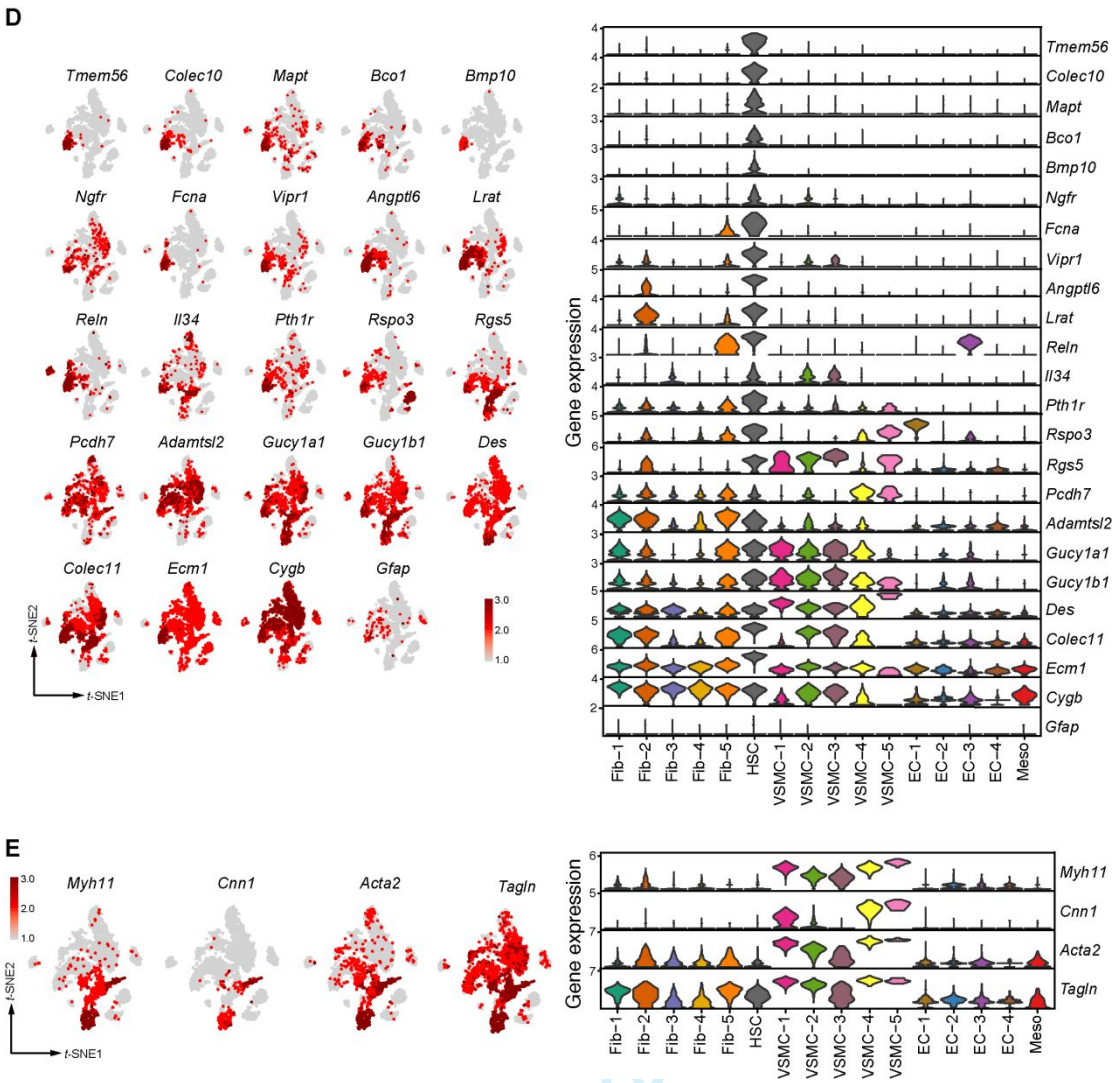

Fig. S4: *t*-SNE and Violin plots across all scRNAseq clusters of gene expressions, that were previously or herein reported to demarcate the following cell types: (A) mesothelial cells (Meso), (B) endothelial cells (EC), (C) fibroblasts (Fib), (D) hepatic stellate cells (HSC), (E) vascular smooth muscle cells (VSMC).

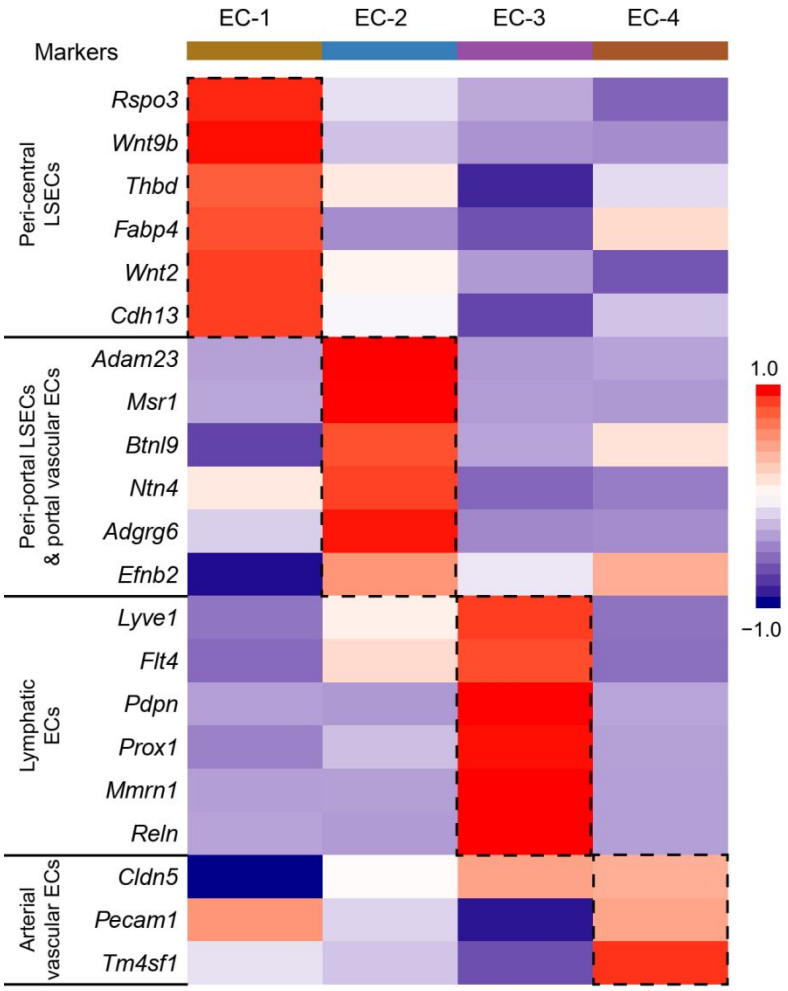

Fig. S5: Heatmap depicting representative genes expressed in the endothelial cell (EC) clusters of the scRNAseq.
Color scale represents the average expression level across all cells within each cluster. LSECs, liver sinusoidal endothelial cells.

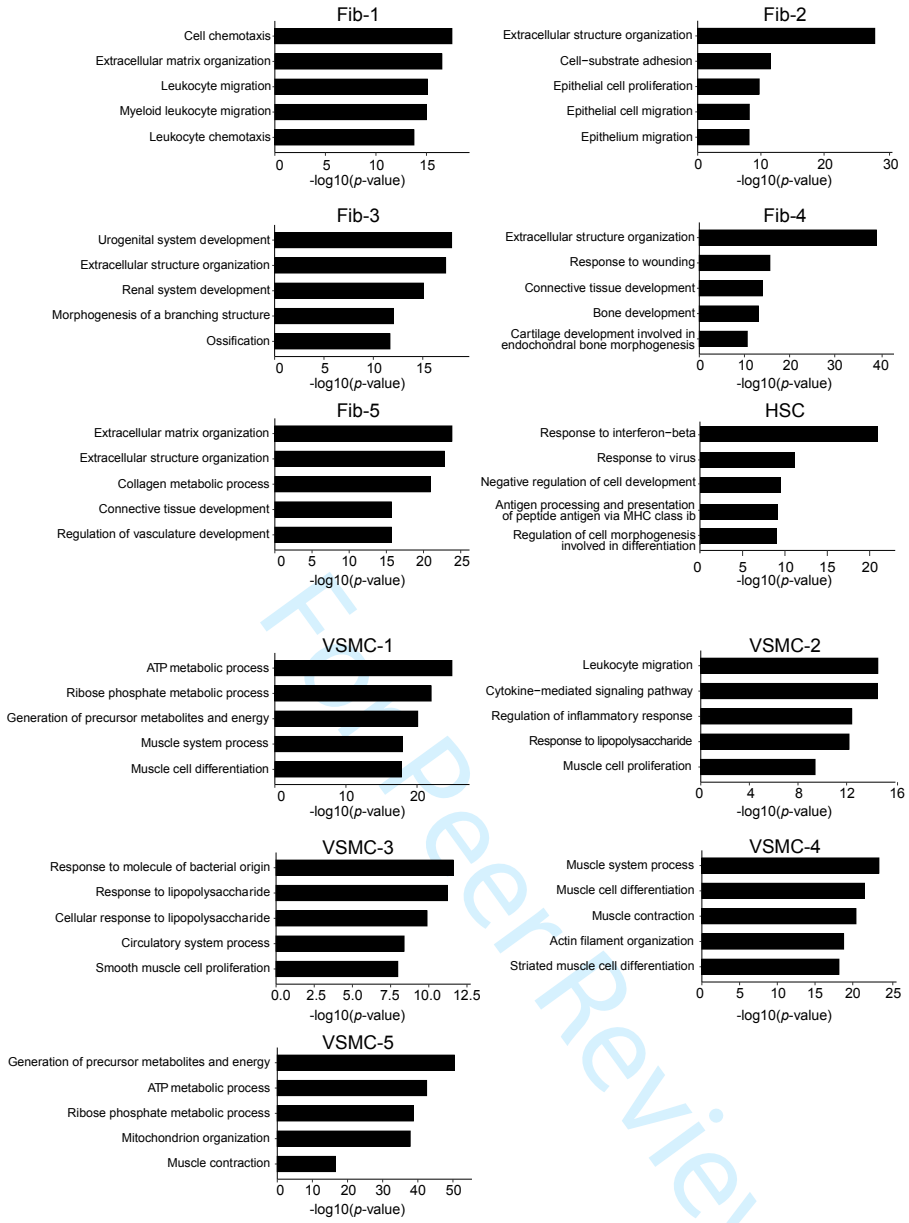

Fig. S6: GO enrichment of genes significantly overexpressed in the different mesenchymal cell clusters of the scRNAseq. (see also Table S5).

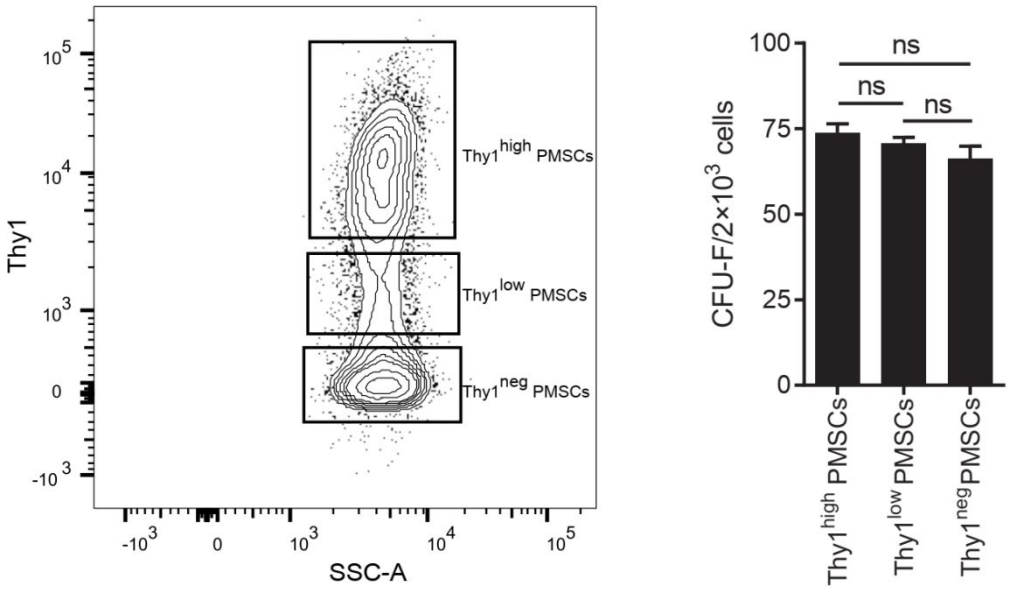

Fig. S7: Clonogenicity of PMSCs according to Thy1 expression.
Left panel: Representative flow cytogram of Thy1 expression on PMSCs. Right panel: CFU-F formed by Thy1^{neg}, Thy1^{low} and Thy1^{high} PMSCs. Data represent means ± SEM (n=3). Statistical significance was evaluated using one-way ANOVA; ns, non-significant.

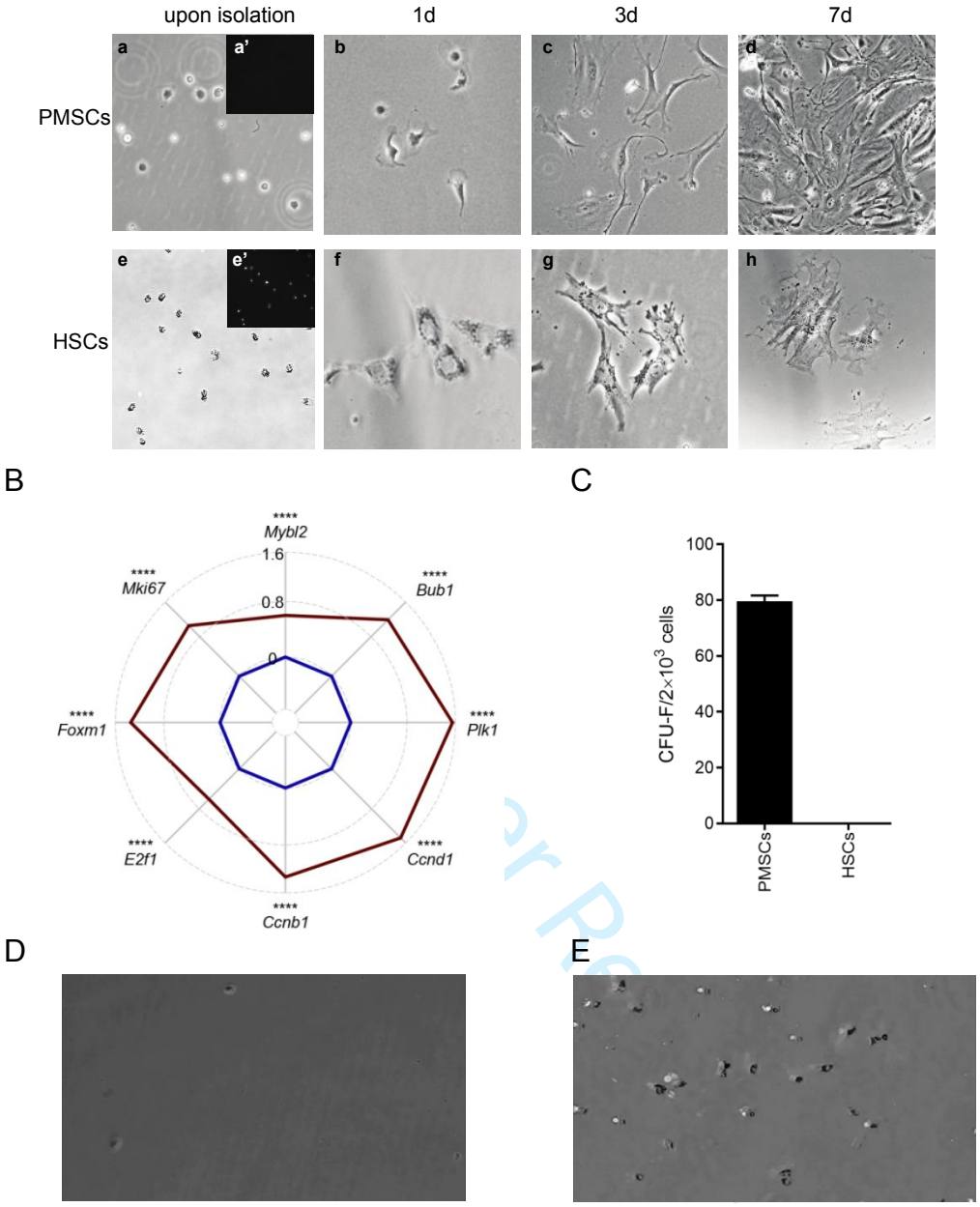

Fig. S8: Phenotypic comparison of PMSCs/PMSC-MFs and HSCs/HSC-MFs.

(A) Microscopic appearance: Cells were observed under phase-contrast microscopy (fluorescence microscopy under 328-nm ultraviolet excitation in insets) (a,e) immediately after cell sorting, (b-d, f-h) at the indicated days (d) of primary culture. (B-E) Proliferative properties: B) Proliferation-related gene expressions in PMSC-MFs *vs.* HSC-MFs. Radar plot showing the log2 fold-difference in the expression of cell proliferation-related genes in bulk RNAseq analysis of PMSC-MFs (red line) and HSC-MFs (blue line) after 7 days in culture. Statistical significance was evaluated using Wilcoxon test; ****p<0.0001; C) CFU-F formed by sorted PMSCs and HSCs (Means ± SEM, n=8); Videomicroscopy (provided separately) of D) PMSCs and E) HSCs between day 1 and day 5 of primary culture (representative of 2 random fields).

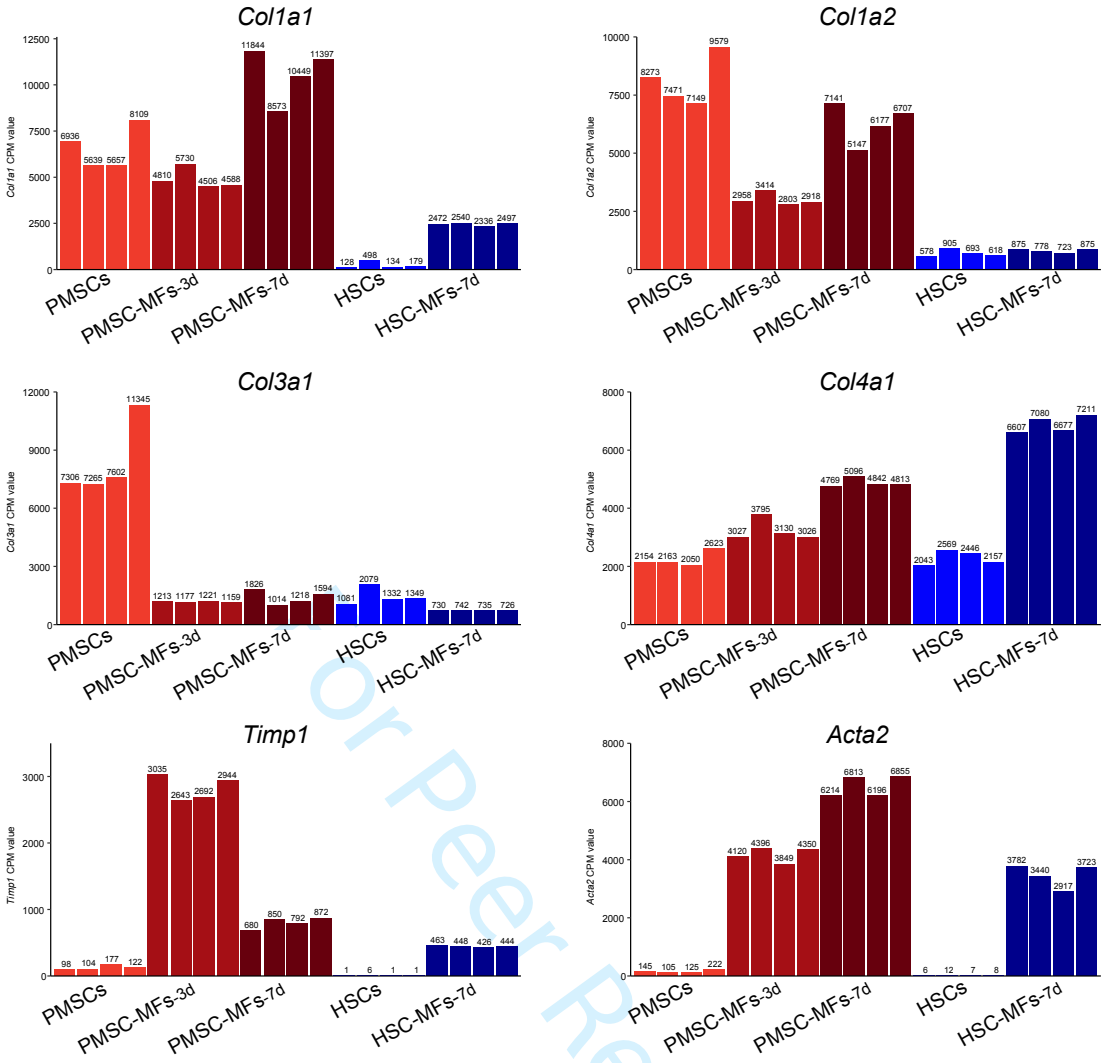

Fig. S9: Expression of pro-fibrotic genes in PMSCs and HSCs, in resting or myofibroblastic states after 3 days (-MFs-3d) or 7 days (-MFs-7d) in primary culture. CPM, counts per million.

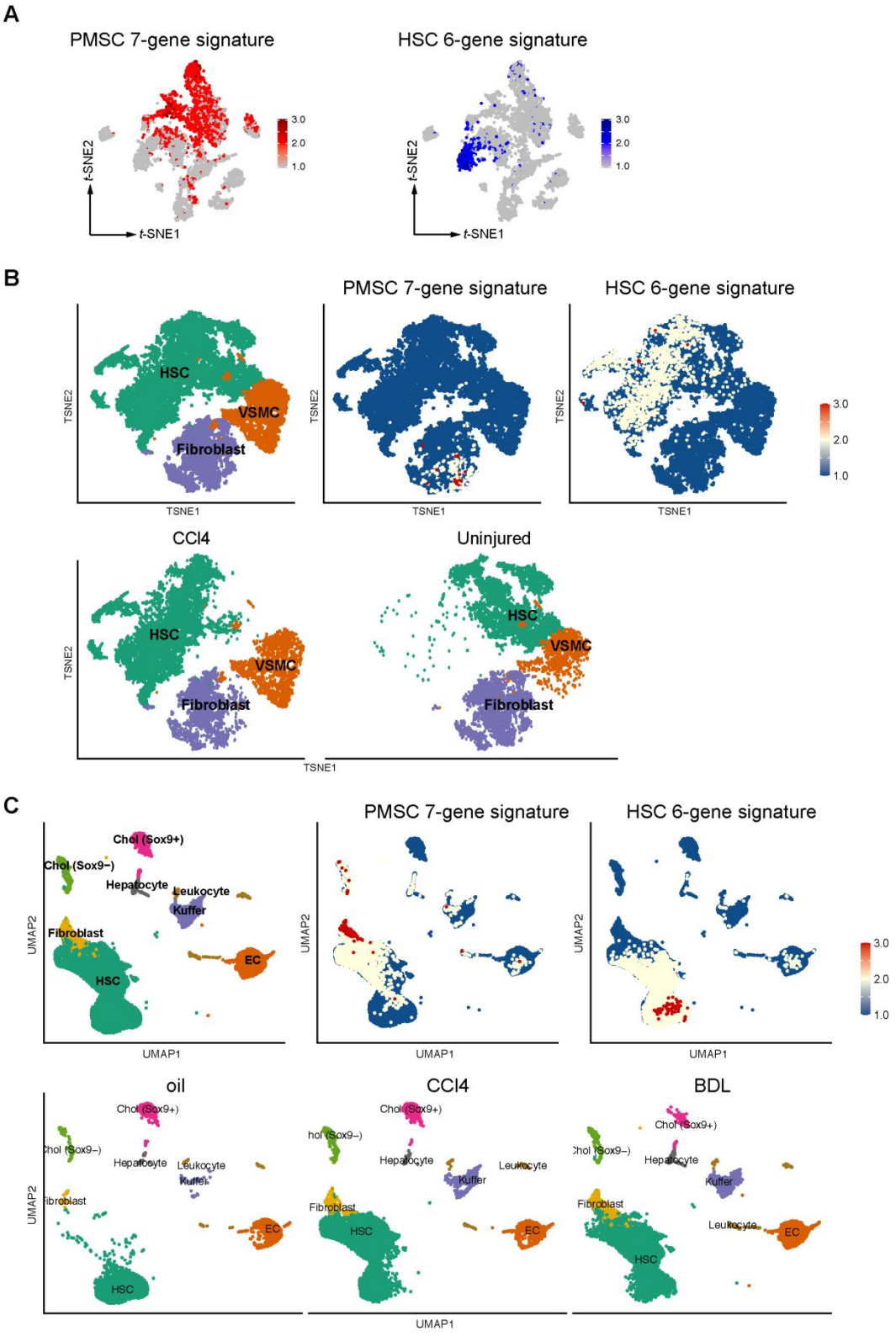

Fig. S10: PMSC/PMSC-MF and HSC/HSC-MF oligogene signatures projected onto (A) current and (B, C) previous scRNAseq data sets.
A) Clustering of portal mesenchymal cells from uninjured mouse liver as in Fig. 1B; B) Clustering of Pdgfrb-GFP+ mesenchymal cells from uninjured and fibrotic (6 weeks CCl4) mouse livers from Dobie *et al*. (GSE137720); C) Clustering of all liver cells from uninjured (oil) and fibrotic (3 weeks CCl4, 10 days BDL) mouse livers from Yang *et al*. (GSE171904). Chol, cholangiocytes.

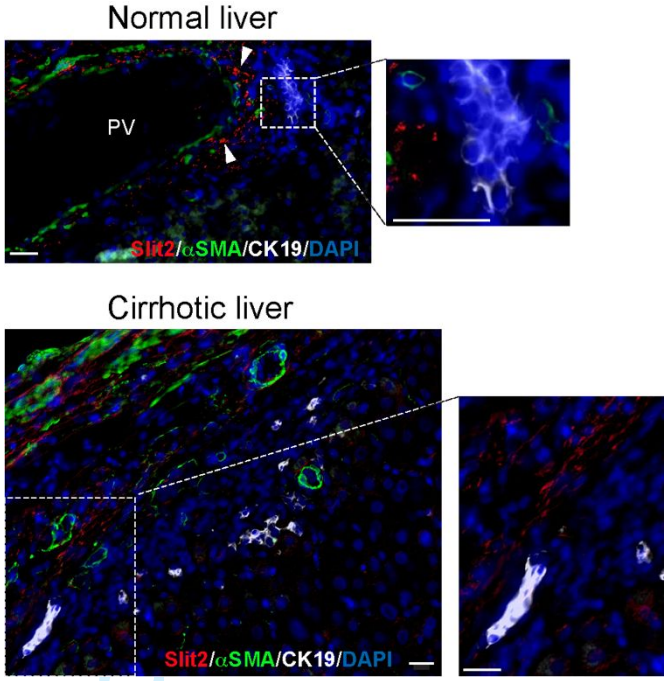

Fig. S11: Distinct localization of SLIT2⁺ cells and cholangiocytes.
SLIT2 FISH and α-SMA or CK19 immunofluorescence were performed on normal and cirrhotic human liver tissue sections. In normal liver (upper panel), perivascular *SLIT2*⁺ cells (arrowheads) in a large portal tract are distinct from α-SMA⁺ VSMCs and from CK19⁺ cholangiocytes (higher magnification in inset), representative of n=2 (PV, portal vein). In cirrhotic liver (lower panel), *SLIT2*⁺ intermingled with *SLIT2*⁻ myofibroblasts in fibrotic septa, are distinct from CK19⁺ cholangiocytes (higher magnification in inset), representative of cirrhosis of alcoholic (n=3), NASH (n=1) or hepatitis C (n=1) origins (Scale bars=50 μm).

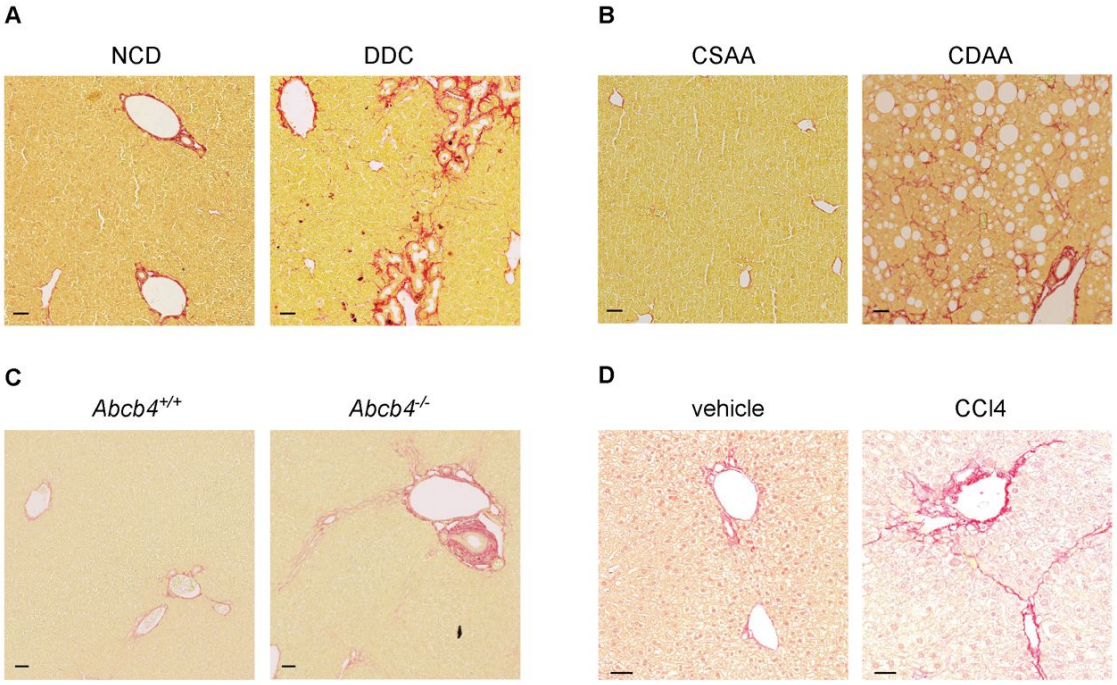

Fig. S12: Mouse models of liver fibrosis.
Sirius red staining of the liver from (A) mice fed NCD or DDC diet for 4 weeks; (B) mice fed CSAA or CDAA diet for 8 weeks; C) *Abcb4*$^{+/+}$ and *Abcb4*$^{-/-}$ mice at the age of 8 weeks; D) vehicle- or CCl4-i.p.-injected mice for 6 weeks. NCD, normal chow diet; DDC, 3,5-diethoxycarbonyl-1,4-dihydrocollidine; CSAA, choline-sufficient L-amino acid-defined; CDAA, choline-deficient L-amino acid-defined diet. Representative of 5 to 17 animals per group. Scale bars=50 µm.

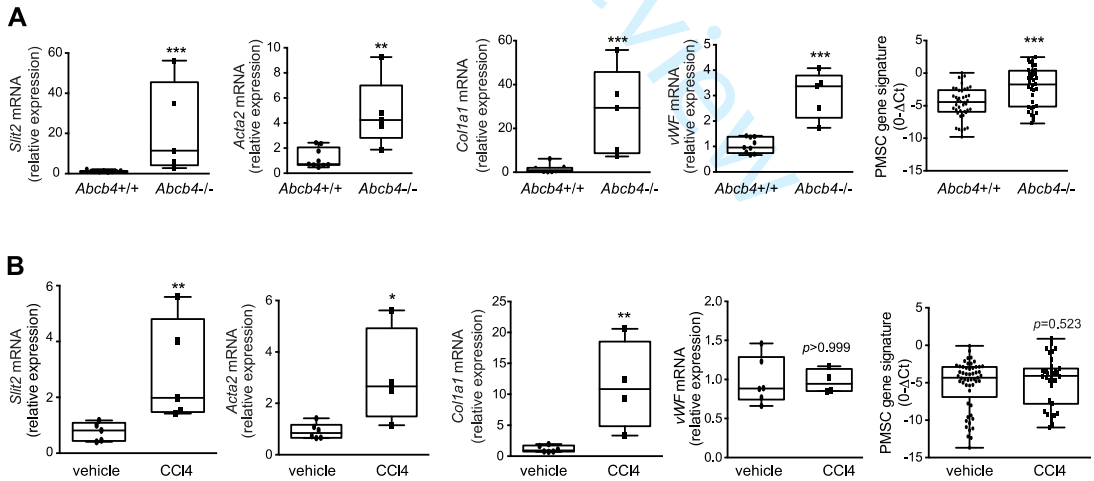

Fig. S13: Expression of SLIT2 and PMSC 7-gene signature in the Abcb4$^{-/-}$ and CCl4 mouse models of liver fibrosis.
Hepatic expression of *Slit2*, *Acta2*, *Col1a1*, *vWF* and of PMSC 7-gene signature was measured by RT-qPCR in liver tissue from (A) *Abcb4*$^{+/+}$ (n=9) and *Abcb4*$^{-/-}$ (n=5) mice at the age of 8 weeks, (B) vehicle- or CCl4-i.p.-injected mice for 6 weeks (n=5/group). Data represent individual values and means ± SEM. **p*<0.05; ***p*<0.01; ****p*<0.001 (Wilcoxon test).

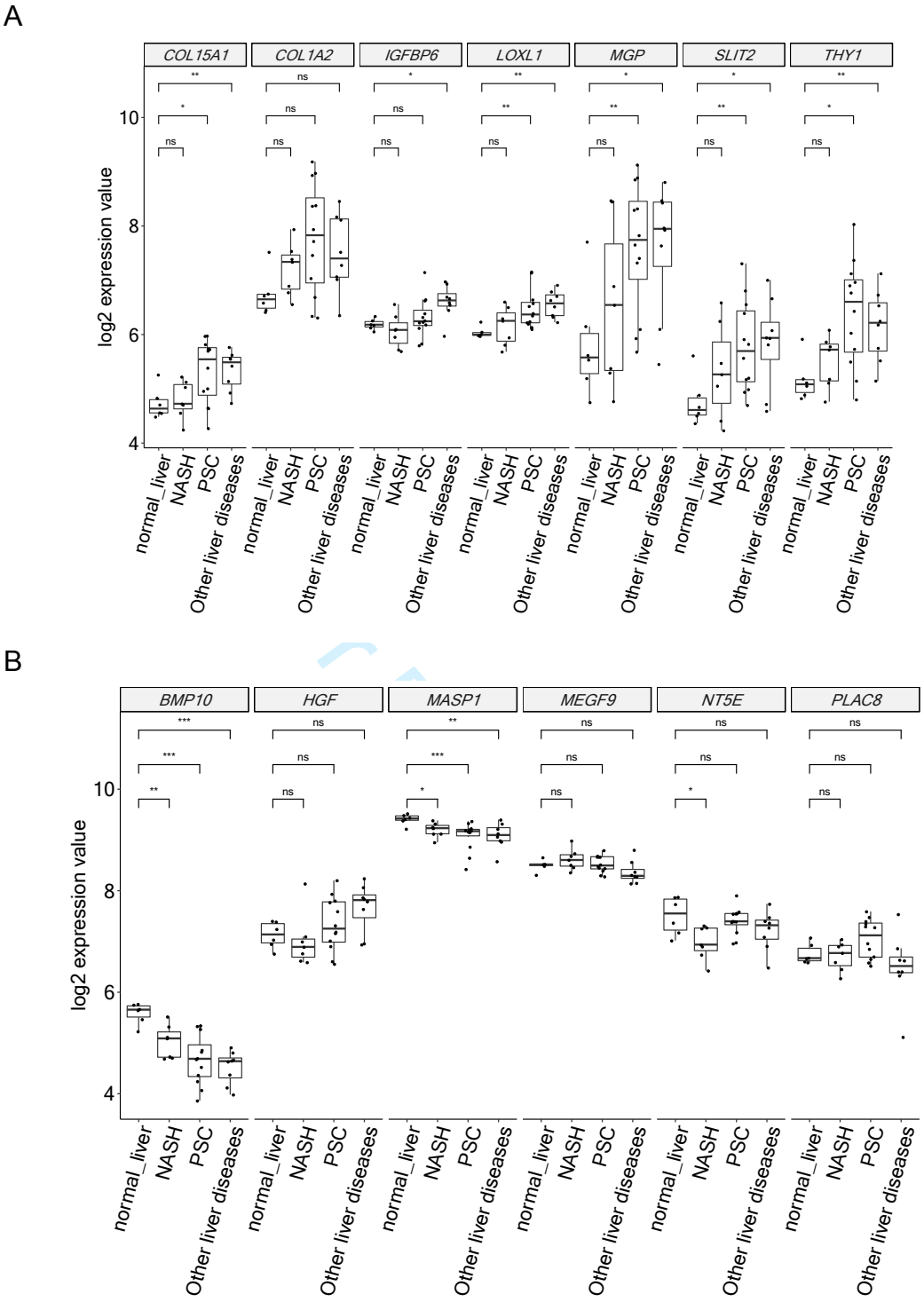

Fig. S14: Individual expression of the PMSC and HSC signature genes in human liver fibrosis.

Hepatic expression of the genes of (A) PMSC/PMSC-MF, and (B) HSC/HSC-MF signatures, was assessed by Affymetrix microarray analysis of normal human liver (n=5 patients) and of liver tissue samples from patients with NASH (n=7 patients), PSC (n=6 patients, 2 biopsies/patient) or other liver diseases (n=8 patients). Data represent individual values and means ± SEM. **p*<0.05; ***p*<0.01; ****p*<0.001; ns, non-significant; statistical significance was evaluated using non-parametric Wilcoxon test.

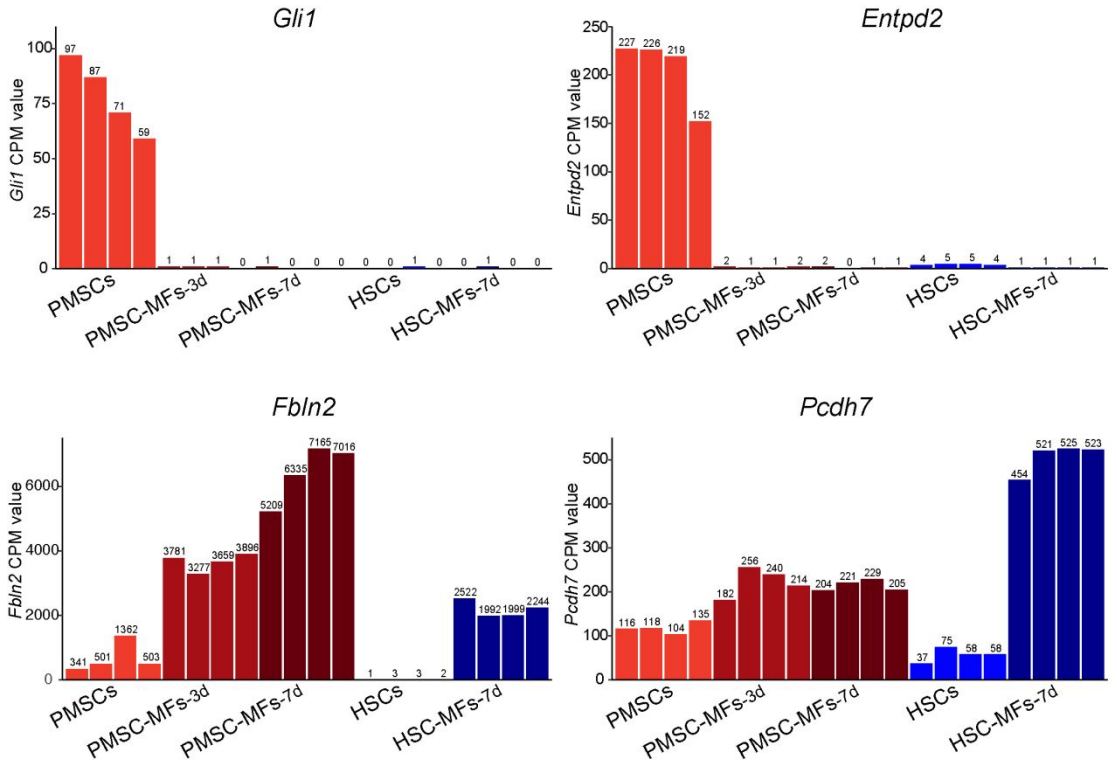

Fig. S15: *Gli1*, *Entpd2*, *Fbln2* and *Pcdh7* expression in the bulk RNAseq analysis of PMSCs and HSCs, in resting or myofibroblastic states after 3 days (-MFs-3d) or 7 days (-MFs-7d) in primary culture.
CPM, counts per million.

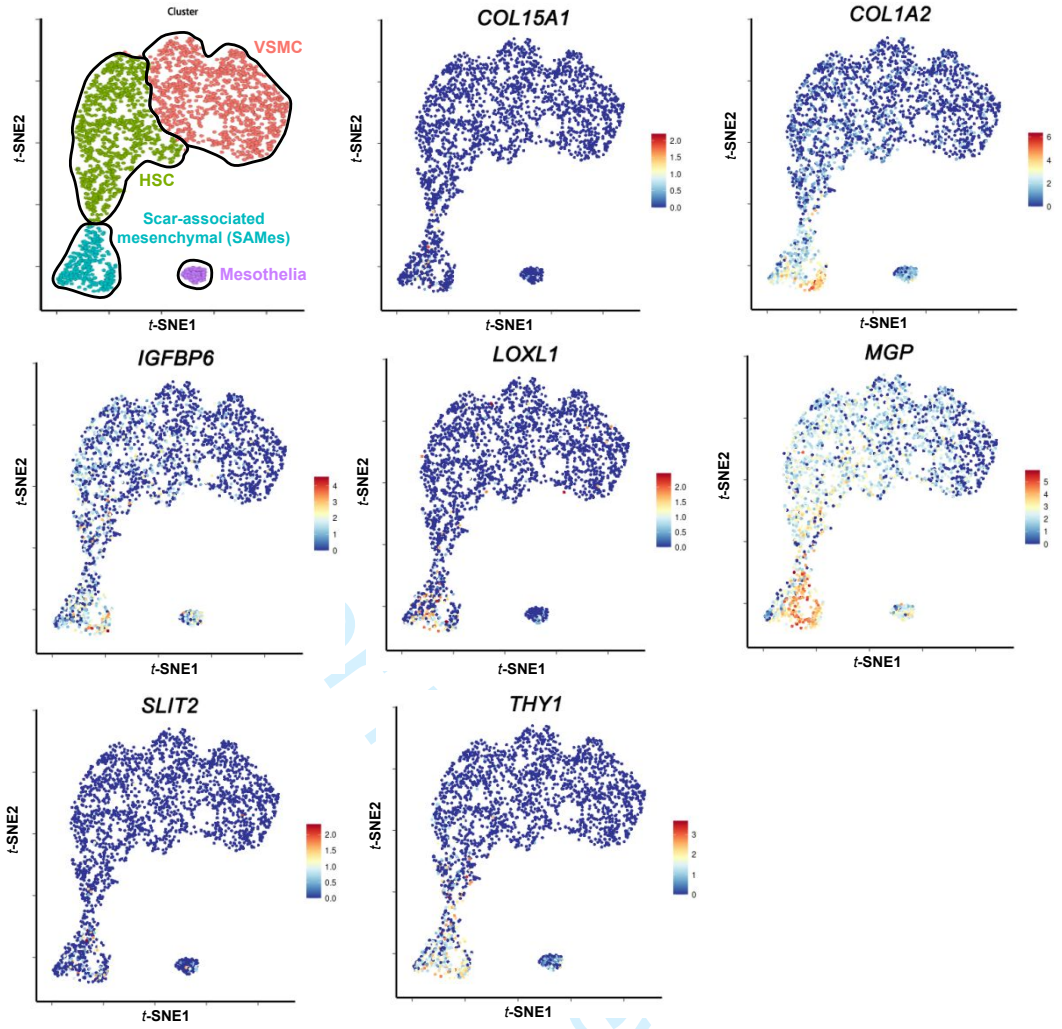

Fig. S16: Comparison of PMSCs/PMSC-MFs with the previously annotated scar-associated mesenchymal cells.
t-SNE plot of PMSC/PMSC-MF signature genes in human mesenchymal cells from Ramachandran et al. (https://www.livercellatlas.ed.ac.uk/).

Table S1: Antibodies used for cell sorting, flow cytometry and immunofluorescence.

Antibody	Company	Cat no.	Clone no.
Cell sorting & Flow cytometry			
rat anti-mouse CD9-BV421	BD Biosciences	564235	KMC8
rat anti-mouse CD11b-FITC	BioLegend	101245	M1/70
hamster anti-mouse CD29-PE/Cy7	BioLegend	102222	HMβ1-1
rat anti-mouse CD31-FITC	BD Biosciences	561813	MEC 13.3
rat anti-mouse CD34-APC	BioLegend	119310	MEC14.7
rat anti-mouse CD45-FITC	BioLegend	103137	30-F11
rat anti-mouse CD105-BV510	BD Biosciences	740188	MJ7/18
rat anti-mouse CD200-APC-R700	BD Biosciences	565546	OX-90
rat anti-mouse Epcam-FITC	BioLegend	118207	G8.8
rat anti-mouse PDGFRa-PE	eBioscience	12-1401-81	APA5
rat anti-mouse Sca1-BV510	BD Biosciences	565507	D7
rat anti-mouse Thy1-PE-Cy7	eBioscience	25-0902-81	53-2.1
Immunofluorescence			
mouse anti-human α-SMA	Agilent	M085129-2	1A4
rabbit anti-human Col15a1	Abcam	ab58717	N/A

Table S2: Primers used for qPCR.

Gene	GenBank	Forward primer	Reverse primer
Mouse			
Acta2	NM_007392.3	CTGTCAGGAACCCTGA	TACTCCCTGATGTCT
Bmp10	NM_009756.3	CGGAGCTTCAAGAACG	TGGTGAGGGATAGAC
Col1a1	NM_007742.4	GCTCCTCTTAGGGGCC	CCACGTCTCACCATT
Col1a2	NM_007743.3	CAAGCATGTCTGGTTA	AGGACACCCCTTCTA
Col15a1	NM_009928.3	AGATTTACGGGTTCCA	CAACGTGTGATTCTTT
Hgf	NM_001289458.1	CACCCCTTGGGAGTAT	GGGACATCAGTCTCA
Hprt	NM_013556.2	TCAAATCCCTGAAGTA	AGGACCTCTCGAAGT
Igfbp6	NM_008344.3	GGGCTCTATGTGCCAA	CCTGCGAGGAACGAC
Loxl1	NM_010729.3	TATGCCTGCACCTCTC	TGTCCGCATTGTATG
Masp1	NM_001359083.1	CCTACAGAGCGGCAG	GGCTCGATTTTCCCG
Megf9	NM_172694.2	ACAACCGGTCTGATAG	TTTGCATTCTTCACAG
Mgp	NM_008597.4	TCACGAAAGCATGGAG	GCTGAGGGGACATAA
Nt5e	NM_001204813	CCATTGATGAGAAGAA	GTCAAATGTCCCTCC
Plac8	NM_139198.3	TGTGTGCCAACTCAAG	GTTGAGCTTCTTCAG
Slit2	NM_178804.5	ATCTGCCTGAGACCAT	CGTCTAAGCTTTTTGT
Thy1	NM_009382.3	GAAAACTGCGGGCTTC	CCAAGAGTTCCGACT
vWf	NM_011708.4	CTACCTAGAACGCGAG	CATCGATTCTGGCCG
18S	NR_003278.3	GAGCGAAAGCATTTGC	GGCATCGTTTATGGT
Human			
ACTA2	NM_001613.4	GACAATGGCTCTGGGC	CTGTGCTTCGTCACC
COL1A	NM_000088.4	GTGCGATGACGTGATC	CGGTGGTTTCTTGGT
HPRT	NM_000194.3	TAATTGGTGGAGATGA	TGCCTGACCAAGGAA
SLIT2	NM_004787.4	GTGTTCGTGCCAGCTA	TTCCATCATTGATTGT
vWF	NM_000552.5	CTCCCACGCCTACATC	GCGGTCGATCTTGCT

Table S3: Probes used for FISH.

Probe name	Sequence
Scrambled	5’ TAGCGAATCTCAGGCAAG – AT 633 3’
SLIT2-1	5’ GGACCACGTCTCGCAGCGGTTCCTGCGGC – 6 Fam 3’
SLIT2-2	5’ CACGGGTCCTTATAGGGGGCGTTGTGGC – 6 Fam 3’
SLIT2-3	5’ CTTACGGTTGTTCTATTTGACGGAAGC – 6 Fam 3’
SLIT2-4	5’ CACCTGCTCCAACTCTTTCACCACTTCACGC – 6 Fam 3’

Table S4: Differentially expressed genes in each scRNAseq cluster compared to all others.

Tab 1: All differentially expressed genes classified according to Seurat R toolkit;
Tab 2: Top 10 differentially expressed genes classified according to average log Fold-Change (avg_logFC).
(Provided separately).

Table S5: GO enrichment of differentially expressed genes in the scRNAseq clusters of Fibroblasts (Fib), Hepatic stellate cells (HSCs), and Vascular smooth muscle cells (VSMCs).

(Provided separately).

Table S6: Differential gene expressions in bulk RNAseq analyses, between PMSCs or HSCs and their myofibroblastic progenies after 3 days (-MFs-3d) or 7 days (-MFs-7d) in primary culture.

Genes (ID) are classified according to average log Fold-Change (logFC) from 4 replicates per condition.
(Provided separately)

Supplementary references

1. Gonzalez-Sanchez E, Firrincieli D, Housset C, Chignard N. Expression patterns of nuclear receptors in parenchymal and non-parenchymal mouse liver cells and their modulation in cholestasis. Biochim Biophys Acta Mol Basis Dis 2017;1863:1699-1708.

2. Mederacke I, Dapito DH, Affo S, Uchinami H, Schwabe RF. High-yield and high-purity isolation of hepatic stellate cells from normal and fibrotic mouse livers. Nat Protoc 2015;10:305-315.

3. Schindelin J, Arganda-Carreras I, Frise E, Kaynig V, Longair M, Pietzsch T, Preibisch S, et al. Fiji: an open-source platform for biological-image analysis. Nat Methods 2012;9:676-682.

4. Stuart T, Butler A, Hoffman P, Hafemeister C, Papalexi E, Mauck WM, 3rd, Hao Y, et al. Comprehensive Integration of Single-Cell Data. Cell 2019;177:1888-1902 e1821.

5. Hafemeister C, Satija R. Normalization and variance stabilization of single-cell RNA-seq data using regularized negative binomial regression. Genome Biol 2019;20:296.

6. Trapnell C, Cacchiarelli D, Grimsby J, Pokharel P, Li S, Morse M, Lennon NJ, et al. The dynamics and regulators of cell fate decisions are revealed by pseudotemporal ordering of single cells. Nat Biotechnol 2014;32:381-386.

7. Yu G, Wang LG, Han Y, He QY. clusterProfiler: an R package for comparing biological themes among gene clusters. OMICS 2012;16:284-287.

8. Yu G, He QY. ReactomePA: an R/Bioconductor package for reactome pathway analysis and visualization. Mol Biosyst 2016;12:477-479.

9. Doench JG, Fusi N, Sullender M, Hegde M, Vaimberg EW, Donovan KF, Smith I, et al. Optimized sgRNA design to maximize activity and minimize off-target effects of CRISPR-Cas9. Nat Biotechnol 2016;34:184-191.

10. Ricano-Cornejo I, Altick AL, Garcia-Pena CM, Nural HF, Echevarria D, Miquelajauregui A, Mastick GS, et al. Slit-Robo signals regulate pioneer axon pathfinding of the tract of the postoptic commissure in the mammalian forebrain. J Neurosci Res 2011;89:1531-1541.